DESIGN AND ANALYSIS OF A COMPLIANT GRASPER FOR HANDLING LIVE OBJECTS

A Thesis
Presented to
The Academic Faculty

by

Xuecheng Yin

In Partial Fulfillment
Of the Requirements for the Degree
Doctor of Philosophy in Mechanical Engineering

Georgia Institute of Technology
Atlanta, Georgia
November 2003

DESIGN AND ANALYSIS OF A COMPLIANT GRASPER FOR HANDLING LIVE OBJECTS

Approved:

_____
Dr. Kok-Meng Lee, Chair

_____
Dr. Shreyes Melkote

_____
Dr. Bruce Webster

_____
Dr. William Singhose

_____
Dr. Chen Zhou

Date Approved: Nov. 19, 2003

DEDICATION

To my parents:

Shisun Yin
Xueyu Liu

To my wife:

Lan Shi

To my son:

Andrew Yifan Yin

ACKNOWLEDGEMENT

I would like to thank Dr. Kok-Meng Lee for many things, his exemplary advisement and guidance throughout the accomplishment of my Ph. D. thesis. Most importantly, he has taught me not only the critical thinking methods to use when facing difficulties in the research problem, but also the professional attitude in the process of the research. He is always so energetic, and very devoted to the broad research areas varying from spherical motor to heat transfer modeling of optic fiber manufacturing and the intelligent transfer project that led to this thesis. I would also like to acknowledge the support and suggestions of my reading committee, Dr. William E. Singhose, Dr. Shreyes N. Melkote, and Dr. Chen Zhou.

This thesis research is funded by the research grants from US Poultry and Eggs Association. Equipment and experiment setup for the project are from the Georgia Agriculture Technological Research Program (ATRP). The author deeply appreciates the support of the GTRI staff Wiley Holcombe and Thomas Sean for system transportation and setup. Inputs from Dr. Bruce Webster of the University of Georgia in this thesis are greatly appreciated.

I would like to extend my thankfulness to the following fellow students, Jeffry Joni, Matt Summer, Chris Shumway, Qiang Li and Chao-Chien Lan, who were or are working in the intelligent transfer group.

My love and appreciation for my beautiful wife, Lan Shi, is immeasurable. She was always there to encourage me when I ran into difficulties in my Ph. D. study and research. I owe a debt to my parents and family for the sacrifices they made during my long time education which started in 1978. Also my parents and parents in law have taken good care of our new born baby, Andrew, so that my wife and I can primarily focus on our Ph. D. researches. My father, an engineer in an under-developed small town of south China, learned almost all his advanced knowledge by himself. He always, from the date when I was very young, encouraged me to do my best to the full extreme of my capability.

Without their support, this thesis cannot be finished.

TABLE OF CONTENTS

LIST OF TABLES

LIST OF FIGURES

NOMENCLATURE

Capitalized	**symbols**
A	Cross-sectional area
	Contact point between object and conveyor
$A1$	Contact point on the object
$A2$	Contact point on the surface of conveyor
$[\boldsymbol{B}]$	Geometry matrix of the object
C_b	Object attached coordinate system
C_d	Drum attached coordinate system (space fixed)
C_{d1}	Drum attached coordinate system
C_f	Finger attached coordinate system
$C_{fi,}$ C_{fi1}, C_{fi2}, C_{fi3}	Finger attached coordinate system of the i^{th} finger
Cw	World coordinate system
C_{ij}	Contact force from the j^{th} finger on i^{th} drum
E	Young's Module
EI	Structural rigidity
F	Contact force; force acting on finger
F_n	Normal component of the contact force
F_t	Tangent component of the contact force
$\boldsymbol{G(X)}$	Function vector defined in FDM
I	Moment of area
$\bar{I}$	Effective moment of area
$[\boldsymbol{J}(X)]$	Jacobian matrix
$[\boldsymbol{I}]$	Inertia matrix
$L_1(p,\zeta)$	First Legendre's standard form
$L_2(p,\zeta)$	Second Legendre's standard form
M	Bending Moment
$[\boldsymbol{M}]$	Mass matrix

N	Normal force from conveyor to object
P_w	Position coordinate in C_W
TOL	Tolerance in recursive numerical method
T_y	Torque from fingers acting on bird
V	Velocity
X_0	the ”initial” position of the object
(X_o, Y_o)	Mass center of the object
XYZ	reference coordinate frame
xyz	coordinate frame attached on object
$X_D Y_D Z_D$	coordinate frame attached on Drum
$x_{fi} y_{fi} z_{fi}$	coordinate frame attached on i^{th} finger

Lower case	**symbols**
a	Coefficient of the parabolic function
$[b_1 \quad b_2 \quad b_3 \quad b_4 \quad b_5 \quad b_6]$	Coefficients of the ellipse equation
d	the spacing between the drum pair
f	Contact force
F_x	Friction force between object and the conveyor in x direction
F_y	Friction force between object and the conveyor in y direction
$f_e(x_f, y_f)$	Hidden form of the ellipse equation
$f_o(x, y)$	Ellipse function for the shape of the object in C_b
$f_o(x_f, y_f)$	Ellipse function for the shape of the object in C_f
h	Step size in Finite Difference Method
l	the length of the finger
m	Mass
p	Modulus governing the shape of the finger and its end slope
$\boldsymbol{q}$	Generalized coordinates

r	Radius of ellipse at contact point; Radius of the drum;
r_D	Radius of the drum;
t	Time variable
u	Normalized finger arc length
(x_i, y_i)	Contact point in finger coordinate system

Greek	***symbol***
α	Angular acceleration
	Direction of the contact force on the finger
α_1	Addition of α and ψ
α_r	Inclined angle of the drum
ω	Angular velocity
θ	Angle of nutation
β	Bird orientation with respect to conveyor
	Step size in Flow chart in Figure 4-2
β_a	Adaptive step size
(φ, θ, ϕ)	Euler angle (precession, nutation, spin)
ψ	Slope of finger at arbitrary point
ψ_o	Slope of finger at the contact point
σ	Engineering Stress
ε	Engineering Strain
η	Bird's half width in x direction
σ_η	Variation of η
λ	Bird's half width in y direction
σ_λ	Variation of λ
γ	Bird's half width in z direction

σ_γ	Variation of γ
ρ	the radius on the neutral axis
ϕ_a	the including angle between two neighbor finger columns
ϕ_i	Initial angular position of the i^{th} finger
ϕ_x, ϕ_y	Configuration angle of the grasper finger
$\phi_z(t)$	Angular position of the finger
μ	Friction coefficient

Subscripts and superscript

a	adaptive
b	bird coordinate
D	drum coordinate
f	finger coordinate
e	ellipsoid
i	drum index
j	finger index
w	world coordinate

SUMMARY

This thesis presents the development of a model for analyzing the design of an automated live-bird transfer system (LBTS) developed at Georgia Tech. One of the most fundamental tasks in the automated transferring is to design and control a grasping system that is capable of accommodating a specified range of objects without causing damage. However, unlike grasping in robotic research that focuses on dexterous manipulation of a single object, repetitive transfer of live objects in a production line requires continuous grasping at high-speed.

This thesis research investigates the use of rotating fingers (capable of undergoing large deflections) to cradle live birds on a moving conveyor for subsequent handling. As compared to fingers with multiple active joints, flexible fingers have many merits, for they are lightweight and have no relative individually moving parts. Their ability to accommodate a limited range of varying sizes, shapes, and the natural reactions of some objects makes rubber fingers an attractive candidate for use as graspers in a high-speed production setting. However, the advantages of flexible fingers are seldom exploited for grasping because of the complex analysis involved in the design. In order to reduce the number of birds and hardware/software design configurations to be tested, a good understanding of the object dynamics throughout the grasping process is necessary. In this thesis, a quasi-static model has been developed for predicting the contact force between a moving object and a rotating finger. The model has been validated with the experimentally measured data and the computed results using finite element (FE)

methods. Finally, an illustrative application of the validated model has been demonstrated in the design of a rotating hand used in the automated LBTS. As illustrated in the simulation results, the computed contact forces can be used as a basis for predicting potential bruises on the bird that may be caused by the rotating fingers.

The analytical model presented in this paper provides a rational basis for predicting the contact forces, optimizing the design of the grasping system, and developing a controller for a high-speed transfer system. It is expected that the analysis presented here can be readily extended to other dynamic systems involving the use of flexible beams.

CHAPTER I

INTRODUCTION AND BACKGROUND

1.1 Background and Motivation

Many people may be familiar with the scene in which suddenly a hawk scoops a rabbit from the ground. The whole process lasts only a few seconds, but it remains a challenging problem for a mechanical system to emulate the grasping of a live, moving object. In this thesis, we explore issues related to grasping of live objects, whose locations are approximately known, at high speed. This system has a number of useful applications. In the assembly industry, vibratory feeders are commonly used to separate parts transported on conveyors for picking up by a programmed robot [Lee and Qian, 1998]. Nomura and Naito [2000] presented an integrated visual servoing system that is able to track and grasp industrial parts moving on a conveyer by controlling a 6-DOF robot arm. Kazerooni and Foley [2003] developed novel end-effectors that can be used with robot manipulators or other material handling devices, and it has been used in picking up the sacks to hold letters and small boxes in postal services. In the health-care area, supporting aging and handicapped people by a service robot could also be modeled as an object-handling problem. In manufacturing food products [Lee, 2000], processing

of natural products requires high speed transferring of live objects from conveyors to moving processing lines.

A specific application for this thesis is to automate a task in the poultry industry, which requires grasping a live bird with one or both legs and inserting both legs into a shackle on a kill-line typically running at 180 shackles per minute. One of the fundamental problems in mechanical transferring of live objects is to design and control a grasping system that is capable of accommodating a specified range of objects without causing damage. Grasping research has received considerable attention in the fields of robotics and artificial intelligence. Grasping in robotics generally focuses on exploring, restraining objects, and manipulating objects, aiming at understanding and emulating the two functions of human hands: stable grasping of objects and dexterous manipulation of objects. However, most of these published works have focused on the grasping of a static, rigid body with human-like hand-eye coordination. As compared to ideal rigid engineering objects, live objects are more difficult to deal with due to their size/shape/weight variations and body compliances. Moreover, processing cycle time is often in the order of 1 second, which limits the application of published techniques. For these reasons, an automated grasper using compliant fingers to cradle live poultry at high speed has been developed at Georgia Tech.

In a survey by Lee *et al*. [1996] it was shown that flexible fingers have widely been used to handle birds over the past two decades. Among these are a singulating system developed by Berry *et al*. [1993] to separate the broilers into a single file on a conveyor, and a pickup system proposed by Briggs *et al*. [1994] for picking up birds off

the ground at the farm and moving them into cages for transportation. Most of these studies were designed empirically. More recently, [Lee, 1999] and [Lee *et al.,* 1999] presented the design, modeling and analysis of a novel compliant mechanism for automating the process of broiler transfer. In [Lee, 1999] an analytical model to predict the forces/moments acting on the live broiler is presented, and in [Lee *et al*., 1999] the criteria for designing the automated system with compliant mechanism were experimentally investigated for live broiler singulation. Built upon the experimental work by Hrishikesh [1998], Joni [2000] performed an in-depth finite element analysis to predict the stresses at the contact areas and the effects of structural stiffness (both with the object and the fingers) on the contact area. Summer [2002] analyzed the leg kinematics of the bird to help optimize the gripper design. Shumway [2002] formulated a method for analyzing the inversion dynamics of the bird while it inverts along a predetermined path.

Prior research has proven the concept feasibility of transferring live broilers from conveyors to a shackle line. The results suggested that flexible rotating fingers can be arranged (by appropriately configuring the fingers) to provide a means to temporarily grasp a live broiler by its body for subsequent handling while they are moving on a conveyor. Continuation of this research is worthwhile since flexible fingers can accommodate a limited range of varying sizes/shapes, and can accommodate some motions due to the birds' natural reaction without the use of real-time sensors. This work has potential in applications where handling of natural moving live-objects at high-speed is essential. The advantages of flexible fingers are seldom exploited for grasping, however, because of complicated analysis involved in their design. The need of a detailed

contact analysis with slipping and friction, together with non-linearity due to the large deflection of the soft finger, makes it a challenging problem to deal with. To facilitate design of a dynamic grasper consisting of soft fingers, there is a need for a good understanding of dynamic grasping that is essential for cost-effective design and control of a high-speed compliant grasper- a topic addressed in this thesis research.

1.2 Overview of Research

In Lee [2000] where the operational principles of a live-bird inverting system were presented along with a leg kinematics analysis of the bird, experimental results show that birds tend to react to long, densely spaced rotating fingers. In order to minimize the bird's reaction to rotating fingers and be able to design the locations at which the fingers are in contact with the bird, there is a need to develop an analytical model upon which the design of a compliant grasper can be analyzed, optimized, and evaluated.

To begin with, we consider the CAD model [Lee, 2000] as shown in Figure 1-1. The transfer system consists of a pair of rotating drums, an inclined conveyor and a shackle-inverter. The two drums, filled with flexible fingers and rotating at the same speed but in opposite direction, move the bird toward the shackle inverter while the fingers constrain the motion of its body. The conveyor, as shown in Figure 1-1(b), is inclined downward with respect to the rotating axes of the drums so that the bird can extend its legs freely between the grasper and the conveyor. Because the bird tends to keep its feet in contact with the conveyor, both legs of the bird can be manipulated by

appropriately controlling the drum speed with respect to the conveyor speed. In other words, the system manipulates the velocity of the bird body with respects to its legs so that both legs of the bird can be inserted into a shackle. Manipulation of the bird body has been accomplished by grasping the body of the bird using the flexible fingers housed in the two rotating drums.

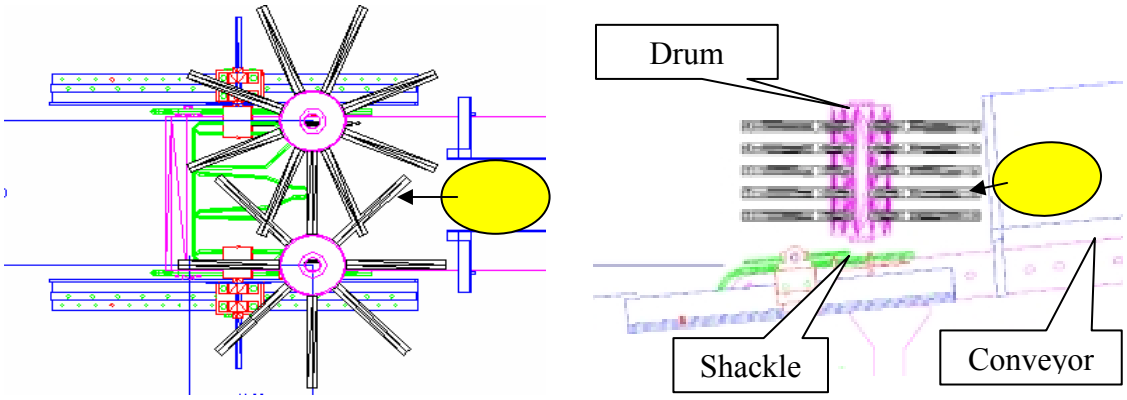

(a) top view (b) side view

Figure 1-1 liver broiler transfer mechanism [Lee, 2000]

Figure 1-2(a) shows a modified design of the grasper or a pair of "rotating mechanical hands", each having *n* appropriately spaced rubber fingers. As shown in Figure 1-2(b), a preliminary investigation suggests an alternative configuration with a relatively small number of fingers can be used to cradle the bird. The advantage is that a deterministic design of fingers not only reduces the anxiety of the incoming bird reacting to noises of the interfering fingers but also avoids bruising the bird body with precise contacts. However, the trade-off is that the rotating grasper and the moving conveyor must be in synchronization, the timing control of which requires an analytical model to characterize the fingers for the design and control of the grasper.

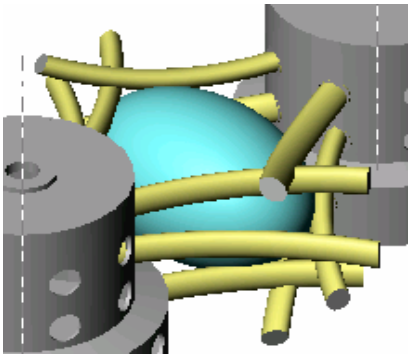

(a) CAD model

(b) Live bird grasping experiment

Figure 1-2 Compliant grasper [Lee, 2001]

The design specifications for synchronizing the motion can be best illustrated using Figure 1-3, where typical contact forces of two fingers are plotted as a function of time. As shown in Figure 1-3, the grasping process can be broadly divided into three steps. The first phase is to engage the bird so that it is guided smoothly into the space formed by a set of fingers that can absorb the impact energy due to their ability to deform. Next, the trapped bird must be supported by the rotating grasper for a short amount of time, during which the maximum contact forces are applied. These forces, however, must not exceed a specified limit, beyond which the bird could be damaged hence downgrading the quality of the meat product. At the same time, these grasping forces should be sufficiently strong to support the weight of the bird, and prevent the object from escaping. While the duration of holding the bird cannot be too long for the bird to react, it must be sustained long enough to allow time for shackling both legs of the bird. Finally, the shackled bird is released from the grasper for subsequent handling.

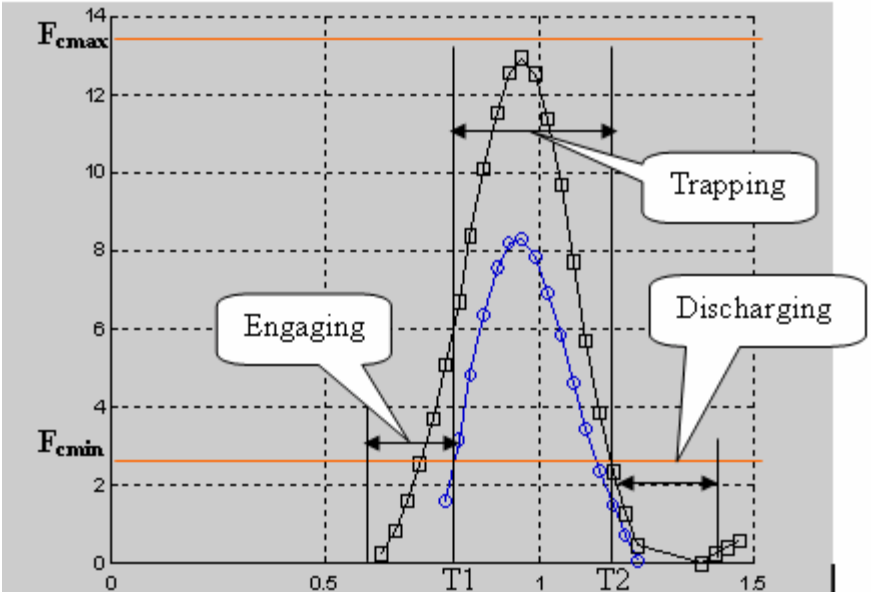

Figure 1-3 Contact force in the grasping

The parameters that could affect the grasping performance can be classified into three categories:

(1) Object parameters describe the weights, sizes and shapes of the birds,

(2) Design parameters that characterize the structure of the grasping system, and

(3) Variables must be specified or controlled for the proper operation of the grasping system.

In this thesis, we model the bird as an ellipsoid characterized by $(\eta,\sigma_\eta;\lambda,\sigma_\lambda;\gamma,\sigma_\gamma)$ where (η, λ, and γ) are the mean radii; and ($\sigma_\eta,\sigma_\lambda$ and σ_γ) are the corresponding standard deviations. The influences of these design parameters and operating variables on the grasping dynamics of the bird are illustrated using Figure 1-4.

Figure 1-4 illustrates the relationship between the arriving bird and the rotating fingers. The design parameter set includes the distance between the drum pair, the drum radius, the angle between two adjacent fingers, and the geometry and properties of the finger. The primary operational variables are the angular velocity of the rotating structure that houses the fingers and the conveyor speed for an initial position (X_0, Y_0) as shown in Figure 1-4, where the bird is moving towards the grasping fingers at a velocity v on the conveyor while the fingers on the drums rotate at an angular velocity ω in the clockwise direction.

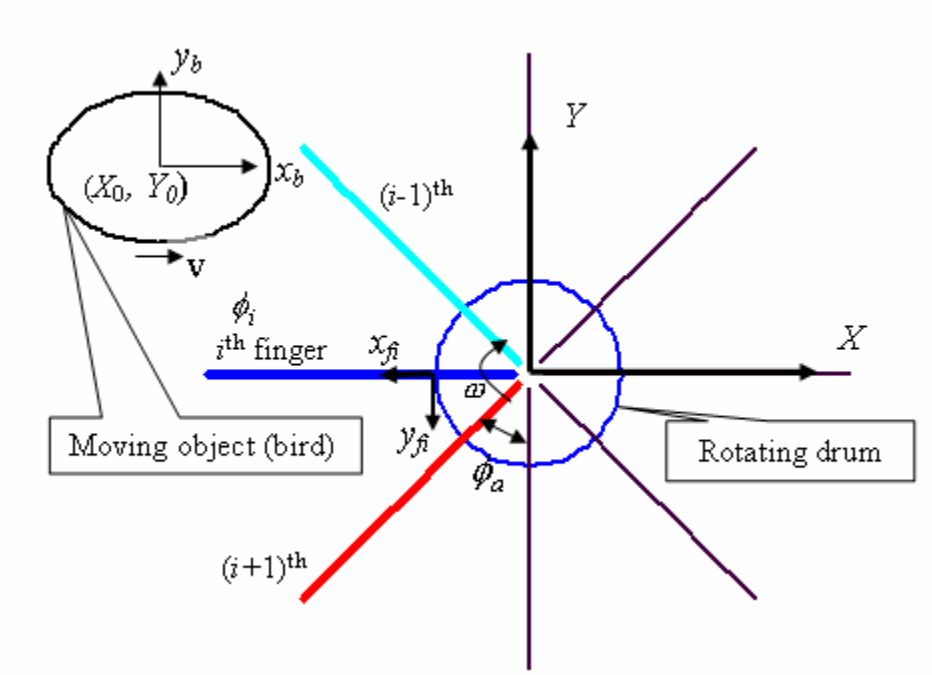

Figure 1-4 Object-finger relationships

The grasping is a non-linear functional of all the parameters and variables presented above. In order to better view the interaction between the grasper and the moving object and the qualitative evaluation of the parameters' effects, typical loci can

be plotted of the un-deflected fingers as viewed in C_b ($x_b y_b$) quasi-statically. It will help visualize the finger/object interaction and the early phase grasper design and parameters evaluation.

The discussion based on un-deflected fingers has identified the parameters and variables involved in the dynamic grasping of a live bird. To determine the optimal set of design parameters, a dynamics analysis that accounts for the large deflection of the rotating fingers is needed. For this reason, this thesis research began with the modeling of a flexible finger followed by developing a method to calculate the contact forces acting on the bird by a rotating finger. On the basis of the finger force model, the dynamics of the birds under the influence of the rotating grasper were then analyzed. It is expected that the ability to simulate the motion of the object being grasped by the soft fingers will provide insights into the control and design of the grasping system.

1.3 Review of Prior Work

As presented in the previous section, this thesis has focused on three basic issues associated with grasping of live objects using flexible fingers. The literature review of prior wok detailed here is broadly divided into three parts: beam theory, contact analysis, and grasping of moving objects.

1.3.1 Beam theory and its applications

The investigation of the deflected beam can date back to the seventeenth century and its theory was closely related to the development of the strength of materials. Daniel

Bernoulli derived the differential equation governing lateral vibrations of prismatic bars and he used it to study particular modes of this motion. Euler used his variational calculus to obtain Jacob Bernoulli's differential equation for elastic curves [Timoshenko, 1953]. Beams are widely used in engineering and scientific research. In this thesis, we focus on cantilever beams. A cantilever is a structural member or an element of a machine that is designed primarily to support forces acting perpendicular to the axis of the member. Generally, the length of a beam is much larger than its cross-sectional dimensions.

Beam theory has also played an important role in the development of flexural joints and compliant mechanisms. Compliant mechanisms are those in which motion and forces are transmitted among various members of the machine through elastic deformation of some or all members, or other non-rigid body effects, in addition to relative rigid body translations and rotations. Applications of compliant mechanisms include micro-motion positioning stages [Lee and Arjunan, 1988]. Another good example is its use in the atomic force microscope (AFM) originally created at Stanford University by Marco Tortonese [1991]. As illustrated in Figure 1-5 [Baselt, 1993], the AFM uses a micro-machined piezo-resistive (100 μm long) cantilever probe to measure sub nano-Newton forces with precise displacements. In a typical configuration, a micro-machined silicon or silicon nitride cantilever with an atomically sharp tip is mounted on a piezoelectric actuator. Forces on the tip that cause deflection of the cantilever can be measured to create an image of the surface. The AFM can achieve a resolution of 10 pico-meters, and unlike electron microscopes, can image samples in air and under liquids. AFM incorporates a number of refinements that enable it to achieve atomic-scale resolution. It requires force feedback, usually with cantilever spring, and laser optical

deflection detection or piezo-resistors. Figure 1-6 shows a schematic illustrating the principle of a piezo-resistive cantilever, where the scan generator moves the sample in the *x* and *y* directions, and the controller adjusts *z* motion to keep atomic force constant such that an image characterizing the contour of the sample surface can be reconstructed. Harley [2000] investigated the optimization of the processing and design of the piezo-resistive cantilevers. Minne *et al.* [1998] increased the throughput of the AFM with parallelism by integrating force sensors onto the cantilever arrays.

(a) Cantilever probe (b) Optical level

Figure 1-5 Concept of AFM and the optical lever [Baselt, 1993**]**

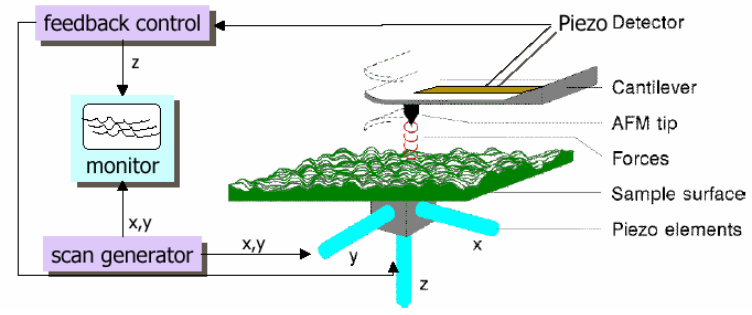

Figure 1-6 Piezo-resistive AFM

Recently, beam theory has been widely used in the Micro-Electro-Mechanical System (MEMS) technology, which has taken advantage of the state-of-art integrated

circuit (IC) fabrication techniques from the semiconductor industry. The cantilever and the double-supported beams are the most common and basic electro-statically-actuated surface micro-machined MEMS. De Los Santos [1997] discussed the cantilever based electrostatic MEM switch. Both the mechanical structure and its design are shown in Figure 1-7. Micro-machined beams have numerous applications. Among these are the arrays of micro-mirrors and micro-lasers proposed by Cheng *et al*. [1997] for replacing conventional laser printing mechanisms to print faster, eliminate synchronization problems, improve image quality, and lower production costs. Each micro-mirror can be a (surface micro-machined piezoelectric) cantilever beam with a reflective surface. Thierry *et al.* [2001] designed, fabricated and tested a micro-machined resonant magnetic field sensor, in which a suspended beam (circulated area) supporting the resonator has been used as shown in Figure 1-8.

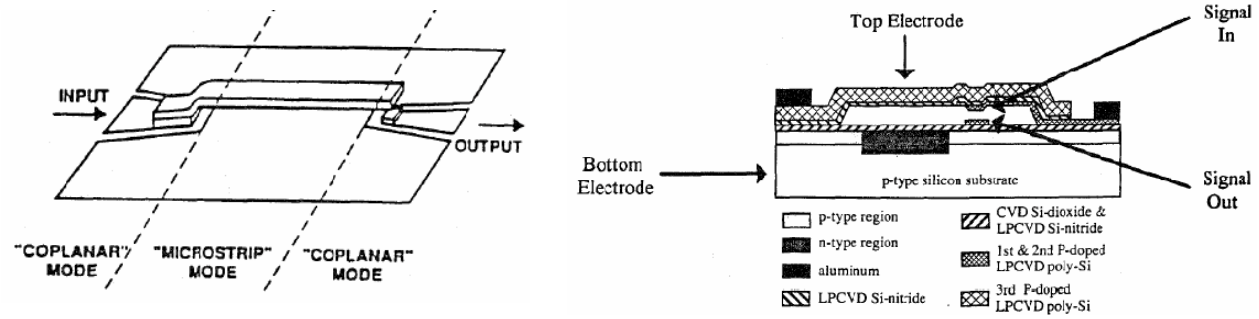

(a) cantilever beam switch (b) doubly-supported cantilever beam switch

Figure 1-7 Transmission line cantilever beam switch [De Los Santos 1997]

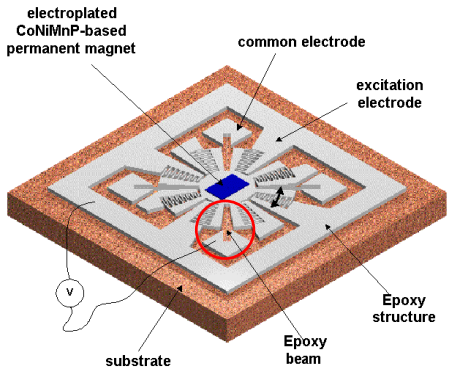

Figure 1-8 Schematic of the rotational comb drive resonator [Thierry, 2001]

More recently, micro-cantilever beams have found their uses in the fast growing field of bio-medical research. Wu *et al*. [2001] developed a cantilevered microscopic chip, no bigger than a hair and coated with antibodies, which can be used to detect prostate specific antigen (PSA) in human blood. As PSA sticks to the antibodies, the cantilevered chip bends like a diving board as shown in Figure 1-9, where the left cantilever bends as the protein PSA binds to the antibody. The other cantilevers, exposed to different proteins found in human blood serum (human plasminogen (HP) and human serum albumin (HSA)), do not bend because these molecules do not bind to the PSA antibody. In Figure 1-9 molecules are represented by ribbons and coils [36]. The cantilevers themselves are about 50 microns wide - half the width of a human hair - 200 microns long (a fifth of a millimeter) and half a micron thick. The micro-cantilever technique has applications beyond prostate cancer. Any disease, from breast cancer to AIDS, with protein or DNA markers in blood or urine could conceivably be assayed by arrays of these micro-cantilevers shown in Figure 1-9. A micro-cantilever array would be one of the first "protein chips" similar to the DNA chip.

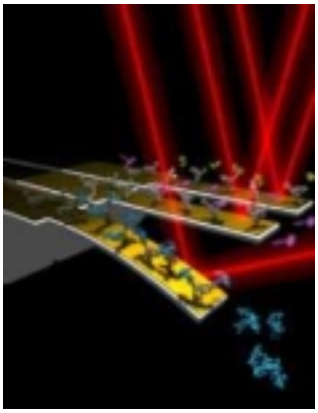

Figure 1-9 Mechanism of cantilevered microscopic chip [36]

Traditionally, designers of mechanical components are accustomed to the assumption of rigid bodies and joints [Vogel, 1995] because of the maturity of the rigid body dynamics analysis. Nevertheless, elastic deformation is seen during design as something that hinders the performance of a machine. However, real life examples demonstrate that compliance can be an advantage in manipulating live objects, to which impact is disallowed. For example, the flexible beam finds an important use in the sport of pole vaulting as shown in Figure 1-10(a), which shows a sequence of movements by a world-class male pole vaulter [Ganslen, 1979]. Linthorne [2000] discussed the flexible pole's advantages in the pole vault by modeling the pole vaulting with flexible pole and predict the optimum take-off technique for a typical world-class pole vaulter. As illustrated in Figure 1-10(b) which shows the vaulter trajectory, the flexible pole acts as an energy transformer that transform the kinetic energy of the vaulter into potential energy in the vaulting process.

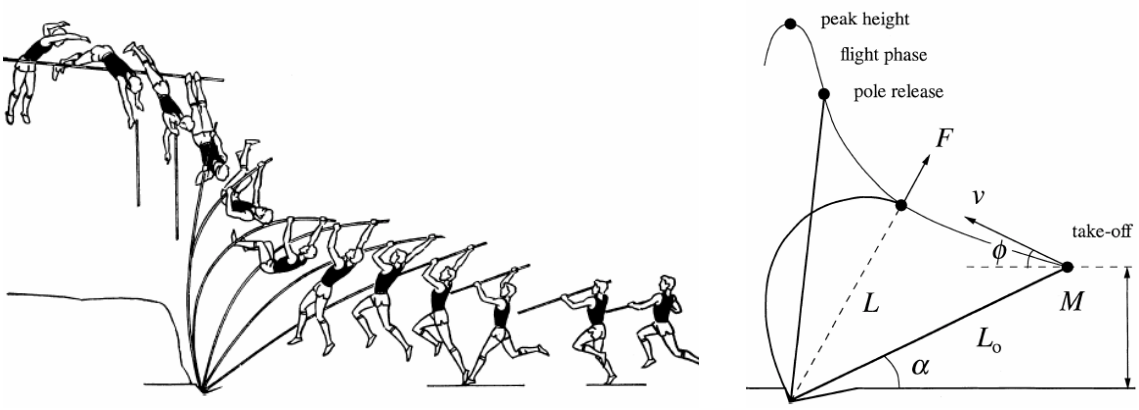

(a) Vaulting (b) Vaulting model

Figure 1-10 Model of the vaulter with a flexible pole [Linthorne 2000]

As mentioned in Section 1.1, flexible fingers have also been widely used in the poultry industry. Primary applications of long flexible fingers (or beams) are for removing feathers from the bird carcass and for singulating birds into a single file to facilitate electronic counting and transportation from farms to the processing plants. Most of these studies were designed empirically because of the complexity of the differential equation describing the large deflection of the flexible finger. The geometrical solution to the second-order, nonlinear differential equation that characterizes large deflections of flexible beams can be found in [Frisch-Fay, 1962], which gives a closed-form solution. The advantage of this solution technique is that it provides closed-form solutions but with cumbersome derivation. Numerical methods, such as the finite element (FE) methods, are capable of solving much more general problems [Yang, 1973]. But the FE method usually involves the huge computations. When the deflection is small, a linearized form that is called the Euler-Bernoulli equation can be used to simplify the analysis. But it is not valid in the case of large-deflection beams. On the basis of beam theory the pseudo-rigid-body model is used to simplify the

analysis and design of compliant mechanism. It is used to unify compliant mechanism and rigid body theory by providing a method of modeling the nonlinear deflection of flexible beams. Burns [1964] and Crossley [1968] approximated flexible couplers as a rigid link with a length five-sixths of the flexible segment. Howell and Midha [1995] analyzed a compliant mechanism with small-length flexural pivots. As shown in Figure 1-11, the model consists of two rigid links, connected by a "characteristic pivot" to represent the displacement, and a torsional spring to model the beam stiffness or resistance to the applied force. The pseudo-rigid-body model is very useful to the analysis of the flexible link or the similar condition where the reaction force always occurs at the same point and for the static cases.

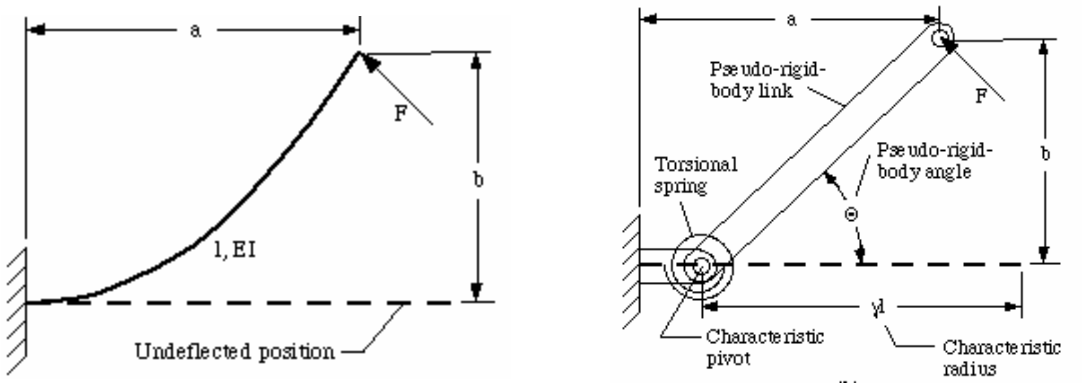

(a) A flexible segment (b) Pseudo-rigid-body model

Figure 1-11 Pseudo-rigid-body modeling [Howell and Midha, 1995]

Another aspect of modeling the flexible beam is from the viewpoint of dynamics; the methods can broadly be divided into three main groups [Javier and Eduardo, 1994]:

a) the simplified methods based on elasto-dynamics,

b) the methods based on defining the deformation with respect to a moving reference frame, and

c) the methods based on defining the overall motion plus deformation with respect to an inertial frame.

The above review has shown that little or no geometrical analyses on beam theory has been treated in the context of compliant grasping of live objects except with the finite element methods, where the nonlinear beam equation combining with the contact theory could be used to solve this problem. But the FE method has difficulties in dealing with the convergence problem encountered in the contact searching process. However, as pointed out in the review by Bicchi and Kumar [2000], there are still difficulties in establishing the uniqueness and existence of solutions of elastic bodies even in the case of static contacts. Most of these studies have been based on the Hertzian contact theory to analyze the contact.

1.3.2 Contact analysis in grasping

The contact analysis in grasping can be categorized into three parts: the geometry of the object and the gripper (grasper or hand), the contact kinematics that includes rolling, sliding, etc., and the dynamics. Based on the contact analysis, quality measures can be developed for optimized grasping. The contact force calculation is the first step to grasping analysis [Liu and Wang, 1998; Sinha and Abel, 1992; Nguyen, 1988; Kerr and Roth, 1986]. It is also investigated widely in many other research fields, such as synthesis of fixture-workpiece system [Wang and Pelinescu, 2003; Wang, 2000; Li and Melkote, 1999; Hurtado and Melkote,1998], physical simulation in graphics [Doug and Pai, 1999& 2003; Baraff, 1994; Gascuel, 1993]. In manufacturing systems, fixture design and

development are purely empirical. The direct application of the fixture-workpiece research is to automatically find the optimal (product quality oriented) layout of the fixture given a workpiece. The contact analysis in the fixture-workpiece systems is featured by large force with a small displacement due to the inherent high stiffness of those systems. In this thesis, the flexible fingers used for the grasping of live object are typically soft (relatively small stiffness) when they come in contact with other objects.

Reuleaux [1876] proposed concepts of form closure and force closure to analyze the functions of bearings in the research field of *mechanism*. He also showed that a minimum of four points contacts (without friction) are needed to completely restrain an object in 2-D space. Based on rigid models, Somoy [1900] in as early as 1897 proved that a minimum of seven points contacts (without friction) are needed to completely restrain an object in 3-D space [Murray, 1997]. Under very general conditions, Marken-scoff *et al*. [1990] showed that four (seven) contacts are sufficient to construct form closure for 2-D (3-D) objects.

Three different modeling approaches are used to calculate the contact force in the literature. The first one, rigid body models, treats the work piece (object) and the fixture (gripper) as perfectly rigid bodies in frictional or frictionless contact. Asada and By [1985] used a frictionless rigid body model to analyze the fixture kinematics. The rigid body model substantially reduces the modeling complexity, which can be used in the early stage design and analysis of grasping and fixture. The major drawback of the rigid body modeling method is that it leads to a statically indeterminate problem, even worse when friction is considered [Demeter, 1998]. The second method analyzes the contact

with finite element model (FEM). It considers the workpiece-fixture (object/grasper) system as an elastic system. Lee and Haynes [1987] were the early users of FEM in the fixture design and analysis. Melkote *et al*. [1995] used this method to analyze the impact of fixturing on workpiece flatness in face milling. FEM is often sensitive to the boundary conditions; it results in large size computer simulation model and it usually requires high computational effort. An intermediate method is to use the contact elasticity models in analyzing the fixture-workpiece system. In [Li and Melkote, 1999] and [Hurtado and Melkote, 1998] a local elastic/plastic contact model is used at each workpiece-fixture contact with assumptions of quasi-static loading conditions. Sinha and Abel [1992] developed a model utilizing a contact stress analysis of an arbitrarily shaped object in a multi-fingered grasp, where both fingers and the object are all treated as elastic bodies, and the region of contact is modeled as a deformable surface patch. This model can predict the normal and frictional contact forces uniquely. However, the experimental validation of the model is lacking.

Akella and Cutkosky [1989] presented a model of a soft fingertip filled with powders or plastic fluids. In this model the contact normal force and torque can be obtained on the basis of a hot metal rolling analogy. Howard and Kumar [1993] derived a minimum potential principle, which can be used in the dynamic analysis of a system with frictional contacts. However, they assumed that at each contact the maximum tangential forces are known a priori, which cannot be available generally in practical system. Moreover, the model neglected the inertial and damping effects when computing the contact.

1.3.3 Grasping of a Moving Object

The grasping of a moving object can be roughly divided into three steps: (1) The end-effector approaches the object with respect to its trajectory. (2) Once the position error between the effector and the object is below a threshold, the hand (or an appropriate multi-fingered gripper) is manipulated to grasp the object. (3) Finally, the object must be stably grasped for subsequent manipulation.

Grasping research has received considerable attention in the fields of robotics and artificial intelligence. Since the late 1970's [Asada, 1978], the early works have been on the design of an appropriate gripper that emulates a human hand. Some other representative grippers (or dexterous hands) widely cited in the robotics grasping [Allen *et al*.,1993] include the four-fingered Utah/MIT Hand [Jacobsen *et al*., 1984] and the three-fingered Stanford/JPL Hand [Salisbury, 1982]. Each of the Utah/MIT fingers has 4-DOF actuated independently using 32 pneumatic actuators and antagonistic tendons. The computing architecture employs an analog controller for tendon management and a VME/VxWorks distributed controller. Controlled by a VME-based open torque control system, the finger of the Stanford/JPL hand (developed by Ken Salisbury in the early 80's) has 3-DOF driven by (n+1) tendons. These fingers are equipped with tension sensors, motor position encoders, and fingertip tactile sensors. The fingertip has a minimum force sensing capacity of 0.01 lbf. These complex multi-sensor and multi-actuator based humanoid graspers are not suitable in the industry application, which usually requires high speed and low cost. In addition, the control and synchronization of multi-fingers are also very complex to be implemented.

Mason and Salisbury [1985] proposed a framework for testing the stability of a grasp on the basis of the grasping Jacobian matrix and internal force. Kerr and Roth [1986] developed a method to determine the squeeze force to ensure the stable grasping of the object. Montana [1988] derived a group of differential equations describing the motion of the point contact between two 3-D rigid objects in the context of lie group theory. Nguyen [1988] investigated how to construct a force closure grasps. Howard *et al.* [1996] developed an optimization method to specify the contact forces given known contact locations and task requirements. Xiong *et al*. [1999] discussed the dynamic stability of the grasp with respect to external disturbance. Other robot grasping research can be found in two recent survey papers. Bicchi and Kumar [2000] conducted a survey in the field of robotic grasping and summarized the works done over the last two decades. Similar overview of the research in the dexterous manipulation can be found in Okamura *et al*. [2000].

Most of the publications that deal with tracking a moving object for grasping have been formulated within the framework of interception originated in the missiles tracking free-flying targets and radar technologies. Some of these examples are [Hunt and Sanderson, 1982; Houshangi, 1990; Koivo, 1991; Allen *et al.*, 1993; Buttazzo *et al*., 1994, Zhang *et al*., 1994; Smith and Papanikolopoulos, 1995; Mehrandezh *et al*., 2000, Hashimoto *et al*., 2001]. Tracking of a moving object for grasping requires the integration of sensing, motion prediction, planning, and sensor-based control system for real-time implementation. Early research focuses have been on the development of non-contact proximity sensors such as vision or other range finding techniques and their uses in tracking. Among these, the vision-based-tracking has been the most popular approach for

grasping, and were used in three primary configurations; eye-in-hand, overhead and static cameras. The earliest robot tracking system with visual servoing dates back to Hill and Park [1978], which used the proportional control method. Their approach was mostly empirical. Hunt and Sanderson [1982] presented a vision based robotic system in which target trajectory predictions enable the robot to track and intercept a moving object. They tested five different predictive algorithms (including the kalman filtering theory) with a 256x256 gray-level image-acquisition system (that has an image-processing-time of 232ms and a control sampling time around 1 second). Allen *et al*. [1993] developed the basis of the stereo optic flow field for grasping of a toy train. Buttazzo *et al.* [1994] presented a control methodology for catching a fast moving object with a robot manipulator. More recently, Mehrandezh *et al*. [2000] presented an online robot-motion planning for the interception of a moving object, which has been developed based on a navigation-based technique commonly utilized in the control of missiles tracking of free-flying targets. Kaneko *et al*. [2002] introduced the concept of dynamic friction closure, which can be used in designing a 2-plate gripper for catching a high-speed moving object. Hashimoto *et al.* [2001] presented a high speed grasping system on the basis of a visuomotor control architecture. The cycle time of its visual feed back (position control of the gripper) is about 1ms, which system has a hierarchical parallel architecture consisting of 7 digital signal processors connected to each other.

Although the vision-based grasping system has the flexibility to deal with dynamically changed, unknown or unexpected events, it has some disadvantages. (1) The problem of extracting motion information from a vision system is often ill-posed, which could occasionally cause the system to fail considering the limited robot task space and

the possible out of focus of the camera. (2) The inherent delay due to the intensive computation associated with the motion prediction algorithm [Houshangi, 1990; Allen *et al*., 1993; Croft *et al*., 1998], particularly when it is incorporated in a real time control system. This increases the complexity of the system. Moreover, the needs for a high-DOF robot in addition to a dexterous hand [Allen *et al*., 1993] often make it rather expensive and too slow to be used in a production line. Moreover, most of the systems presented in the literature have been dealing with rigid moving objects. In this thesis project that requires high-speed grasping of live, moving objects on a production line, we seek an alternative approach where vision is used only in the detection and classification problems.

In the above literature review in the vision based grasping system, it appears that there has been no manufacturing and processing systems dealing with grasping of live objects at high speed on the order of one second cycle-time. This thesis focuses on developing a detailed model for design, analysis and control of a compliant grasping mechanism for automating the process of transferring broilers from a conveyor to a shackle line. Unlike most of the published works that have focused on the deflection of a uniform beam under a point load applied at a known location, this thesis considers the effects of the large deflection and the beam geometry (including beams with non-uniform cross-section) on the grasping performance, where the locations of contact forces are not known a priori.

1.4 Scope of Research

The grasper to be designed is essentially a pair of drums filled with flexible fingers as already shown conceptually in Figure 1-2. The two drums, rotating at the same speed but in opposite directions, grab and hold the body of the bird while the moving conveyor drives both legs of the bird into the shackle inverter. The particular interest of this thesis is to study the motion of the bird, as it enters the rotating grasper. In other words, the model described in this thesis begins at the entry point of the rotating drum pair and ends before the bird body is released from the compliant grasper. Consequently, the grasping of the bird is essential to the success of the live broiler transfer. The following assumptions have been assumed throughout this thesis:

(1) It is assumed in this thesis that the birds have been singulated before their entering the housing space of the compliant grasper.

(2) To make the model and analysis tractable, we will be more concerned in the body of the bird to be grasped. The ellipsoid (ellipse), the model for the body of the object or bird, will be used throughout the thesis for discussion and analysis.

(3) The effects from the legs and the neck part of the bird will not be considered in the model of this thesis.

The overall goal of this thesis research is to develop a theoretical framework for modeling, analysis and simulation of a live bird grasping system. Although the focus of the work is on live bird grasping, many of the analytical models and tools developed in

this research will be applicable to other similar grasping and processing problems. The goal above will be achieved through the following specific tasks.

The research will first develop an analytical model to determine the shape of a flexible beam undergoing large deflection. Both uniform and non-uniform beams are considered in this thesis. Two numerical methods, shooting and finite difference method (FDM), have been developed for the shape calculation of the non-uniform beam in large deflection. In order to test and compare against a closed-form solution based on Frisch-Fay flexible bar theory, which is deflection calculation of a uniform beam under point force, the shooting method and FDM can be also used to calculate the deflection of the uniform beam. To take advantage of the closed-form solution of Frisch-Fay theory, the concept of effective *EI*, characterizing the ability of the beam to resist deformation, will be introduced for approximating the deflection of the non-uniform beam by a uniform beam.

The second task is to develop a model for solving the contact kinematics and the corresponding reaction force between a flexible, rotating finger and a moving object. Two algorithms, the uniform approximation with effective EI and the FDM, to solve the non-uniform contact equations will be discussed and simulated. The Algorithm I, built upon the Frisch-Fay flexible bar theory for the uniform beam, provides an approximate closed–form solution for determining the contact points and forces. Because of its good stability for solving the contact problem, the uniform beam contact analysis together with the effective *EI* will be used in the third task of this thesis, the dynamic analysis of a compliant grasper. The contact model will be verified by experiments and FEM. The

comparison results will show that the contact model developed is valid and can be used in the dynamic analysis when the drum rotates at a low angular velocity of around 20rpm.

The third task, on the basis of the uniform beam contact analysis, is to develop a dynamic model for the live bird transfer system. First a design algorithm, upon which a near optimal set of design and operating parameters will be suggested for a grasper used in the LBTS. On the basis of the contact model and the grasper, dynamics analysis and simulation of the grasping process are presented. A football will be used in the analysis since it has been a well-defined shape similar to that of a live bird, yet it allows for an experimental test in a controlled environment. Then an existing testing prototype system will be used to verify the dynamic model using the football. Finally the dynamics model can be used to evaluate the performance of the grasper using characteristic data of live birds.

It is expected that this thesis research will contribute to the design process of a high-speed dynamic grasper for handling live moving objects. While the motion simulation cannot fully predict the birds' natural reflexes to the mechanical processes, it can effectively be used to study the effects of the transfer system design parameters: the bird sizes, the hardness of the finger used in the grasper design, etc. It will also reduce the number of hardware prototype configurations that need to be built, and the number of live birds to be evaluated. During a system development and engineering design process, modeling of the system will help improve the system design and find the right direction. A few iterations of design-modification-test procedure are required to get to the finalized

design. The grasping dynamics modeling and its simulation developed in this research will be a necessary tool.

This thesis research will contribute in the following:

- Solutions to the equations that characterize the large deflection of a flexible beam (with non-uniform cross-section) under a point force have been derived.
- Develop a quasi-static model for predicting the contact force between a moving object and a rotating finger.
- Develop a dynamic grasping model and numerically simulate the grasper performance using statistical data of live birds.

1.5 Thesis Outline

The remainder of this thesis is organized as follows: Chapter II starts with the very basic constructing element of the grasper, flexible beam. It discusses the large deflection of both the uniform and non-uniform beams. An ordinary differential equation (ODE) with boundary value conditions is presented to describe the large deflection of the beam. Methods to solve this nonlinear ODE, the shooting and FDM, are discussed and compared.

Chapter III focuses on the finger/bird contact force analysis, which is the core content of the thesis. It provides the basis for the system dynamic analysis. The analytical method to obtain the contact force in 2-D is implemented in the simulation using

MatLAB. The results will be compared to those obtained from experiments and FE Analysis.

Chapter IV presents the dynamic analysis of the grasping of the live bird. A set of Differential Algebraic Equations (DAE) will be derived to describe the motion dynamics of the object being grasped. Numerical solution to solve the DAEs will be given. A 3-D simulation program is developed in MatLAB to evaluate the system parameters.

Chapter V begins with the design considerations of a grasper used in the live object transfer with 2-D kinematic simulation program. Then the results of a detailed study on the effects of the finger stiffness (on the bird motion, the contact forces, and the duration within which the rotating fingers are able to support the bird) are presented. The experimental results will be obtained using a specific grasper with an ellipsoid (football) on an existing prototype developed at Georgia Tech. The results are then compared with the motion predictions of the football. The simulation results are supposed to further improve the prototype experimental system.

Finally, the conclusions and recommendations of the thesis are presented in Chapter VI. Several aspects of potential future work are addressed to increase the applicability of the analysis and modeling discussed in this thesis, and to improve and optimize the transfer system.

CHAPTER II

FLEXIBLE BEAM ANALYSIS

With the application of poultry processing in mind, it is important to analyze the grasping forces applied by the flexible finger on the bird because excessive forces can bruise its body and thus, downgrade the meat quality. Moreover, a good prediction of the contact force and the grasping dynamics will help improve the design and control of the grasper. This chapter begins with deriving the equations to characterize the deflection of the flexible beam under a point force, where following assumptions are used:

(1) The finger is modeled as a flexible beam with one end clamped.

(2) The dimensions of the cross-section are assumed to be small as compared to the length of the beam. The moment of area $I(x)$ of the cross-section is a continuous function along the x direction.

(3) The analysis of the beam deflection assumes that the beam is stationary.

Then numerical methods are investigated for the deflection calculation, and the simulation results will be shown.

2.1 Uniform Flexible Beam Theory

The shape of a deflected beam about its neutral axis, which can be derived on the basis of the Bernoulli-Euler law, is given by Equation (2.1):

$$\frac{1}{\rho} = -\frac{M}{EI} \tag{2.1}$$

where M (in Nm) is the moment acting on the beam;

E (in GPa) is the Young's module of the beam material;

ρ (in m) is the radius of curvature at the point of interest;

I (in m^4) is the 2nd order moment of area of the beam; and

the negative sign defines that downward deflections are positive.

We model the finger as a flexible beam with one end clamped. In other words, the dimensions in the *y*- and *z*-directions are assumed to be small as compared to that in the *x*-direction as shown in Figure 2-1, where *x* is the coordinate along the neutral axis of the beam before it is deflected; *y* is the transverse deflection; α defines the direction of the force $\boldsymbol{F}$ acting on the finger; and ψ_o is the slope of the finger at the contact point. In Figure 2-1, $C(x_c, y_c)$ denotes the point at which the force is acting; Q(*x*, *y*) denotes an arbitrary point on the deflected finger; and the corresponding arc lengths from the base of the finger to Q(*x*, *y*) and $C(x_c, y_c)$ are represented by *s* and *L* respectively.

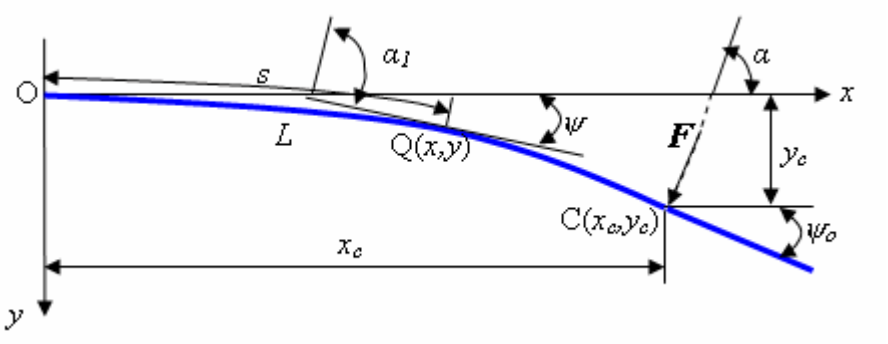

Figure 2-1 Model of a bent flexible finger

The equation governing the beam deflection can be derived by substituting the curvature at any point Q(*x, y)* into Equation (2.1). In rectangular coordinates, the result is

$$M = EI(s)\frac{d\psi}{ds} = -EI(s)\frac{\dfrac{d^2y}{dx^2}}{\left[1+\left(\dfrac{dy}{dx}\right)^2\right]^{\frac{3}{2}}} \tag{2.2}$$

where $\dfrac{d\psi}{ds}$ is the rate of change of angular deflection along the length of the beam, or the curvature at the point considered. Equation (2.2) shows that the shape of the deflected finger for a given design (material and geometry) depends on the moment *M*. From Figure 2-1, the bending moment *M* at the point Q(*x*, *y*) can be shown to be

$$M = EI(s)\frac{d\psi}{ds} = F\sin\alpha(x_c - x) + F\cos\alpha(y_c - y) \tag{2.3}$$

Small deflection

For small deflection such that the square of the slope, or $\left[\dfrac{dy}{dx}\right]^2$ in Equation (2.2), is small as compared to unity, the curvature can be approximated by the second

derivative of *y,* i.e. $\frac{d^2y}{dx^2}$. The small deflection assumption also implies that the second term in the moment Equation (2.3) is negligible, which leads to the classical, linear beam moment-curvature equation:

$$F\sin\alpha(L-x_f) = EI(x)\frac{d^2y}{dx^2}. \tag{2.4}$$

where $y(0)=0$ and $y'(0)=0$

For a uniform beam, the solution is given by

$$y = \frac{FL^3\sin\alpha}{2EI}\cdot\left(\frac{x}{L}\right)^2\left(1-\frac{1}{3}\cdot\frac{x}{L}\right) \tag{2.5}$$

Equation (2.5) becomes invalid when the slope of the transverse deflection is no longer small. For large deflection applications such as rubber fingers considered in this thesis, the small-deflection beam theory is inadequate and the principle of superposition is not applicable.

Large deflection

To obtain a general equation that governs the beam deflection, we differentiate Equation (2.3) with respect to *s*:

$$E\frac{dI(s)}{ds}\frac{d\psi}{ds} + EI(s)\frac{d^2\psi}{ds^2} = -F\sin\alpha\cos\psi - F\cos\alpha\sin\psi \tag{2.6}$$

When the beam has a uniform cross-section and is acted upon by a known load (F, α), Equation (2.6) reduces to a form of Newton's equation:

$$\frac{d^2\alpha_1}{du^2} + (kL)^2 \sin\alpha_1 = 0 \tag{2.7}$$

where $$u = s/L \tag{2.7a}$$

$$\alpha_1 = \psi + \alpha \tag{2.7b}$$

and $$k = \sqrt{\frac{F}{EI}} \tag{2.7c}$$

In Equation (2.7), $u \in [0,1]$ and $\alpha_1 \in [\alpha, \alpha + \psi_0]$. The corresponding boundary conditions are

$$(\alpha_1)_{u=0} = \alpha \tag{2.8a}$$

$$\left(\frac{d\alpha_1}{du}\right)_{\alpha_1 = \psi_0 + \alpha} = 0 \tag{2.8b}$$

The differential Equation (2.7) along with the boundary conditions given by Equations (2.8a) and (2.8b) have been solved by Frisch and Fay [1962] for the deflected shape of a flexible beam subjected to a point load at a known location. The Frisch-Fay solution describing the shape of the beam is given below.

$$x = \frac{1}{k}\left[2p\sin\alpha(\cos\varsigma - \cos\xi) - h(\psi_o)\cos\alpha\right] \tag{2.9a}$$

$$y = \frac{1}{k}\left[2p\cos\alpha(\cos\varsigma - \cos\xi) + h(\psi_o)\sin\alpha\right] \tag{2.9b}$$

where $$h(\psi) = \left[L_1(p,\xi) - L_1(p,\zeta) - 2L_2(p,\xi) + 2L_2(p,\zeta)\right]; \tag{2.10a}$$

$$p = \sin[(\psi_o + \alpha)/2]; \tag{2.10b}$$

$$\varsigma = \sin^{-1}\left[\frac{\sin(\alpha/2)}{p}\right]; \tag{2.10c}$$

$$\xi = \sin^{-1}\left[\frac{\sin[(\psi+\alpha)/2]}{p}\right]; \tag{2.10d}$$

k is defined in Equation (2.7c); and $F(p,\varsigma)$ and $E(p,\varsigma)$ are Legendre's standard form of the first and second kinds respectively:

$$L_1(p,\zeta) = \int_0^{\zeta} \frac{d\zeta}{\sqrt{1-p^2\sin^2\zeta}} \tag{2.11a}$$

$$L_2(p,\zeta) = \int_0^{\zeta} \sqrt{1-p^2\sin^2\zeta}\, d\zeta\,. \tag{2.11b}$$

The modulus p, which governs the deflected shape of the finger, is related to the property of the finger by

$$kL = \left[L_1(p,\pi/2) - L_1(p,\varsigma)\right] \tag{2.12}$$

The deflected shape of the finger under a known point force (F, α) can be computed as follows:

(1) For a given flexural rigidity and a given force, calculate k from Equation (2.7c).

(2) Solve for the module p from Equation (2.12) implicitly. This involves constructing a function of p, $g(p) = \left[L_1(p,\pi/2) - L_1(p,\varsigma)\right] - kL$. Note that from the definition of p given in Equation (2.10b), $0 < p < 1$. The

equation $g(p) = 0$ is solved numerically, for example using the Bisection Method.

(3) Calculate ψ_0 from Equation (2.10b).

(4) Calculate ζ and $\xi_0 = \xi\big|_{\psi=\psi_0}$ from Equations (2.10c) and (2.10d) respectively.

(5) Calculate the deflected shape of the finger in terms of (x and y) from Equation (2.9a) and (2.9b) respectively.

2.2 Non-uniform beam

In this section, we consider a flexible beam with a non-uniform cross-section. Recall the equation governing the shape of a deflected beam given by

$$M = EI(s)\frac{d\psi}{ds} = F\sin\alpha(x_c - x) + F\cos\alpha(y_c - y) \tag{2.3}$$

and the notations introduced in Equations (2.7a) and (2.7b):

$$u = s/L \tag{2.7a}$$

$$\alpha_1 = \psi + \alpha \tag{2.7b}$$

Substituting the following derivatives

$$\frac{d\psi}{ds} = \frac{1}{L}\frac{d\alpha_1}{du} \tag{2.13a}$$

and
$$\frac{d^2\psi}{ds^2} = \frac{1}{L^2}\frac{d^2\alpha_1}{du^2} \tag{2.13b}$$

into Equation (2.3), a general non-linear second order differential equation that governs the shape of a deflected beam is obtained as follows:

$$I(s)\frac{1}{L^2}\frac{d^2\alpha_1}{du^2} + \frac{dI(s)}{ds}\frac{1}{L}\frac{d\alpha_1}{du} + \frac{F}{E}\sin\alpha_1 = 0 \tag{2.14}$$

The corresponding boundary conditions are given by Equations (2.8a) and (2.8b).

Since a closed-form solution for the above second-order nonlinear differential equations is not available, Equation (2.14) is solved numerically. For this purpose, we rewrite Equation (2.14) and its boundary conditions in a standard form:

$$\begin{cases} \alpha_1'' = f(u, \alpha_1, \alpha_1'), \quad 0 \le u \le 1 \\ \alpha_1(0) = \alpha, \\ \alpha_1'(1) = 0 \end{cases} \tag{2.15}$$

where

$$f(u, \alpha_1, \alpha_1') = -L\frac{I'(uL)}{I(uL)}\alpha_1' - \frac{FL^2}{EI(uL)}\sin\alpha_1 .$$

Once the solution of Equation (2.15) is obtained, the finger shape (in the rectangular coordinates) can be computed from the following pair of equations:

$$x(u_0) = L\int_0^{u_0}\cos\psi du \tag{2.16a}$$

$$y(u_0) = L\int_0^{u_0}\sin\psi du \tag{2.16b}$$

where u_0 is any value between 0 and 1.

Note that Equation (2.15) has a standard form of boundary value problems (BVP), two different numerical methods to obtain the solution to Equation (2.15) are discussed in the following subsections; namely, the shooting method and the finite difference method.

2.2.1 Shooting method

The basic idea of the shooting method [Burden, 1997] to solve the standard Boundary Value Problem (BVP), Equation (2.15), is to first construct an initial value problem for the ODE:

$$\begin{cases} \alpha_{10}'' = f(u, \alpha_{10}, \alpha_{10}') \\ \alpha_{10}(0) = \alpha, \alpha_{10}'(0) = \varepsilon \end{cases} \tag{2.17}$$

where ε is a guessed slope at one end of the boundary. The initial value problem is then solved. The guessed value ε can be adjusted by using the difference between $\alpha_1'(1)$ and the $\alpha_{10}'(1)$ computed from Equation (2.17):

$$m(\varepsilon) = \alpha_{10}'(1, \varepsilon) - \alpha_1'(1) \tag{2.18}$$

The recursive algorithm is to find the correct value ε with $m(\varepsilon)=0$ as follows:

Step 1: use $\alpha_{10}(0) = \alpha, \alpha_{10}'(0) = \varepsilon(1)$ to calculate the error $m(1)$;

Step 2: use $\alpha_{10}(0) = \alpha, \alpha_{10}'(0) = \varepsilon(2)$ to calculate the error $m(2)$;

Step 3: use the secant method to obtain a new estimate

$$\varepsilon(i) = \varepsilon(i-1) - \frac{\varepsilon(i-1) - \varepsilon(i-2)}{m(i-1) - m(i-2)} m(i-1), \text{ i=3, 4, …;}$$

Step 4: iterate until $|\varepsilon(i)-\varepsilon(i-1)| \le tol$, where *tol* is a small positive value governing the accuracy of the numerical calculation.

The shooting methods can be used for both linear and nonlinear boundary-value problems.

2.2.2 Finite Difference Method

The essence of the finite difference method for solving an ODE is to transform a calculus problem into an algebra problem. For clarity, it can be decomposed in two parts; namely, finite difference formulation of Equation (2.15) and Newton's method of solving the nonlinear difference equations.

2.2.2.1 Formulation of the finite difference beam equations

The formulation includes the domain discretization, finite difference approximation, boundary conditions and the algebraic finite difference equations, which can be solved by the Newton's method.

Domain discretization

The continuous solution domain [0, 1] is discretized into (*N+1*) equal subintervals with endpoints at $u_i = ih$ for i=0, 1, …, and $N+1$, each of which has a width $h = 1/(N+1)$.

Finite difference approximation

The exact derivatives in Equation (2.15) are then approximated by appropriate central finite difference formula given by Equations (2.19) and (2.20). This assumes that the exact solution has a bounded fourth derivative to allow for replacing $\alpha_1''(x_i)$ and $\alpha_1'(x_i)$.

$$\alpha_1''(u_i) = \frac{1}{h^2}[\alpha_1(u_{i+1}) - 2\alpha_1(u_i) + \alpha_1(u_{i-1})] - \frac{h^2}{12}\alpha_1^{(4)}(\xi_i) \tag{2.19}$$

$$\alpha_1'(x_i) = \frac{1}{2h}[\alpha_1(u_{i+1}) - \alpha_1(u_{i-1})] - \frac{h^2}{6}\alpha_1^{(3)}(\eta_i) \tag{2.20}$$

The substitution of Equations (2.19) and (2.20) into Equation (2.15) leads to a set of finite difference equations:

$$\frac{\alpha_1(u_{i+1}) - 2\alpha_1(u_i) + \alpha_1(u_{i-1})}{h^2} = f\left(u_i, \alpha_1(u_i), \frac{\alpha_1(u_{i+1}) - \alpha_1(u_{i-1})}{2h} - \frac{h^2}{6}\alpha_1^{(3)}(\eta_i)\right) + \frac{h^2}{12}\alpha_1^{(4)}(\xi_i) \tag{2.21}$$

for some ξ_i and η_i in the interval (u_{i-1}, u_{i+1}), where i=1, 2, …, N.

Boundary Conditions

For simplicity, we define

$$w_i = \alpha_1(u_i) \tag{2.22}$$

From Equation (2.15) directly we have

$$w_0 = \alpha \tag{2.23}$$

for the boundary condition at u=0.

In Equation (2.15) the boundary condition at u=1 is a 1st order derivative, $\alpha_1'(1) = 0$. An approximation formula of w_{N+1} can be expressed as the following equation from a truncated Taylor series expansion at point u=1.

$$w_{N+1} = \frac{1}{3}(4w_N - w_{N-1} + 2hw'_{N+1}) \tag{2.24}$$

where

$$w_N = w_{N+1} - hw'_{N+1} + \frac{h^2}{2}w''_{N+1} \tag{2.25a}$$

$$w_{N-1} = w_{N+1} - (2h)w'_{N+1} + \frac{(2h)^2}{2}w''_{N+1} \tag{2.25b}$$

Substituting the boundary condition $w'_{N+1} = 0$ into Equation (2.24) leads to

$$w_{N+1} = \frac{1}{3}(4w_N - w_{N-1}) \tag{2.26}$$

Finite Difference Equation (FDE)

The difference approximations represented in Equation (2.21) are substituted into the Equation (2.15) to obtain an algebraic finite difference equation, and the following $N \times N$ nonlinear system is obtained:

$$G(W) = \begin{bmatrix} G_1(W) \\ G_2(W) \\ \vdots \\ G_{N-1}(W) \\ G_N(W) \end{bmatrix} = 0, \tag{2.27}$$

$$G_1(W) = 2w_1 - w_2 + h^2 f\left(u_1, w_1, \frac{w_2 - w_0}{2h}\right) - w_0$$

$$G_2(W) = -w_1 + 2w_2 - w_3 + h^2 f\left(u_2, w_2, \frac{w_3 - w_1}{2h}\right)$$

where $\vdots$

$$G_{N-1}(W) = -w_{N-2} + 2w_{N-1} - w_N + h^2 f\left(u_{N-1}, w_{N-1}, \frac{w_N - w_{N-2}}{2h}\right)$$

$$G_N(W) = -w_{N-1} + 2w_N + h^2 f\left(u_1, w_1, \frac{w_{N+1} - w_{N-1}}{2h}\right) - w_{N+1}$$

and $W = [w_1 \quad w_2 \quad \cdots \quad w_{N-1} \quad w_N]$.

Equation (2.27) can be directly used to solve for the solution by replacing w_0 and w_{N+1} with appropriate boundary conditions given in Equations (2.23) and (2.26). It leads to Equation (2.28):

$$G(W) = \begin{cases} 2w_1 - w_2 + h^2 f\left(u_1, w_1, \frac{w_2 - w_0}{2h}\right) - \alpha \\ -w_1 + 2w_2 - w_3 + h^2 f\left(u_2, w_2, \frac{w_3 - w_1}{2h}\right) \\ \vdots \\ -w_{N-2} + 2w_{N-1} - w_N + h^2 f\left(u_{N-1}, w_{N-1}, \frac{w_N - w_{N-2}}{2h}\right) \\ -\frac{2}{3} w_{N-1} + \frac{2}{3} w_N + h^2 f\left(x_N, w_N, \frac{2}{3h}(w_N - w_{N-1})\right) \end{cases} = 0 \qquad (2.28)$$

2.2.2.2 Newton's method to solve the finite difference beam equations

Newton's method is used to generate a sequence of iterations $\left\{(w_1^{(k)}, w_2^{(k)}, ..., w_N^{(k)})^t\right\}$ that converge to the solution of Equation (2.28). The convergence is possible provided that

(1) the initial approximation $\left\{(w_1^{(0)}, w_2^{(0)}, ..., w_N^{(0)})^t\right\}$ is sufficiently close to the solution $\left\{(w_1, w_2, ..., w_N)^t\right\}$, and that

(2) the Jacobian matrix for the system is nonsingular.

The Jacobian matrix $J(w_1, w_2, ..., w_N)$, which is defined as

$$J(w_1, w_2, ..., w_N) = \begin{bmatrix} \frac{\partial G_1}{\partial w_1} & \frac{\partial G_1}{\partial w_2} & 0 & \cdots & 0 & 0 \\ \frac{\partial G_2}{\partial w_1} & \ddots & \ddots & & & \vdots \\ 0 & \ddots & & \frac{\partial G_i}{\partial w_j} & & 0 \\ \vdots & & 0 & & \ddots & \frac{\partial G_{N-1}}{\partial w_N} \\ 0 & \cdots & 0 & 0 & \frac{\partial G_N}{\partial w_{N-1}} & \frac{\partial G_N}{\partial w_N} \end{bmatrix}_{N \times N}; \qquad (2.29)$$

is tri-diagonal with the *ij*-th entry for the first (N-1) rows

$$J(w_1, w_2, ..., w_N)_{i,j} = \begin{cases} -1 + \frac{h}{2} f_{y'}\left(u_i, w_i, \frac{w_{i+1} - w_{i-1}}{2h}\right), & i = j-1 \text{ and } j = 2, ..., N, \\ 2 + h^2 f_y\left(u_i, w_i, \frac{w_{i+1} - w_{i-1}}{2h}\right), & i = j \text{ and } j = 1, ..., N-1, \\ -1 - \frac{h}{2} f_{y'}\left(u_i, w_i, \frac{w_{i+1} - w_{i-1}}{2h}\right), & i = j+1 \text{ and } j = 1, ..., N-2, \end{cases}$$

(2.30a)

and for the N^{th} row

$$J(w_1, w_2, ..., w_N)_{N,N-1} = -\frac{2}{3} - \frac{2}{3} h f_{y'}\left(u_N, w_N, \frac{2}{3h}(w_N - w_{N-1})\right) \qquad (2.30b)$$

$$J(w_1, w_2, ..., w_N)_{N,N} = \frac{2}{3} + h^2 f_y\left(u_N, w_N, \frac{2}{3h}(w_N - w_{N-1})\right) + \frac{2}{3} h f_{y'}\left(u_N, w_N, \frac{2}{3h}(w_N - w_{N-1})\right)$$

(2.30c)

At each of the iterations, the Newton's method solves for $v_1, v_2, ..., v_{N,}$ from the $N \times N$ linear system

$$J(w_1, ..., w_N)(v_1, ..., v_N)^T = -G(W) \tag{2.31}$$

the approximation is then updated with

$$w_i^{(k)} = w_i^{k-1} + v_i \tag{2.32}$$

Since *J* is tri-diagonal, the Crout Factorization Algorithm can be applied.

Similar to the shooting method, the shape of the deflected finger can be calculated by Equation (2.16a) and (2.16b).

2.3 Simulations of uniform beam deflection

In previous sections, methods to solve the differential equation of beam have been discussed for both uniform and non-uniform beams. This section presents some simulations of the uniform beam using MatLAB. The objectives of these simulations are the following:

(1) The non-linearity effect of the large deflection on the deflected shape of a beam is analyzed. Comparisons between large and small deflections are made.

(2) The numerical approximation in the computation of a uniform beam undergoing large deflection is examined, where closed-form solutions are available for comparisons.

Since closed-form solutions for predicting the deflected shape of a uniform beams under a point load at a location are available, this section validates the numerical computations and examines the effects of non-linearities by comparing the difference among a few methods of calculating large deflection of a beam by means of simulation. The simulation parameters are listed in Table 2-1.

Table 2-1 Simulation parameters (uniform beam)

Parameters	Values
E	4.8 MPa
I	1.67×10-8 m^4
EI	0.08 Nm^2
L	101.6 mm (4 inches)
F	15 N
α	90°

Four methods discussed in the previous sections are used to predict the shape of a deflected finger under a point load; namely, linear approximation, Frisch-Fay's solution, and two numerical methods (shooting and FDM). For the case of large deflection, both the shooting and the FDM are compared against the closed-form solution given by Frisch and Fay [1962] and the linear approximation given by Equation (2.4).

The results (simulation parameters listed in Table 2-1) are compared in Figure 2-2. The solid line in the figure represents the deflected beam calculated with the Frisch-Fay method and the dashed line for the small or linear deflection of the uniform beam. The dotted line and left-triangle in Figure 2-2 shows the results from shooting method and FDM respectively. From Figure 2-2 we can draw following conclusions:

(1) The small deflection approximation is valid only when the acting force is small. When the force becomes large as shown in Figure 2-2, the small deflection theory fails to give an accurate prediction of the finger shape, especially at the free end of the beam.

(2) The predicted shapes of the uniform beam from both numerical methods agree very well with the result from the Frisch-Fay method as shown in Figure 2-2.

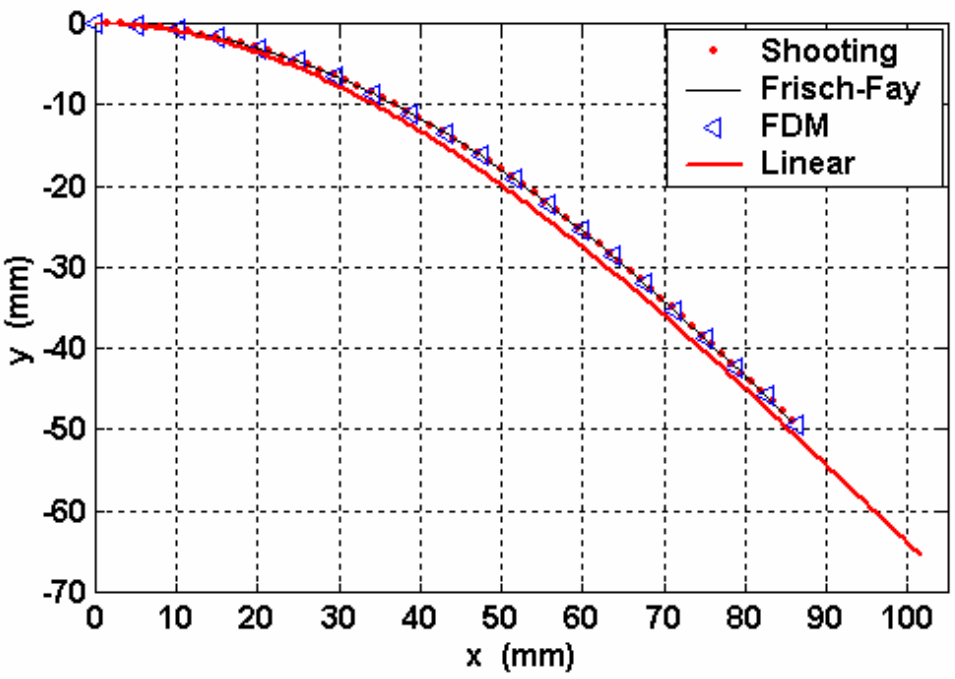

Figure 2-2 Comparison of methods (uniform beam)

2.4 Deflection shape calculation for a non-uniform finger

In this section, simulations using the shooting method and the FDM to solve Equation (2.15) for the shape of a non-uniform beam will be discussed. The focuses of these simulations are given below:

(1) Of particular interest is to study the effect of non-uniform cross-sectional area on the computed shape of a beam undergoing large deflection. The two numerical methods for calculating the deflected shape are compared.

(2) Since it is desired to have a closed-form solution to characterize the beam deflection for dynamic analysis and control, attempts have been made in this research to determine an effective flexural rigidity for approximating a non-uniform beam.

2.4.1 Simulation example

Figure 2-3 shows a typical finger used in grasping a live bird [Lee *et al.*, 2000]. Table 2-2 lists the geometrical properties of the beam that is characterized by four different types of cross-sections. Section 1 is a circular cone (10 mm in length) while Sections 3 and 4 are elliptical, which repeat themselves alternatively at the last part of the finger and thus considered as one section. Section 2 tapers down over the 101.76 mm (4 inches) from the end of Section 1 to Sections 3 and 4.

To solve for the solution from Equation (2.15), $I(x)$ must be represented in a closed form (or by means of a lookup table). Equation (2.15) also requires that the first order derivative of $I(x)$ exists in the effective domain of independent variable x. In other

words, $I(x)$ is a continuous function along the x direction. For the simulation of the non-uniform beam, an exponential function is used to approximate $I_z(x)$ of the beam shown in Figure 2-3:

$$I(x) = Ae^{\alpha x} + Be^{\beta x} + C\ ; \tag{2.33}$$

and its 1st and 2nd derivatives are

$$I'(x) = A\alpha e^{\alpha x} + B\beta e^{\beta x} \tag{2.33a}$$

and

$$I''(x) = A\alpha^2 e^{\alpha x} + B\beta^2 e^{\beta x} \tag{2.33b}$$

respectively.

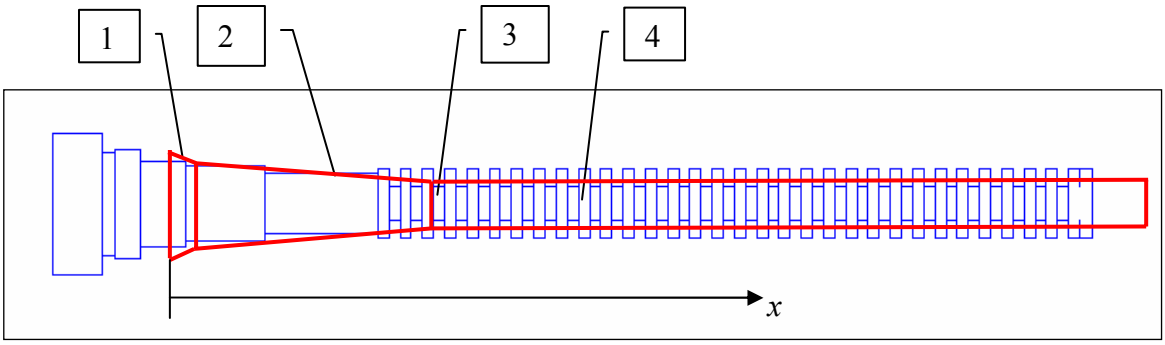

Figure 2-3 Geometrical approximation of the beam [Adapted from Joni, 2000]

Table 2-2 Approximation of finger geometry

Section	Shape	Radius (m)	Modeled I_{zz} (m^4),	Approximation	
				x_i (mm) inches	I_{zz} (m^4),
1	Cone (Circular) (13 mm length)	0.030 (begin), 0.026 (end)	3.976 E-8, 2.570 E-8	0.0 (0.0)	3.976 E-8
2	Non-regular (101.76 mm)	NA	NA	13.0 (0.512)	2.570 E-8
3	Ellipse	0.0170, 0.024	5.7071 E -9	111.76 (4.4)	3.2102 E-9
4	Ellipse	0.0085, 0.024	7.1339 E-10		

Figure 2-4 shows the comparison between the approximation (exponential function in solid line) and the actual values (star) for the moment of area along the length of the finger. The coefficients of Equation (2-33) are also given in Figure 2-4. Other simulation parameters of the deflection of the non-uniform beam are listed in Table 2-3.

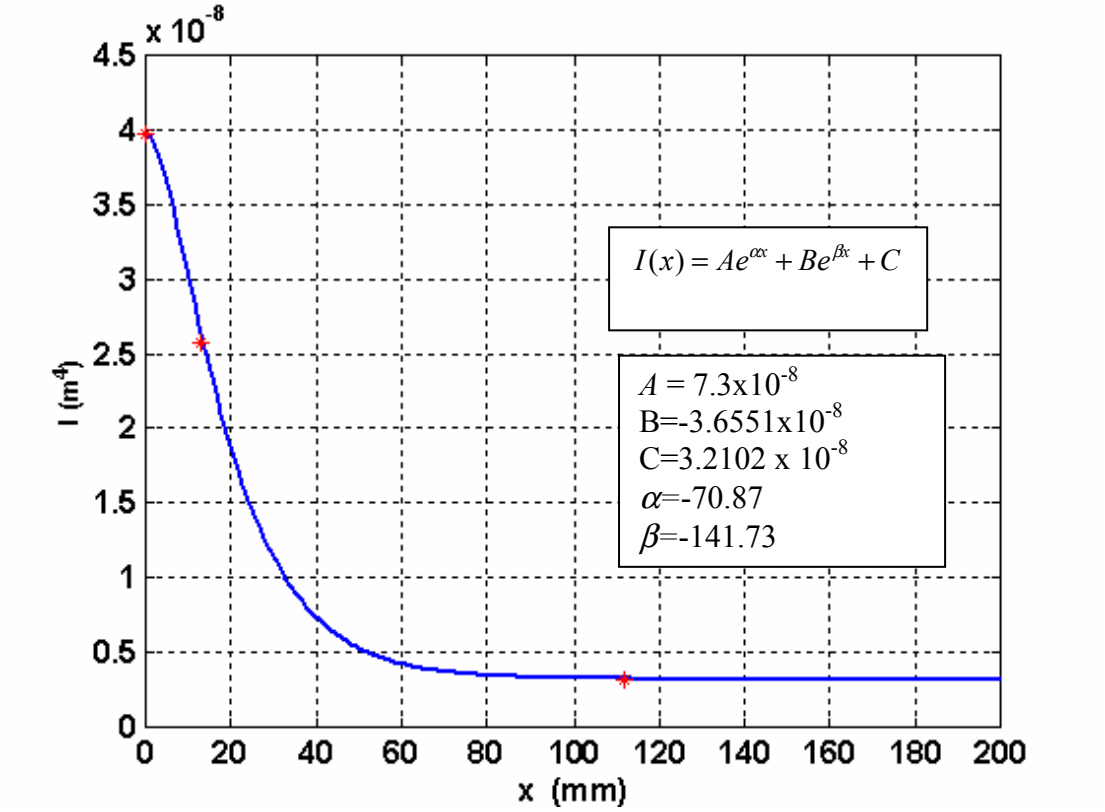

Figure 2-4 Function approximating the beam moment of area

Table 2-3 Simulation parameters (Non-uniform beam)

Parameters	Values
E	4.8MPa
I	Given in Figure 2-3
L	76.2 mm (3 inches)
F	15 N
α	90°

2.4.2 Comparisons between the Shooting Method and the FDM

The shooting method requires two initial guesses of the derivatives at one end for iteratively estimating for the boundary conditions at the other end. Figure 2-5 shows the values for α_1 and $\alpha_1^{'}$. The dashed lines and black dotted lines are the solutions of the ODEs given by Equation (2.17) for initial guess of $\alpha_1^{'}$ being 0 and 1 respectively. After six iterations (intermediate results not plotted) the algorithm converges to the solid lines, the final solution of the boundary value problems defined by Equations (2.15).

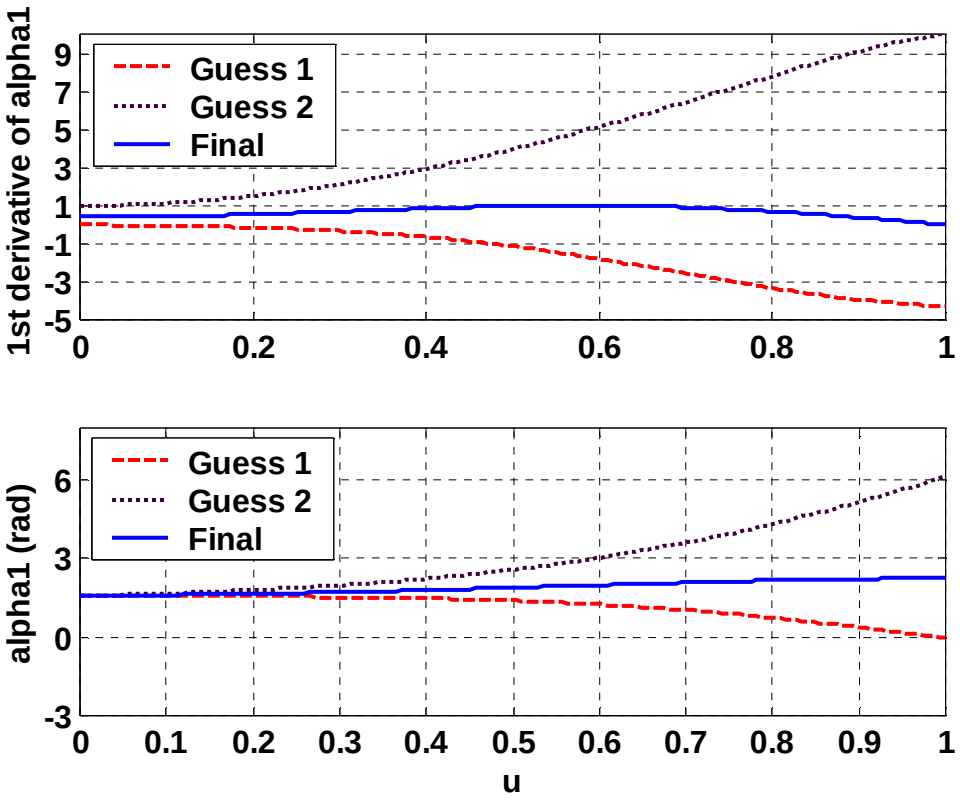

Figure 2-5 Solution of non-uniform beam differential Equation

The FDM, often referred to as a global method, satisfies the boundary conditions automatically. Thus, it does not need a recursive algorithm to estimate for the boundary condition, which is the basis of the shooting method.

Figure 2-6 shows the solution of Equation (2.15) from both the shooting and FDM methods.

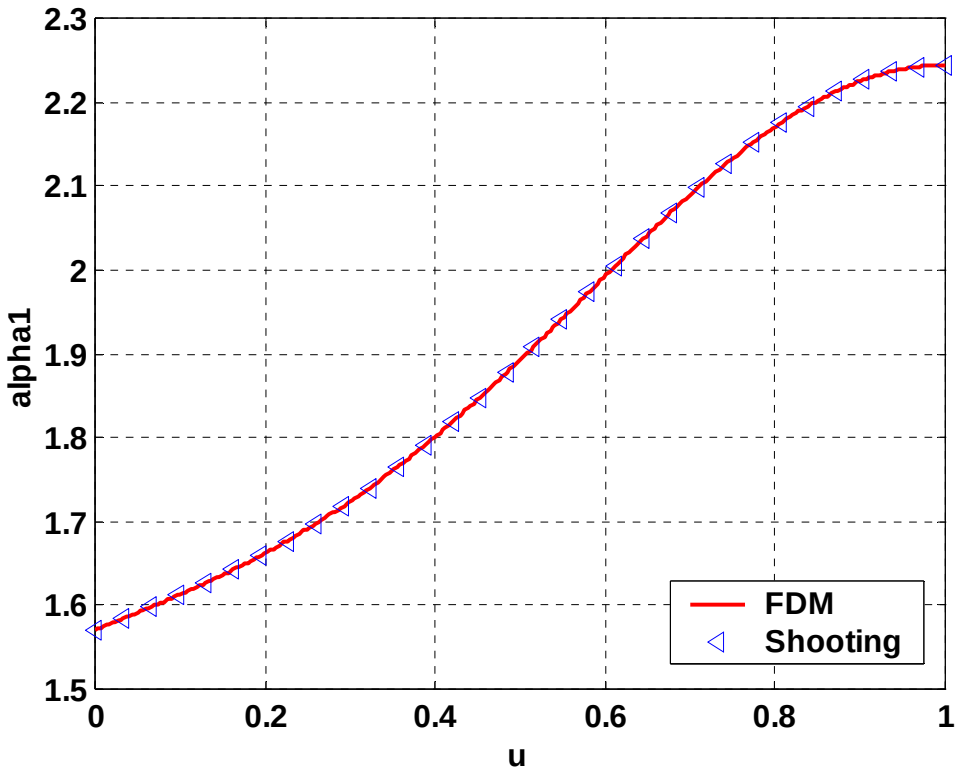

Figure 2-6 α_1 comparison (FDM and shooting)

The resolution of the shooting method depends on the method that solves the ordinary differential equation generalized in the shooting process. So it is easy to achieve fourth- or higher order accuracy. But for FDM it is difficult to have higher than second-order accuracy. We assume the solution from shooting is closer to the exact solution of

the problem at hand. The differences between the shooting and FDM are shown in Figure 2-7.

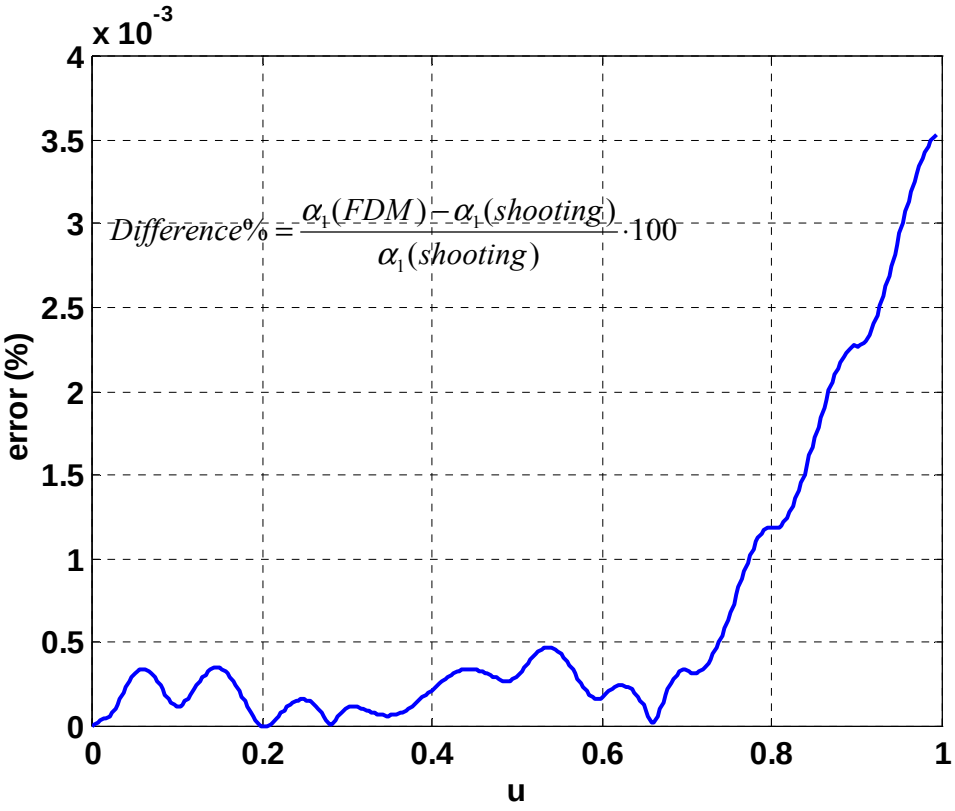

Figure 2-7 Difference estimation: FDM and Shooting (N=300)

Figure 2-7 shows that the difference between the shooting method and the FDM calculation is far less than 0.1 percent when the beam is divided in 300 units. When reducing the mesh number N in the simulation, the error is below 0.5% when N =40.

After α_1 has been solved, Equation (2.16) is used to calculate the finger shape in *x-y* coordinates. The finger shape calculated from FDM method is plotted in Figure 2-8

together with the one from the shooting method. As we expected the two methods get the same shape describing the deflected non-uniform finger.

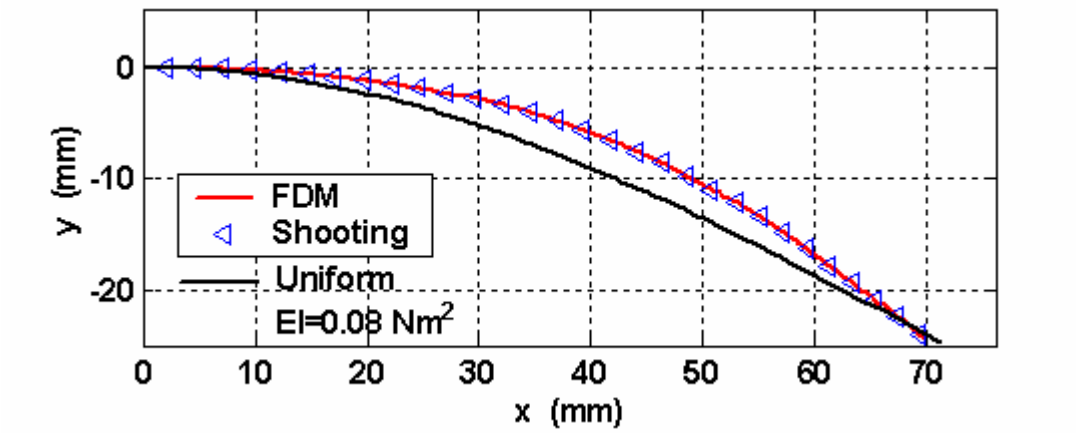

Figure 2-8 Finger deflection

2.4.3 Effects of the non-uniformity

The uniform beam model has a closed form solution that makes it valuable in the contact force analysis, which will be discussed in the later chapters. As discussed in Section 2.2, the uniform beam is characterized by the flexural rigidity, *EI*. Thus, the interest here is to find out whether the shape of a non-uniform deflected beam can be predicted using the F-F's solution with an appropriate effective *EI*.

The steps for finding an effective *EI* of a non-uniform beam under the loading of a point force F at a location denoted by the length L and at an angle α are given as follows:

1. Calculate the shape of the deflected non-uniform beam by one of the numerical methods. The slope of the finger at the contact point, ψ_o, can then be obtained from Equation (2.7b)
2. From Equation (2.10b) calculate *p*.
3. From Equation (2.12) calculate *k*.
4. From Equation (2.7c) calculate the effective *EI*.
5. Multiply a calibration coefficient $C_{EI,}$ in our case, 1.48. (The calibration coefficient can be obtained by trying a few cases in the range of interest and using the average value.)

As shown in Figure 2-8, the dashed line is the shape of a uniform beam using the same simulation parameters listed in Table 2-3 with *EI* 0.08. We can say that the "flexural rigidity" of the non-uniform beam is about 0.08 at length of 76.2mm. The effective *EI* for the case shown in Figure 2-8 is calculated as 0.081. In next Chapter the *EI* as a function of the acting position of the force will be presented when we discuss the contact analysis.

2.5 Summary

In this chapter, a few methods to calculate the flexible beam deflection have been discussed. The beam defection problem basically is a nonlinear boundary value problem. In this thesis, it is classified into uniform and non-uniform according to the geometrical property along the finger. For the uniform beam the analytical model, built upon the Frisch-Fay flexible bar theory, provides a closed–form solution; while the shooting, FDM

have been used to solve the non-uniform deflection problem. Following the analysis are some simulations for the beam deflection. Finally the concept of effective *EI* is presented for approximating the deflection of the non-uniform beam by uniform beam. The reason to do so will be expressed in next Chapter.

The beam deflection calculation provides a solid basis for contact analysis. In the next Chapter, on the basis of the beam analysis, a contact model will be developed and the simulation will be presented and discussed.

CHAPTER III

ROTATING FINGER/MOVING OBJECT CONTACT ANALYSIS

In Chapter II, methods of predicting the shape of a deflected beam under a point force have been discussed. For a uniform beam, the Frisch-Fay's solution is used to describe the shape of the deflected finger. For a non-uniform beam, the differential equation that governs the shape of the finger is solved using two different numerical methods in MatLAB; namely, the shooting method and the finite difference method. This chapter models the contact force between a rotating finger (grasper) and a moving object (bird).

When a rotating finger is in contact with an object, the reaction force causes the finger to deflect. The force acting on the live object and the contact point must be calculated using the geometrical properties of the object, and the mechanical properties of the finger. The deflection of the finger depends on the coefficient of friction at the contact interface, the object geometry, the shape of the deflected finger, and the location at which the force is applied. Most of the methods available to predict contact force in the context of grasping treat the object and fingers as rigid bodies. This thesis addresses compliant

contact as a result of a soft elastic finger. The contact problem is characterized by a set of coupled nonlinear equations, and it is rather involved because of the compliant property of the finger.

3.1 Formulation of a 2D Compliant Contact Force Model

The following assumptions are made in this model:

(1) The basic shape of a broiler can be best described by an ellipsoid. In two-dimensions, it is essentially an ellipse; or mathematically given by Equation (3.1):

$$f_o(x,y) = \begin{pmatrix} x & y \end{pmatrix} [B] \begin{pmatrix} x \\ y \end{pmatrix} - 1 = 0 \tag{3.1}$$

$$[B] = \begin{bmatrix} 1/\eta^2 & 0 \\ 0 & 1/\lambda^2 \end{bmatrix} \tag{3.1a}$$

where η and λ are the characteristic radii of the ellipse.

(2) The finger is flexible in its *xy* plane but rigid in its *xz* plane.

(3) The object is treated here as a rigid body, because it has been shown experimentally in [Lee *et al.*, 2000] that the object has a relatively high stiffness as compared to that of the finger, and its stiffness effects on the contact force [Jeffery, 2001] can be ignored.

(4) Point contact is assumed for the contact model.

(5) For a relatively slow rotational speed, the contact force of a rotating finger can be determined quasi-statically. In other words, the rotating finger will be treated as "quasi-static", and the contact equations are solved approximately using static mechanics. The equations of static mechanics can be applied at each instant in time sequences as though the deflected finger were in static equilibrium.

(6) With the grasping in mind, an important phenomenon is the potential of the slipping in the tangent direction at the contact point. Therefore, the finger is always at the edge of sliding on the surface of the sliding for each moment investigated quasi-statically.

Coordinate systems

Figure 3-1 shows a plane contact model for describing the kinematic relationship between the object (ellipse) and the rotating finger, where the ellipse is shown to have orientation at an arbitrary angle of θ. In Figure 3-1, C_w (XYZ) is the fixed (reference) coordinate frame assigned at the center of a rotating drum with its normal Z pointing along its rotating axis. The bird coordinate frame C_b ($x_b y_b z_b$) is attached with its mass center (X_o, Y_o), where the x_b-axis and y_b-axis are along its principal axes. The finger coordinate frame C_f ($x_f y_f z_f$) is attached at the base of a rotating structure.

When the finger is in contact with an object, the reaction force F acting at an angle α causes the finger to deflect, as did the flexible beam model discussed in Chapter 2, the slope of the finger at the contact point is denoted by ψ_o. The contact force can be

decomposed into two orthogonal components, parallel and perpendicular to a tangent line at the contact point (x_i, y_i).

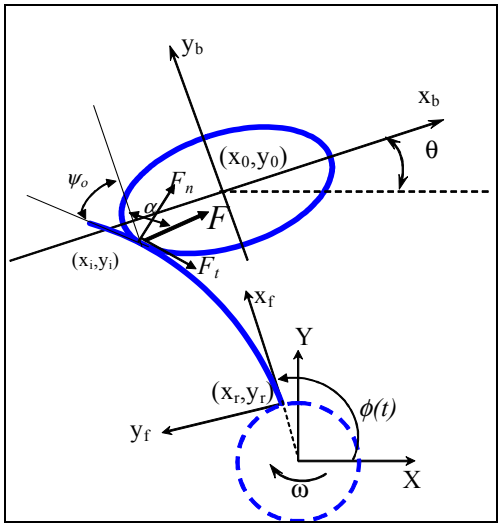

Figure 3-1 Kinematic model of the finger/ellipse interaction

Ellipse in finger coordinate system

To solve for the contact point and forces, we express points on the ellipse with respect to C_f. The points on the ellipse are described with respect to C_w by

$$P_w = [R_z(\theta)]P_b + P_{b0} \tag{3.2}$$

where P_{b0} is the position vector $(X_0, Y_0)^T$ of the ellipsoid in C_w frame; $P_b = (x_b, y_b)^T$ and $P_w = (X, Y)^T$ are the position vectors describing points on the broiler with respect to C_b and C_w respectively; and

$$[R(\theta)] = \begin{bmatrix} \cos\theta & -\sin\theta \\ \sin\theta & \cos\theta \end{bmatrix} \tag{3.2a}$$

is a rotational matrix describing the orientation of the bird with respect to C_w. Similarly, we have points on the finger in C_w:

$$P_w = [R_z(\phi(t))]P_f + P_{f0} \tag{3.3}$$

where

$$P_{f0} = [r\cos\phi, r\sin\phi]^T; \tag{3.3a}$$

$$[R_Z(\phi(t))] = \begin{bmatrix} \cos\phi & -\sin\phi \\ \sin\phi & \cos\phi \end{bmatrix}; \tag{3.3b}$$

$$\phi(t) = 2\pi - \omega t; \tag{3.3c}$$

ω is the angular speed and r is the radius of the drum. Hence, the coordinate transformation from C_f to C_b is

$$P_b = [R_{bf}]P_f + P_{bf0} \tag{3.4}$$

where

$$[R_{bf}] = [R_z(\theta)]^T[R_Z(\phi(t))]; \tag{3.4a}$$

and

$$P_{bf0} = [R_z(\theta)]^T(P_{f0} - P_{b0}) \tag{3.4b}$$

Substituting Equation (3.4) into Equation (3.1), after some algebraic manipulations the resulting equation of an ellipse in the finger coordinate system becomes

$$f_o(x_f, y_f) = P_f^T[R_{bf}]^T[B][R_{bf}]P_f + 2P_{bf0}^T[B][R_{bf}]P_f + P_{bf0}^T[B]P_{bf0}^T - 1 = 0 \tag{3.5}$$

Expansion of Equation (3.5) results in Equation (3.6), the equation of an ellipse in the finger coordinate system:

$$f_o(x_f, y_f) = b_1x_f^2 + b_2y_f^2 + b_3x_fy_f + b_4x_f + b_5y_f + b_6 = 0, \tag{3.6}$$

where

$$\begin{bmatrix} b_1 & \frac{b_3}{2} \\ \frac{b_3}{2} & b_2 \end{bmatrix} = [R_{bf}]^T [B][R_{bf}]; \tag{3.6a}$$

$$\begin{bmatrix} b_4 & b_5 \end{bmatrix} = P_{bf0}^T [B][R_{bf}]; \tag{3.6b}$$

and

$$b_6 = P_{bf0}^T [B] P_{bf0}^T - 1. \tag{3.6c}$$

Contact model

The shape of the deflected finger may be solved from Equation (2.15) in which the reaction force F and its acting direction α are unknowns. The unknown force and direction must be solved along with the constraints imposed at the contact as follows:

The first is imposed by the friction at the contact, which governs the direction of the reaction force:

$$\mu = \frac{F_t}{F_n} = \tan(\alpha + \psi_o - \frac{\pi}{2}) \tag{3.7}$$

where μ is the coefficient of friction between object and finger; F_t and F_n the forces tangent to and normal to tangent line at the contact point (x_i, y_i). At the contact point, the ellipse and the finger share the same slope

$$-\frac{\partial f_e(x_f, y_f)/\partial x_f}{\partial f_e(x_f, y_f)/\partial y_f}\Big|_{(x_f = x_i, y_f = y_i)} = \tan\psi_0 \tag{3.8}$$

where $f_e(x_f, y_f) = 0$ is the hidden form of equation (3.6) describing the shape of the broiler.

Summary

Equations (2.15), (3.6)-(3.8) form a basic system of nonlinear equations which have five unknowns; namely, the contact point (x_i, y_i), the slope ψ_o at the contact point governing the shape of the deflected finger, and the reaction force F and its direction α.

In Sections 3.2 and 3.3 we discuss two methods to solve the non-uniform beam contact problems. The first method approximates the non-uniform finger with a uniform finger which is characterized by a function of effective *EI*. Then Equation (2.15) describing the deflection of the beam can be replaced by Equations (2.9a) and (2.9b). After solving the nonlinear equations the contact force can be calculated using the effective *EI*.

The second method, as presented in Section 2.2.2, will approximate the differentials in Equation (2.15) with the FDM. But it is formulated in a variable describing the slope of the deflected finger. Unlike the first method that has a direct formula for the finger shape, the second method needs two more equations, Equation (2.16a) and (2.16b), to compute for the shape of deflected finger; a more complex procedure.

3.2 Algorithm I: Uniform Finger with Effective *EI*

In the last Chapter, we presented the method of calculating the effective *EI* from the shape of a non-uniform finger. The physical meaning of the effective *EI* is that it describes the overall ability of the non-uniform finger to resist deformation under external force or moment. A recursive numerical algorithm is developed to find the

solution from the set of nonlinear equations. The computing procedure illustrated by the flowchart is given in Figure 3-2. The algorithm provides a good understanding of the solution approach for computing the forces on the object at the contact point. It is also an essential basis for formulating the grasping dynamics to be discussed in Chapter IV.

The method requires an initial guess as illustrated using the flowchart shown in Figure 3-2. In order to speed up the convergence of the solution, the shape of the deflected finger is approximated by a parabolic function for providing a good initial guess of the contact points (x_i, y_i):

$$y_f = ax_f^2 \tag{3.9}$$

In other words, $x_f = x_i$, $y_f = y_i$ and a can be solved simultaneously from Equations (3.6), (3.8) and (3.9).

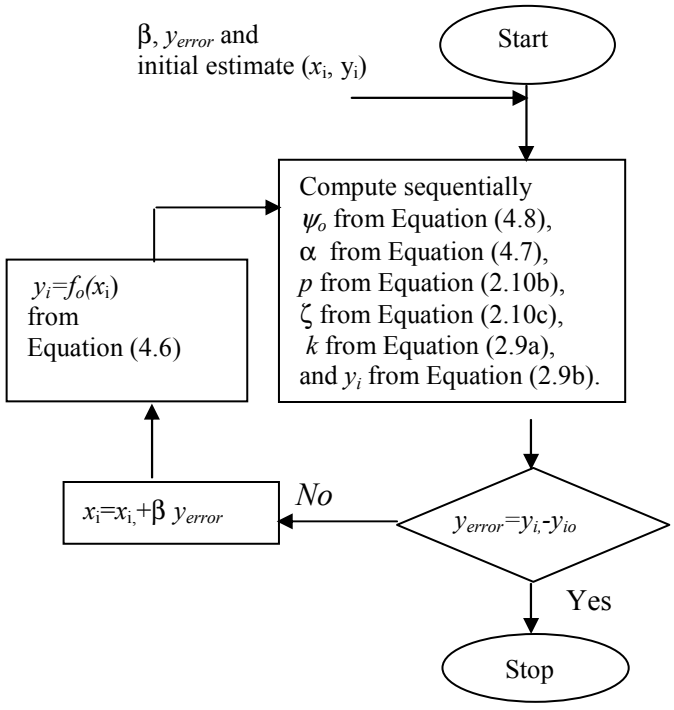

Figure 3-2 Flowchart illustrating the computational procedure

Using Equation (3.9), Equation (3.6) can be re-written as

$$2ax_f = -\frac{2b_1x_f + b_3y_f + b_4}{2b_2y_f + b_3x_f + b_5} \tag{3.10}$$

Note that the substitution of y_f from Equation (3.9) into Equation (3.6) and (3.10) leads to a 4th order equation of x_f and a quadratic equation of a respectively. The solution of x_f can be obtained by first solving for a in terms of x_f from the quadratic equation and then the 4th order equation for x_f.

Alternatively, the problem may be more conveniently computed numerically from the 4th order equation for x_f by stepping a, and examining the form of the solutions, which is known as follows:

Case 1: All the solutions will be imaginary if the finger does not intercept the ellipse.

Case 2: If $x_f > 0$ and the finger intercepts the ellipse, two of the solutions will be real and distinct.

Case 3: For a particular a, the specific solutions that we are looking for characterized by two real repetitive roots and a pair of complex conjugates. The value of this particular a is what we are look for and the repetitive roots are the estimated contact points.

With the computed contact point (x_i, y_i), the arc length L can be approximated from Equation (3.11):

$$L = \int_0^{x_i} \sqrt{1 + (2ax)^2}\, dx \tag{3.11}$$

and k and F can be computed for the initial guess from Equations (2.12) and (2.7c) respectively. This method is only an approximation method for the guess of the contact point. The results here will also be used in the initial guess of the FDM non-uniform contact analysis in the next section.

For the solution searching process presented in Figure 3-2, after the first initial guess (x_i, y_i) has been calculated, sequentially the values of ψ_0, α, p, ζ and k can be calculated from the equations specified in the flow chart. Finally a new y_i can be obtained. The difference, y_{error}, between this new and old y_i can be used to update the x_i. Then the ellipse Equation (3.6) can be solved for the corresponding updated y_i. The process continues until the y_{error} is less than the pre-specified error tolerance. Then other contact information, such as the contact force F and the contact length L, can be obtained.

3.3 Algorithm II: Non-uniform finger using FDM

We have derived the method to predict the contact force for a uniform beam. This section extends the use of FDM (described in Chapter 3) to predict the contact point of a non-uniform finger. The primary difference here is that the parameters F, L, and α are unknowns. Thus, Equation (2.15) must be solved along with the geometry of the object and the contact model.

The finite difference equations are in the form:

$$\begin{bmatrix} G_1(W) \\ G_2(W) \\ \vdots \\ G_{N-1}(W) \\ G_N(W) \end{bmatrix} = 0 \tag{3.12}$$

where $W = [w_1 \quad w_2 \quad \cdots \quad w_{N-1} \quad w_N]^T$;

$$\begin{aligned} G_1(W) &= 2w_1 - w_2 + h^2 f\left(u_1, w_1, \frac{w_2 - w_0}{2h}, F, L\right) - w_0 \\ G_2(W) &= -w_1 + 2w_2 - w_3 + h^2 f\left(u_2, w_2, \frac{w_3 - w_1}{2h}, F, L\right) \\ &\vdots \\ G_{N-1}(W) &= -w_{N-2} + 2w_{N-1} - w_N + h^2 f\left(u_{N-1}, w_{N-1}, \frac{w_N - w_{N-2}}{2h}, F, L\right) \\ G_N(W) &= -w_{N-1} + 2w_N + h^2 f\left(u_1, w_1, \frac{w_{N+1} - w_{N-1}}{2h}, F, L\right) - w_{N+1} \end{aligned};$$

and the boundary conditions are given by

$$w_0 = \alpha \tag{3.12a}$$

and

$$w_{N+1} = \frac{1}{3}(4w_N - w_{N-1}) \tag{3.12b}$$

The contact point (x_i, y_i) can then be calculated from Equations (2.16a) and (2.16b) numerically approximated by

$$x_i = L\frac{h}{3}\sum_{i=0}^{(N-1)/2}\left[g_1(w_{2i}) + 4g_1(w_{2i+1}) + g_1(w_{2i+2})\right] \tag{3.13a}$$

and $$y_i = L\frac{h}{3}\sum_{i=0}^{(N-1)/2}[g_2(w_{2i}) + 4g_2(w_{2i+1}) + g_2(w_{2i+2})] \tag{3.13b}$$

where

$$g_1(\alpha_1) = \cos(\alpha_1 - \alpha) \tag{3.13c}$$

$$g_2(\alpha_1) = \sin(\alpha_1 - \alpha) \tag{3.13d}$$

Note that the Simpson's Rule is used here to approximate the integral in Equations (2.16a) and (2.16b), which has the form:

$$\int_{x_i}^{x_{i+2}} g_j(x)dx = \frac{h}{3}[g_j(x_i) + 4g_j(x_{i+1}) + g_j(x_{i+2})] - \frac{h^5}{90}g_j^{(4)}(\xi),\ j=1, 2 \tag{3.13e}$$

if the 4th order differential of $g_j(x)$ exists.

Other contact constraints are the same as described in last section. Specifically, they are Equations (3.6), (3.7) and (3.8). The overall system of equations consists of (N+6) nonlinear equations and (N+6) unknowns, which can be represented by defining a function $\boldsymbol{G(X)}$

$$\boldsymbol{G(X)} = \begin{bmatrix} G_1(X) \\ G_2(X) \\ \vdots \\ G_{N-1}(X) \\ G_N(X) \\ G_{N+1}(X) \\ \\ G_{N+2}(X) \\ G_{N+3}(X) \\ G_{N+4}(X) \\ G_{N+5}(X) \\ G_{N+6}(X) \end{bmatrix}_{(N+6)\times 1} = 0 \qquad (3.14)$$

where $X = \begin{bmatrix} w_1 & w_2 & \cdots & w_{N-1} & w_N & w_{N+1} & x_i & y_i & F & \alpha & L \end{bmatrix}^T$;

$G_1(X), G_2(X), \cdots, G_{N-1}(X)$ and $G_N(X)$ are defined in Equation (3.12);

$$G_{N+1}(X) = \frac{1}{3} w_{N-1} - \frac{4}{3} w_N + w_{N+1};$$

$$G_{N+2}(X) = x_i - L\frac{h}{3}\sum_{i=0}^{(N-1)/2}\left[g_1(w_{2i}) + 4g_1(w_{2i+1}) + g_1(w_{2i+2})\right];$$

$$G_{N+3}(X) = y_i - L\frac{h}{3}\sum_{i=0}^{(N-1)/2}\left[g_2(w_{2i}) + 4g_2(w_{2i+1}) + g_2(w_{2i+2})\right];$$

$$G_{N+4}(X) = f_o(x_f, y_f) = b_1 x_f^2 + b_2 y_f^2 + b_3 x_f y_f + b_4 x_f + b_5 y_f + b_6 = 0;$$

$$G_{N+5}(X) = \tan(w_{N+1} - \frac{\pi}{2}) - \mu;$$

$$G_{N+6}(X) = -\frac{\partial f_e(x,y)/\partial x}{\partial f_e(x,y)/\partial y}\Big|_{(x=x_i, y=y_i)} - \tan(w_{N+1} - \alpha);$$

The above system can be solved numerically using Newton's method [Burden *et. al*., 1997], which requires the computation of the Jacobian matrix [***J****(X)*]:

$$\boldsymbol{J}(X)_{ij} = \frac{\partial G_i}{\partial X_j},$$

for the nonlinear system described in Equation (3.14) is

$$[\boldsymbol{J}(X)] = \begin{bmatrix} A_1 & B_1 & 0 & 0 & 0 & 0 & 0 & 0 & F_1 & C_0 & L_1 \\ C_1 & A_2 & \ddots & 0 & \vdots & \vdots & \vdots & \vdots & F_2 & 0 & L_2 \\ 0 & \ddots & \ddots & B_{N-2} & 0 & 0 & 0 & 0 & \vdots & 0 & \vdots \\ \vdots & 0 & C_{N-2} & A_{N-1} & B_{N-1} & 0 & 0 & 0 & F_{N-1} & 0 & L_{N-1} \\ 0 & \vdots & 0 & C_{N-1} & A_N & B_N & 0 & 0 & F_N & 0 & L_N \\ 0 & \cdots & 0 & \frac{1}{3} & -\frac{4}{3} & 1 & 0 & 0 & 0 & 0 & 0 \\ D_1 & D_2 & \cdots & D_{N-1} & D_N & D_{N+1} & 1 & 0 & 0 & Q_1 & L_{N+2} \\ E_1 & E_2 & \cdots & E_{N-1} & E_N & E_{N+1} & 0 & 1 & 0 & Q_2 & L_{N+3} \\ 0 & 0 & \cdots & 0 & 0 & 0 & H_1 & H_2 & 0 & 0 & 0 \\ 0 & 0 & \cdots & 0 & 0 & K & 0 & 0 & 0 & 0 & 0 \\ 0 & 0 & \cdots & 0 & 0 & M_1 & M_2 & M_3 & 0 & Q_3 & 0 \end{bmatrix}_{(N+6)\times(N+6)} \tag{3.15}$$

where

$$A_i = 2 + h^2 f_{\alpha_1}\left(u_i, w_i, \frac{w_{i+1} - w_{i-1}}{2h}, F, L\right), \quad i = 1,\ldots,N, \text{ where } f_{\alpha_1} = -\frac{FL^2}{EI(uL)}$$

$$B_i = -1 + \frac{h}{2} f_{\alpha_1'}\left(u_i, w_i, \frac{w_{i+1} - w_{i-1}}{2h}, F, L\right), \quad i = 1,\ldots,N$$

$$C_{i-1} = -1 - \frac{h}{2} f_{\alpha_1'}\left(u_i, w_i, \frac{w_{i+1} - w_{i-1}}{2h}, F, L\right), \quad i = 2,\ldots,N-1, \text{ and } f_{\alpha_1'} = -L\frac{I'(uL)}{I(uL)}$$

$$C_0 = -1 - \frac{h}{2} f_{\alpha_1'}\left(u_1, w_1, \frac{w_2 - w_0}{2h}, F, L\right),$$

$$D_{N+1} = \frac{Lh}{3}\sin(w_{N+1} - \alpha),$$

$$D_{2i+1} = \frac{4Lh}{3}\sin(w_{2i+1} - \alpha), \quad i = 0,1,2,\ldots,(N-1)/2$$

$$D_{2i} = \frac{2Lh}{3}\sin(w_{2i} - \alpha), \quad i = 1,2,...,(N-1)/2$$

$$E_{N+1} = -\frac{Lh}{3}\cos(w_{N+1} - \alpha),$$

$$E_{2i+1} = -\frac{4Lh}{3}\cos(w_{2i+1} - \alpha), \quad i = 0,1,2,...,(N-1)/2$$

$$E_{2i} = -\frac{2Lh}{3}\cos(w_{2i} - \alpha), \quad i = 1,2,...,(N-1)/2$$

$$F_i = -\frac{L^2}{EI(u_i L)}\sin w_i, \quad i = 1,2,\cdots,N$$

$$Q_1 = -L\frac{h}{3}\sum_{i=0}^{(N-1)/2}\left[\sin(w_{2i} - \alpha) + 4\sin(w_{2i+1} - \alpha) + \sin(w_{2i+2} - \alpha)\right],$$

$$Q_2 = L\frac{h}{3}\sum_{i=0}^{(N-1)/2}\left[\cos(w_{2i} - \alpha) + 4\cos(w_{2i+1} - \alpha) + \cos(w_{2i+2} - \alpha)\right], Q_3 = \sec^2(w_{N+1} - \alpha),$$

$$H_1 = 2b_1 x_i + b_3 y_i + b_4, \qquad H_2 = 2b_2 y_i + b_3 x_i + b_5,$$

$$K = \sec^2(w_{N+1} - \frac{\pi}{2}),$$

$$L_i = h^2\begin{bmatrix} -\dfrac{I'(u_i L)}{I(u_i L)}\dfrac{w_{i+1} - w_{i-1}}{2h} - Lu_i\dfrac{w_{i+1} - w_{i-1}}{2h}\dfrac{I''(u_i L)I(u_i L) - [I'(u_i L)]^2}{I^2(u_i L)} \\ -\sin w_i \dfrac{FL}{E}\dfrac{2I(u_i L) - I'(u_i L)u_i L}{I^2(u_i L)} \end{bmatrix}, i = 1,2,\cdots,N$$

$$L_{N+2} = -\frac{h}{3}\sum_{i=0}^{(N-1)/2}\left[\cos(w_{2i}-\alpha)+4\cos(w_{2i+1}-\alpha)+\cos(w_{2i+2}-\alpha)\right]$$
$$L_{N+3} = -\frac{h}{3}\sum_{i=0}^{(N-1)/2}\left[\sin(w_{2i}-\alpha)+4\sin(w_{2i+1}-\alpha)+\sin(w_{2i+2}-\alpha)\right],$$

$$M_1 = -\sec^2(w_{N+1}-\alpha),$$
$$M_2 = -\frac{(4b_1b_2-b_3^2)y_i+(2b_1b_5-b_3b_4)}{(2b_2y_i+b_3x_i+b_5)^2}$$

and
$$M_3 = -\frac{(-4b_1b_2+b_3^2)x_i+(b_3b_5-2b_2b_4)}{(2b_2y_i+b_3x_i+b_5)^2}.$$

The algorithm using Newton's method is given as below [Burden *et al*., 1997]:

Input: Number *n* of equations and unknowns; tolerance *TOL*; discretization number of the beam *N*; maximum number of iterations *Num*

Output: Solution $X = \begin{bmatrix} w_1 & w_2 & \cdots & w_{N-1} & w_N & w_{N+1} & x_i & y_i & F & \alpha & L \end{bmatrix}^T$ or a message that the number of iterations was exceeded.

Step 1) Find the initial approximation of the solution by have an initial guess of the contact points (x_i, y_i). In the algorithm, the finger shape could be approximated by a parabolic function as described in Equation (3.9).

Step 2) Set k=1

Step 3) While ($k \le Num$) do Steps 4)-8).

Step 4) Calculate $G(X)$ and $J(X)$ defined in Equations (3.14) and (3.15).

Step 5) Solve the $n \times n$ linear system $[J(X)]Y = -G(X)$.

Step 6) Set $X = X + Y$

Step 7) If $\|Y\| < TOL$ then output (X);

(Procedure completed successfully)

STOP

Step 8) Set $k = k + 1$

(Procedure completed unsuccessfully.)

STOP

3.4 Simulation and Model Validation

In previous sections, two specific methods to solve for the contact point and the force imposed by a non-uniform finger on the object have been discussed; namely, approximated finger with an effective *EI* and FDM. This section addresses the following issues:

(1) We examine the convergence of the two numerical algorithms. The results of the two algorithms are then compared. It is of particular interest to determine the validity of approximating the non-uniform finger using a uniform finger with an effective *EI*.

(2) We validate the analytical model by comparing the computed results against those computed using the finite element method and those obtained experimentally.

Simulations have been performed for two separate cases as shown in Figure 3-3. The corresponding parameters used in the simulation are compared in Table 3-1. As shown in Figure 3-3, the primary difference between Case 1 and Case 2 is the slope, which has a significant effect on the convergence of Algorithm I, at the contact point in the finger coordinate system. The function describing the moment of area of the finger has been given in Equation (2.33) and Figure 2-3.

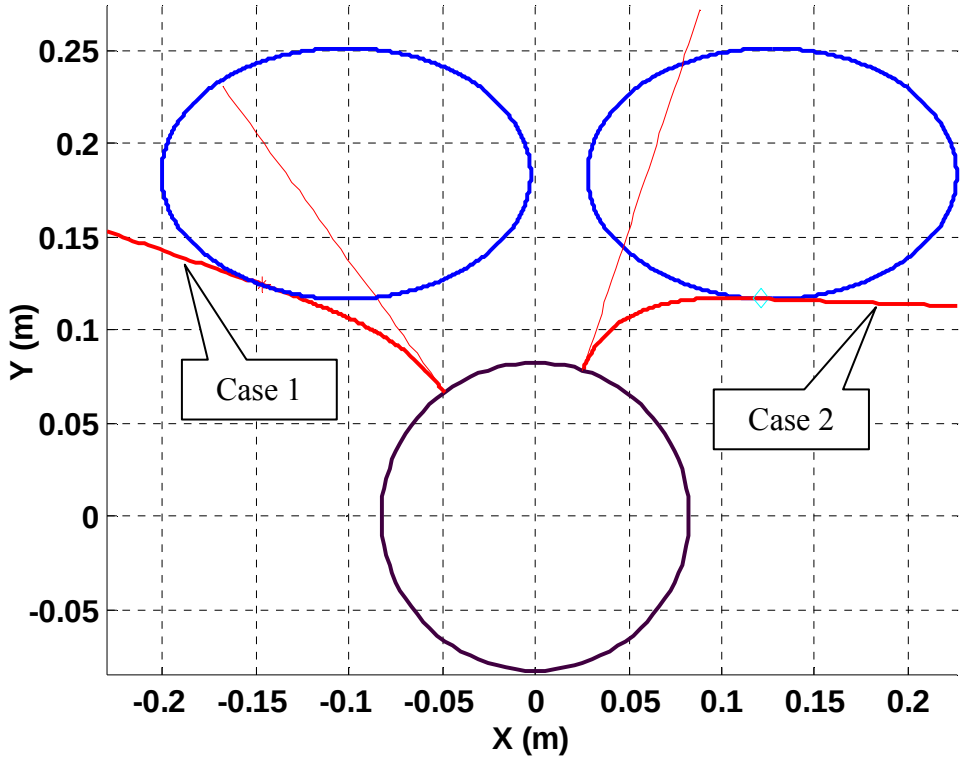

Figure 3-3 Simulation example in world coordinate system

Table 3-1 Simulation parameters

Simulation Parameters	**Case 1**	**Case 2**
Ellipse		
η, λ, in mm (inches)	99.1, 67.3 (3.9, 2.65)	99.1, 67.3 (3.9, 2.65)
(X_0, Y_0) in mm (inches)	**-101.6, 184 (-4, 7. 25)**	**127, 184 (5, 7. 25)**
Orientation θ in degrees	0	0
Velocity in m/s (inches/s)	0.508 (20)	0.508 (20)
Finger		
Angular position of finger (ωt)	**126˚**	**72˚**
Length of finger in m (inches)	0.203 (8)	0.203 (8)
Young's module E (MPa)	4.8	4.8
Drum		
Radius of the roller in m (inches)	0.0825 (3.25)	0.0825 (3.25)
Angular velocity (rpm)	20	20
Coef. Of friction μ, object/finger	0.6	0.6

3.4.1 Simulation of Algorithm I and its convergence

Simulation written in MatLAB has been performed for two cases. The first case illustrates the simulation algorithm and results. The second case helps illustrate the effect of the contact position on the convergence of the algorithm and the selection of the step size.

The contact force (predicted using Algorithm I shown in Figure 3-2) requires an explicit representation of the flexural rigidity *EI* of the finger. Figure 3-4 shows a cluster of solid lines of the effective *EI* as a function of the x_f for a range of forces and angles. They are calculated using the algorithm presented in Chapter 2; and the effective *EIs* of the finger are also listed in the table beside the figure.

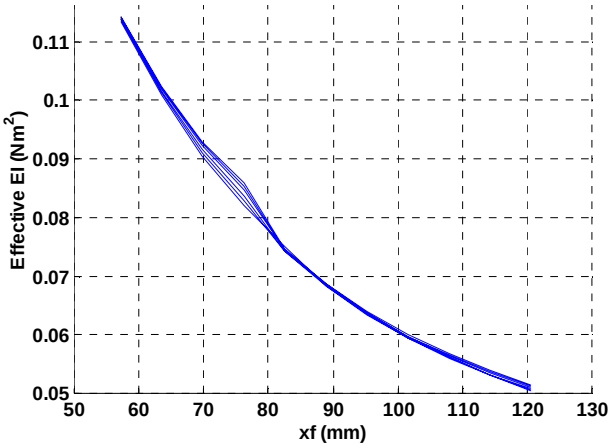

x_f mm (inch)	*EI* Nm² (soft)
50.80 (2.0)	0.1108
66.04 (2.6)	0.0915
81.28 (3.2)	0.0786
96.53 (3.8)	0.0694
111.76 (4.4)	0.0627
127.00 (5.0)	0.0506

Figure 3-4 Effective *EI* plot

The parameters required in the flow chart are listed in Table 3-3 together with the simulated results. The computed shapes of the finger for both cases are shown in Figure

3-3. The error threshold ERR is set manually to be 0.0005m (or 0.5mm) since further reduction does not have much effect on the result.

The step sizes used to simulate Case 1 and Case 2 are 0.6 and 0.05 respectively. Figure 3-5 illustrates the convergence of the solution, which plots the shape of the finger for Case 1 in the finger coordinate system. The circle is the initial approximation of the contact point from the parabolic approximation of the finger deflection. The stars are the locus of the intermediate contact points when the solution converges to the final position. We have noticed that the step size has a significant effect on the convergence of Algorithm I, the choice of which depends significantly on the slope of the finger.

Table 3-2 Simulation parameters and results for Algorithm I

Parameters	**Case 1**	**Case 2**
Controlling variables		
Step size β	0.6	0.05
Tolerance *ERR* (mm)	0.5	0.5
Simulation Results		
Contact point (*xi, yi*) (m)	(0.104, 0.045)	(0.0662, 0.040)
α(°)	85.39	46.83
$\lvert F \rvert$ (N)	8.77	18.72
ψ_0(°)	**35.6**	**74.13**
L (mm)	118.8	111.4

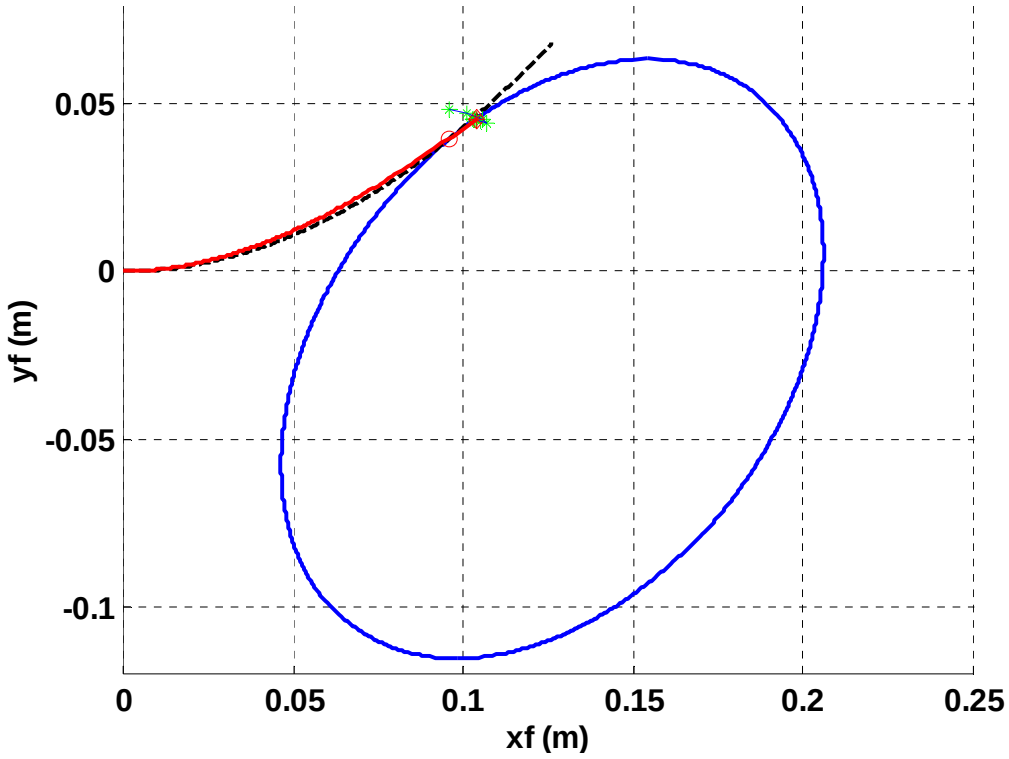

Figure 3-5 Finger/object contact simulation result plot in C_f

The step size coefficient β has been tested computationally for convergence. From the simulation it is found that the selection of step size β depends on the contact condition, more specifically the slope at the contact point. We notice that when the slope around the contact point has a value near 90˚, the recursive method may not converge if β is more than 0.4. Thus, the step size is chosen between 0.01 and 0.3. Tests have shown that when the slope is near infinity (or the tangent line at the contact point becomes vertical), the computation oscillates around that point. To avoid this, we decrease the step size or the coefficient β, and when the slope approaches infinity, the x_{error} is used as a criterion of convergence. In the following, we discuss in greater detail the effect of step size using the two different cases.

Case 1

Figure 3-6 compares the convergence of different step sizes used for the case where the finger experiences a moderate slope. Recall that the parameters are given in Table 3-1 and Table 3-3. Different step sizes β were tried. When β=1.15 the solution oscillates around the real solution but cannot converge as shown in Figure 3-5(c). When β=0.05 the algorithm as shown in Figure 3-6(a) converges to the final solution after 58 iterations. As expected, when we increase the step size coefficient β=0.6 the algorithm converges faster to the final solution after 9 iterations as shown in Figure 3-6(b).

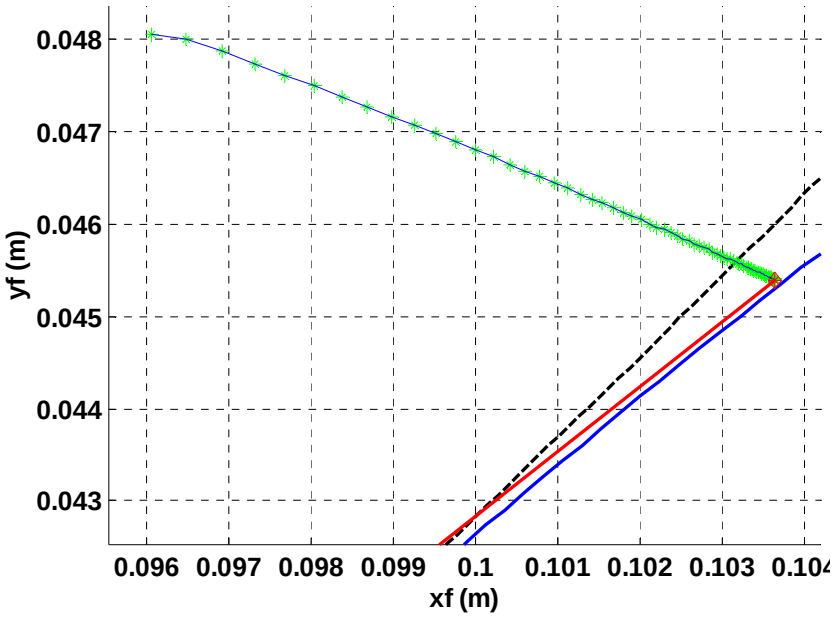

(a) Step size β=0.05, 58 iterations

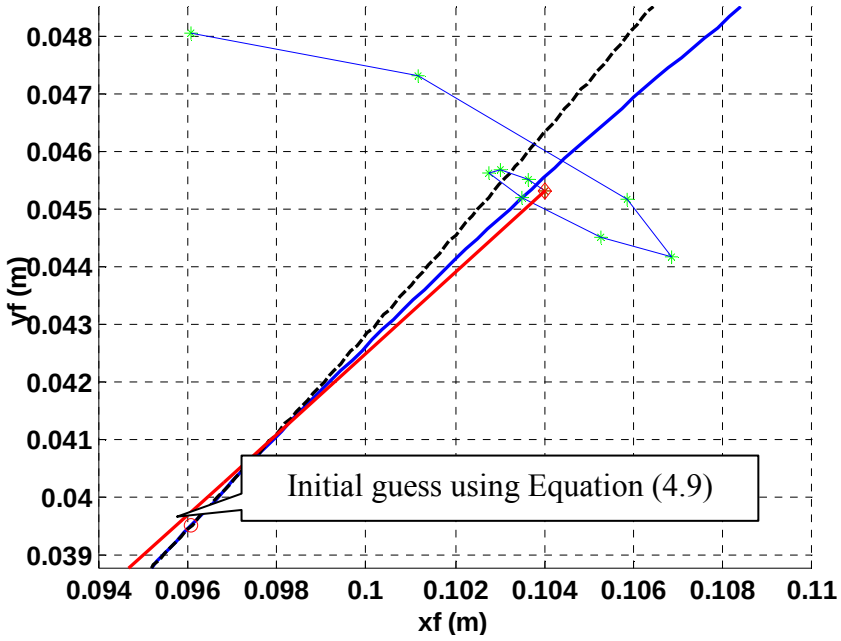

(b) Step size β=0.6, 9 iterations

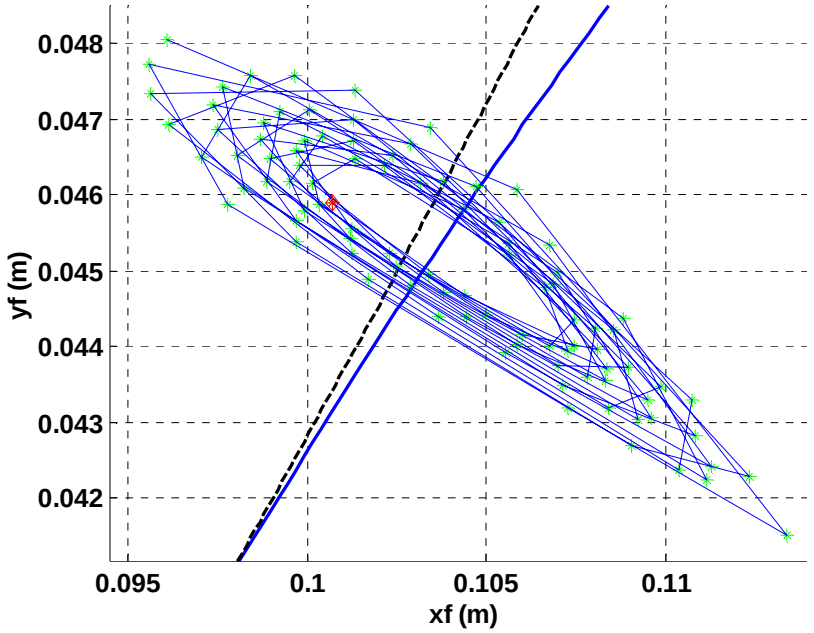

(c) Step size β=1.15, oscillation

Figure 3-6 Effect of the step size β (Case 1)

Case 2

Figure 3-7 shows the effects of the step size for the case when the finger experiences a large slope. When the step size is around 0.1, the solution starts to oscillate around as shown in Figure 3-7(c) and needs a very long step to converge. When β=0.01 the algorithm converges to the final solution after 48 iterations as shown in Figure 3-6(a). As expected and shown Figure 3-7(b), when increase the step size coefficient β = 0.05 the algorithm converges faster to the final solution after 20 iterations.

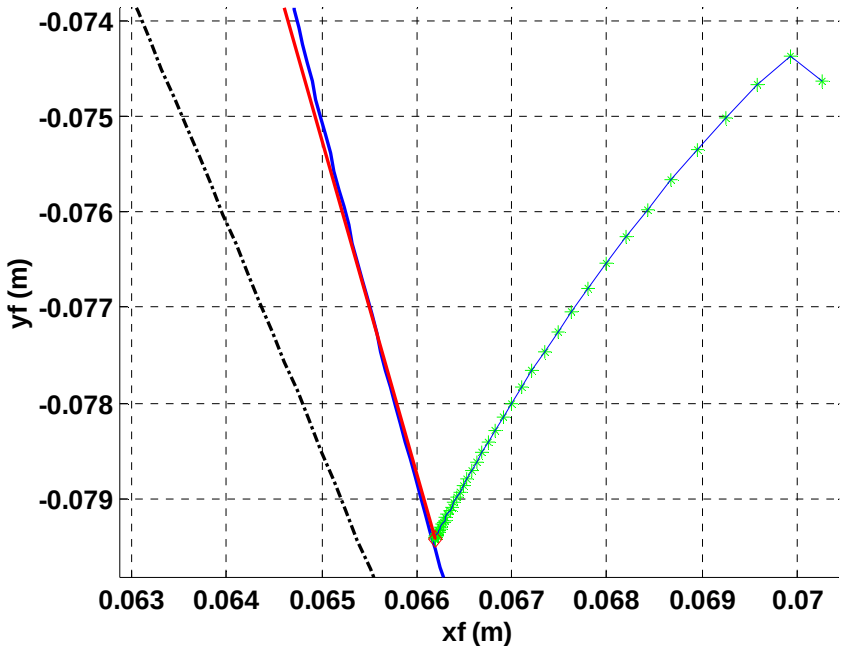

(a) Step size β=0.01, 48 iterations

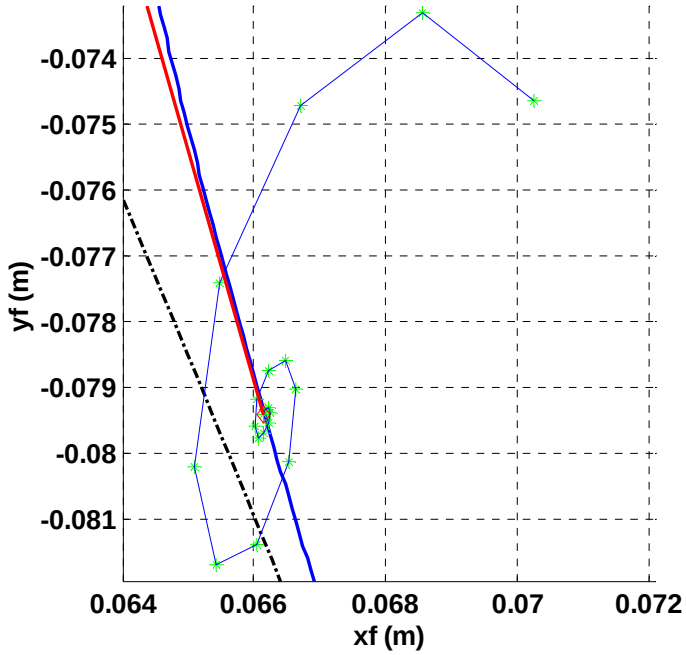

(b) Step size β=0.05, 20 iterations

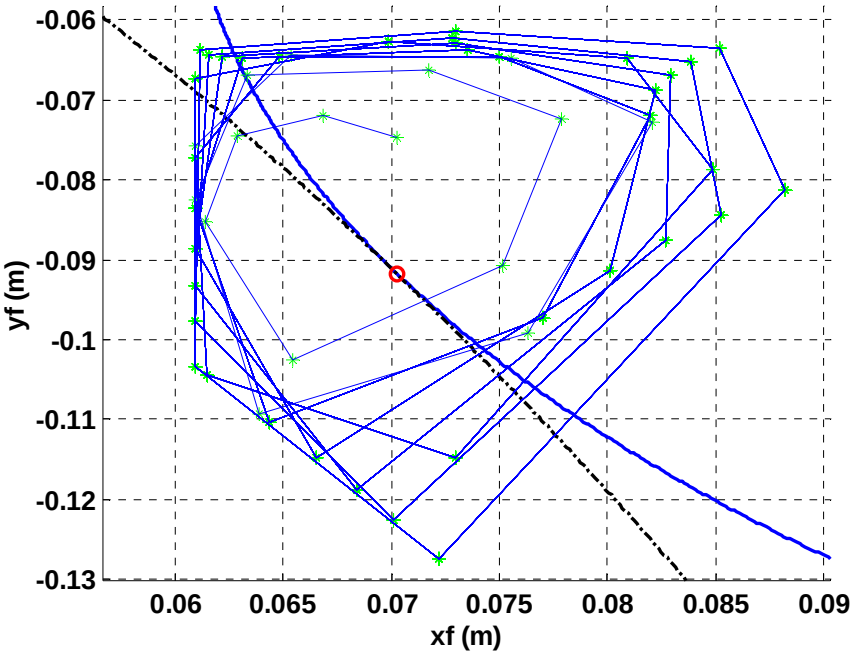

(c) Step size β=0.1, oscillation

Figure 3-7 Effect of the step size β (Case 2)

Discussion

One way to improve the algorithm is to add the slope information to update equation in the flow chart, or to use an adaptive step size, β_a, which can be defined as:

$$\beta_a = \beta / \tan\psi_0 \tag{3.16}$$

where β is a constant, in our case around 0.3, and $\tan\psi_0$ is the slope at the current estimated contact point.

3.4.2 Simulation of Algorithm II

In this section, the finite difference method has been incorporated in the contact model to solve the contact problem. Unlike Algorithm I, the Newton method is used to search for the contact point and other unknowns. The simulation parameters are from Table 3-1, which is also used Algorithm I discussed in last section. Other parameters used only in Algorithm II are listed in Table 3-4 together with the simulation results.

Table 3-3 Simulation parameters and results for Algorithm II

Simulation Parameters	**Case 1**
Unit number in FDM, N	155
Tolerance TOL	0.05
Simulation Results	
Contact point (x_i, y_i) (m)	(0.103, 0.044)
α (°)	44.33
$\lvert F \rvert$ (N)	7.49
ψ_0(°)	34.4
L (mm)	115.8

Compared to Algorithm I, Algorithm II is more complex because it involves the solution to a group of linear equations, especially when a greater unit number is used in

the discretization of the finger. But Algorithm II provides a more accurate solution because it includes a more accurate beam model in its formulation.

As discussed in the FDM contact analysis, Equation (3.15) requires the evaluation of the geometrical moment of inertia and its 1st and 2nd derivatives. They are given in Equations (2.33), (2.33a) and (2.33b) respectively. When decreasing the step size (or increasing the unit number) of FDM, the simulation in MatLAB shows that the solution becomes unstable.

In Figure 3-8, the contact between the finger and the object has been plotted in the finger coordinate system C_f. The stars in the figure are the temporary contact points (also see Figure 3-9) calculated in the recursive process of the Newton method.

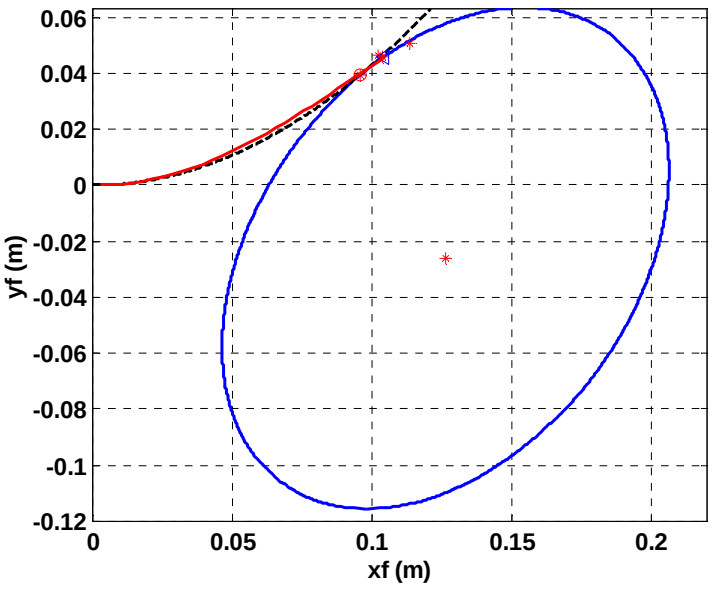

Figure 3-8 Non-uniform deflected finger shape

In Figure 3-9, the finger shapes from the FDM and the Frisch-Fay method are compared. The dotted line is the shape obtained from Frisch-Fay method. The solid line is the shape of the non-uniform finger. The green stars are the temporary contact points calculated from the F-F method and the red from the FDM. The contact force from FDM is 7.49 N, and 8.77 N from the Frisch-Fay methods.

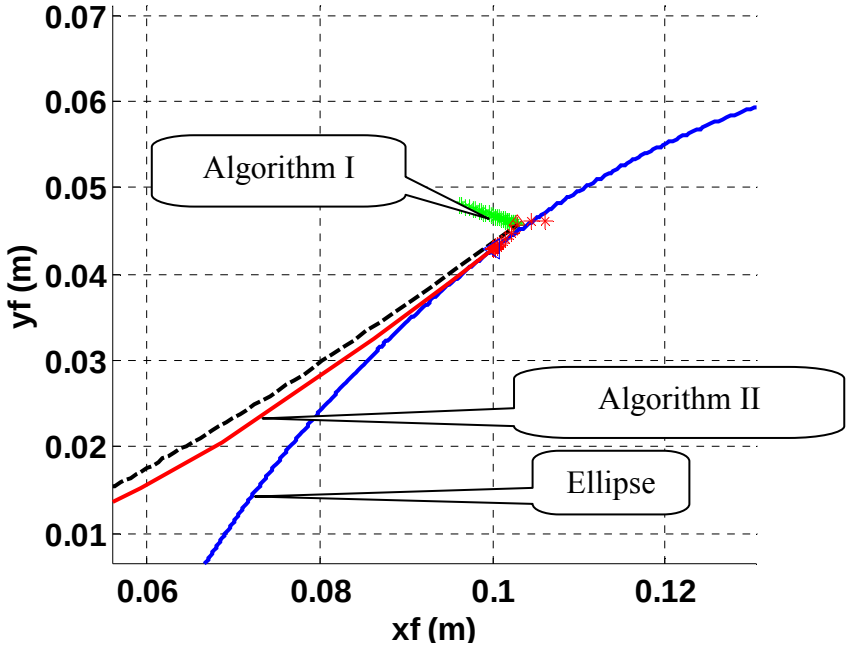

Figure 3-9 Comparison between Frisch-Fay and FDM contact methods

From Equations (2.19), (2.20) and (2.21), the error introduced by FDM is of the order h^2. Other error sources are from Equations (3.13a) and (3.13b) whose integrals are approximated with Simpson's formula. To accurately model the non-uniform finger it is important that the step size used to digitize the beam is small enough. But, in the simulation we found that when the step size, h, is too small, the Newton's method easily

goes unstable. Another problem is the multiple solutions from the highly nonlinear equations system. The system evolves to a fake solution which largely depends on the initial guess of the solution for the Newton's method.

So in the rest of the thesis, the *uniform beam model with effective EI describing the non-uniform property* will be used in the dynamics equation to calculate the contact force. The solution to the FDM contact problem needs a better algorithm.

3.4.3 Contact Model Verification

In this section we validate Algorithm I (approximated uniform finger with an effective EI) experimentally and compare the results against those obtained using finite element method (FEM). Figure 3-10 shows the simulated shape of a flexible finger as it exerts force on the bird using the parameter values listed in Table 3-4

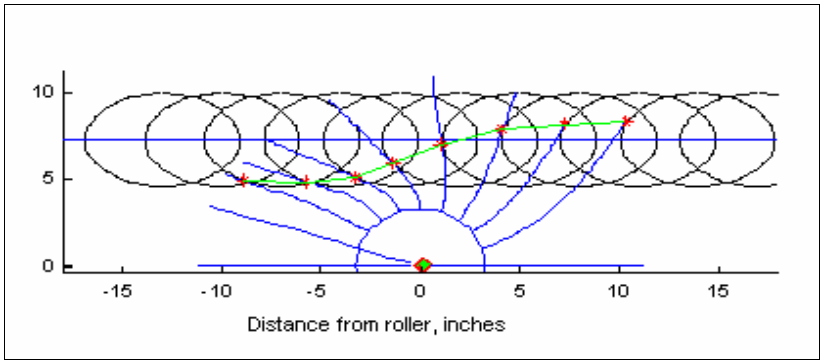

Figure 3-10 Force prediction and deformed finger

Table 3-4 Simulation parameters and values (Ref. Figure 3-1)

Simulation Parameters	Values
Bird's half width along major axis	0.099 m (3.9 inches)
Bird's half width along minor axis	0.067 m (2.65 inches)
Initial Location of the ellipse	X_0=-0.332 m (-13 inches) Y_0=0.184 m (7.25 inches), θ=0˚
Initial angular position of finger	ωt=180˚
Length of finger	0.203 m (8 inches)
Radius of the drum	r= 0.0762 m (2 inches)
Coef. of friction μ, object/finger	0.6041
EI of the rubber finger	0.08 Nm^2
Conveyor speed	0.508 m/s, 20 inches/second
Angular speed of drums	20 rpm
Step size β	0.05
Tolerance ERR	0.5 mm

Results that characterize the contact are given in Table 3-5, which shows that the maximum force acting on the broilers is in the order of 25N.

Table 3-5 Simulated values describing the deflected finger

ϕ(°)	x_i (m)	y_i (m)	ψ_0(°)	$\|\boldsymbol{f}\|$ (N)	α(°)
144	0.1731	0.032	15.7	1.685	105.26
126	0.1029	0.046	35.6	8.77	85.39
108	0.0662	0.040	46.1	23.365	74.88
90	0.0673	0.035	41.1	21.885	79.87
72	0.0959	0.029	25.2	8.055	95.78
54	0.1401	0.031	18.8	2.975	102.17
36	0.1901	0.059	25.7	2.08	95.30
18	0.234	0.119	40.0	1.795	80.92

Finite Element Contact Force Verification

Results of FEA computation [Lee *et al*., 2000] have been used to verify the analytical model for the contact analysis. As in the beam theory, the FEM model is also based on the Bernoulli-Euler beam theory that considers a large deflection analysis on the model. Commercial software, ANSYS will be used in the FEM analysis to verify Algorithm I.

Using ANSYS, the finger is modeled as a 2-D elastic beam element (Beam3), which is a uni-aixal element with tension, compression, and bending capabilities. The element has 3 DOF at each node, translations in the nodal *x*- and *y*-directions and a rotation about the nodal *z*-axis. It has a large deflection analysis capability and the transverse shear strain is nonzero. As for the ellipse, the element type Plane42, a 4-node quadrilateral structural solid with 2 DOF (*x*- axis and *y*- axis), is chosen since the ellipse is constrained and thus, considered fixed in the analysis.

A surface-to-surface contact assumption is used in the ANSYS because our contact is made up of two compliant surfaces. The TARGE169 and CONTA171 were used to define the 2-D contact pair between the finger and the object. The object, which is both stiffer and has markedly larger surface, is chosen as the target surface. The values of the parameters are the same as those of the analytical model given in Table 3-4. Figure 3-11 shows the simulation results of the FEM contact analysis which is applied to the positions that have contact between the flexible finger and moving object. For each position, the contact force in *x*- and *y*- directions can be obtained from FEM; and the

reaction contact forces $\boldsymbol{F}$ are computed and listed in Table 3-6. Figure 3-12 compares the deflected shape of the flexible finger for the FEM and analytical model.

Table 3-6 Contact forces from FEM

X mm (inches)	F_X (N)	F_Y (N)	F (N)	M_Z (N·m)
-254 (-10)	0	0	0	0
-177.8 (-7)	0.495	0.444	0.665	-0.101
-101.6 (-4)	4.935	5.859	7.661	-0.711
-25.4 (-1)	24.381	20.412	31.797	-2.004
50.8 (2)	7.329	29.823	30.710	-1.226
127.0 (5)	5.262	5.646	7.718	-0.462
203.2 (8)	1.442	0.600	1.562	-0.145
254.0 (10)	0.849	0.137	0.860	-0.109
279.4 (11)	0.360	0.137	0.676	-0.122

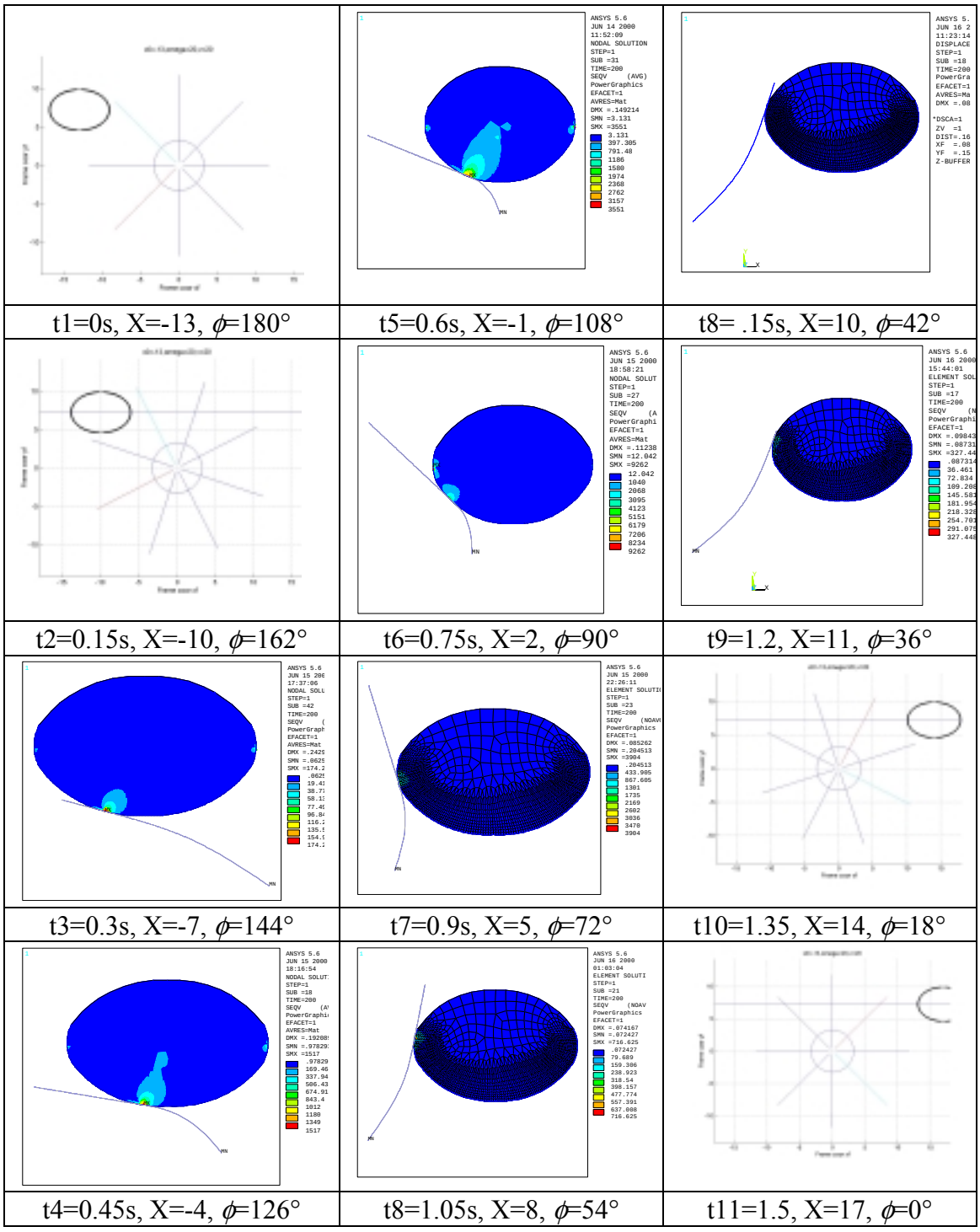

Figure 3-11 Quasi-static FEM contact analysis (*X* in inches)

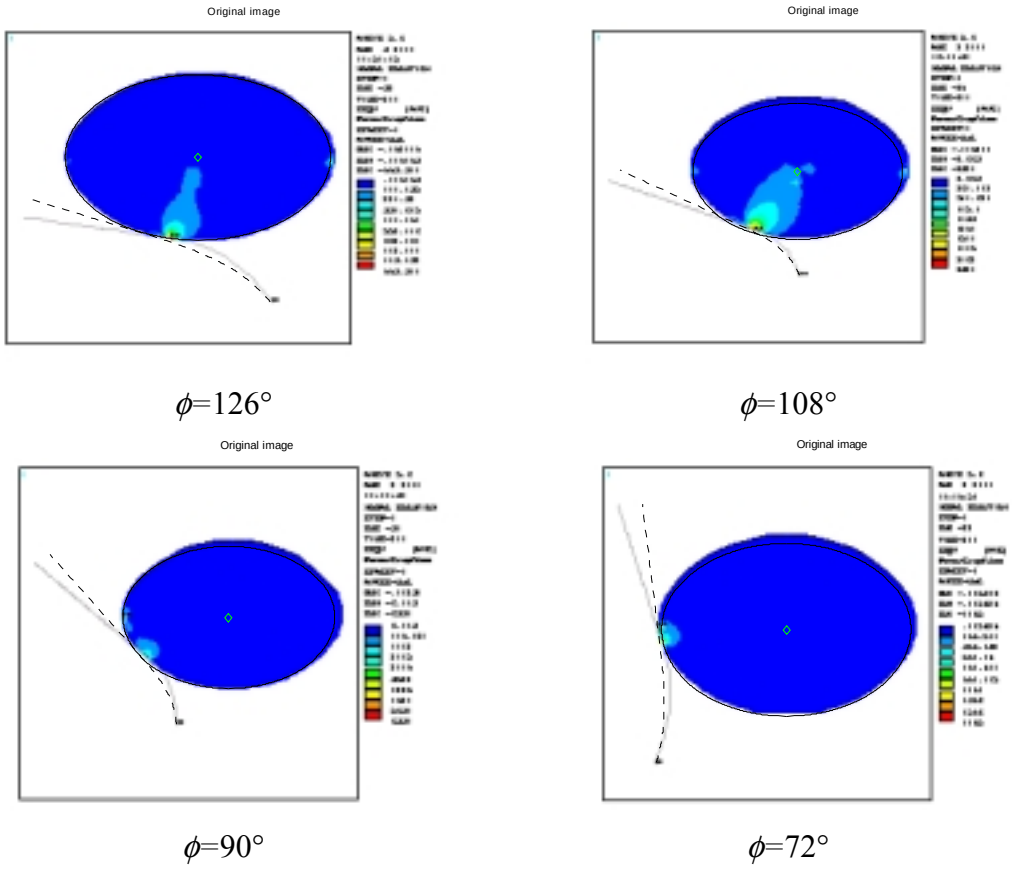

Figure 3-12 Finger shape comparison between analytical model and FEA

Experimental Verification

- Experimental Setup

To verify the finger model, an 8-inch (203.2mm) long finger [Joni, 2000] was chosen for this experiment. An aluminum elliptical cylinder (25mm thick) was fabricated as a model representation of a bird in the plane of the rotating finger [Lee *et al.*, 2000]. As shown in Figure 3-13, the elliptical object was mounted on a 6-DOF-force/torque transducer to deduce the force/torque at the contact between the fingers and object. The object was positioned at a specific position from drum. At each position, the force/torque

data as a function of time were recorded as the drum rotates at a specified speed, and the contact force between the finger and the object were then computed from the equation of static mechanics.

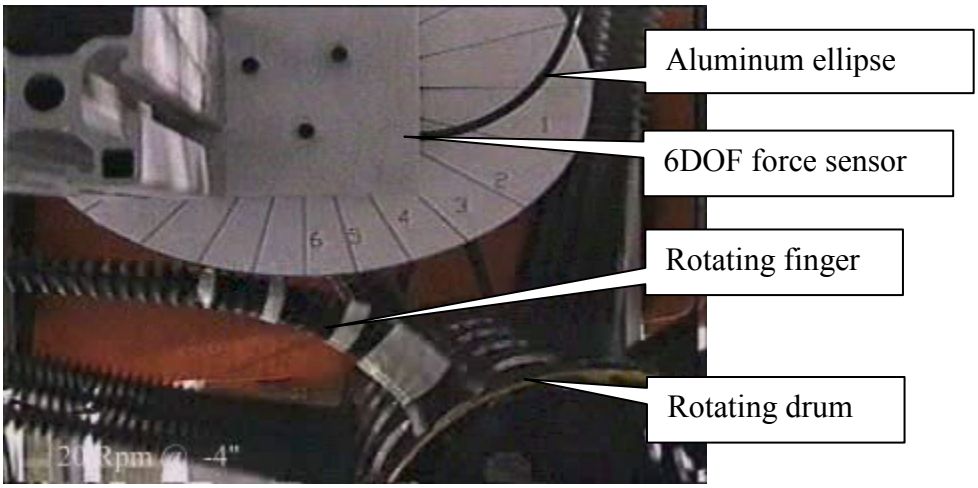

Figure 3-13 Experiment setup

- Experiment Results

The force on the object (moving along *X* direction) was measured for a range of angular speeds typically used in dynamics grasping. Figures 3-14 and 3-15 show a sample plot of force trajectory obtained experimentally. Figure 3-14, which plots the measured forces on the object at X_0=-25mm for 5 different angular speeds (15, 20, 22, 24, 25rpm), shows that the *finger dynamics do not have significant effects on the contact forces* for the range of speeds up to 25rpm. The similarity in the force curve suggests that for a relatively slow constant drum speed, the force acting on the object is primarily a function of the finger deflection and that the contact mechanics can be determined quasi-statically. Figure 3-14 shows the measured force as a function of the fingers' angular position for five different values of X_0 at a constant speed of 20rpm.

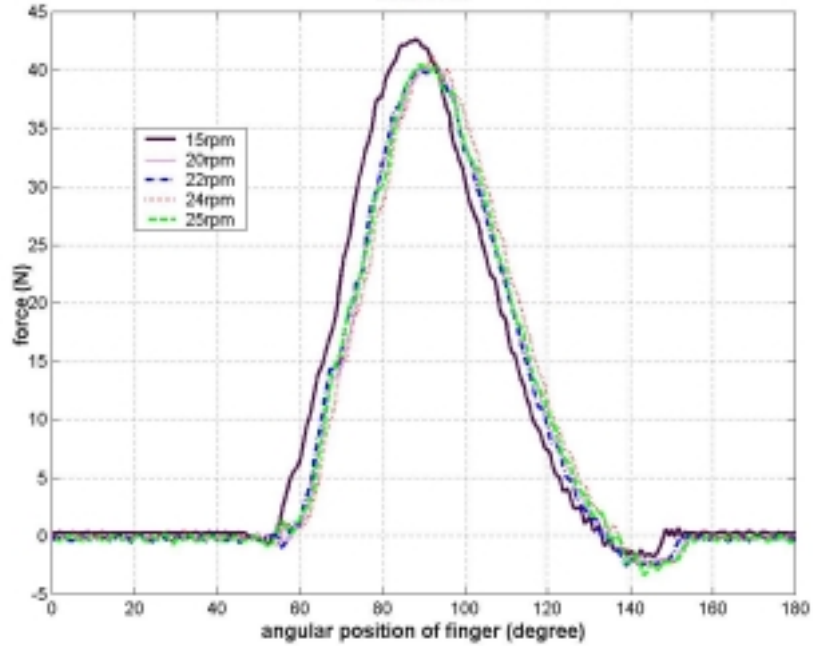

Figure 3-14 Different angular velocities at X0=-25mm

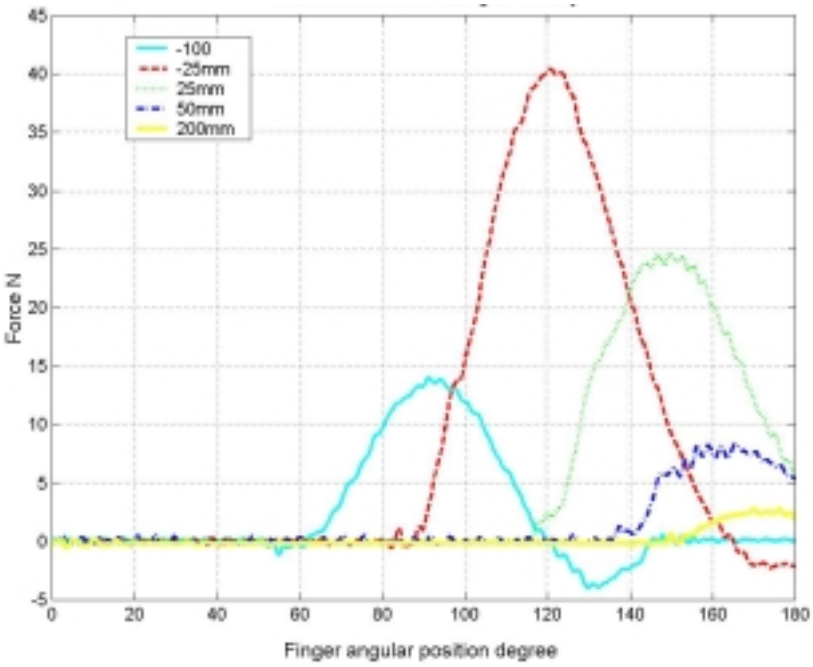

Figure 3-15 Different X0 at a constant speed of 20rpm

Figure 3-16 compares the computed shape of the deflected finger against the shape found in the images captured experimentally for four different instants highlighted (shaded in gray) in Table 3-6.

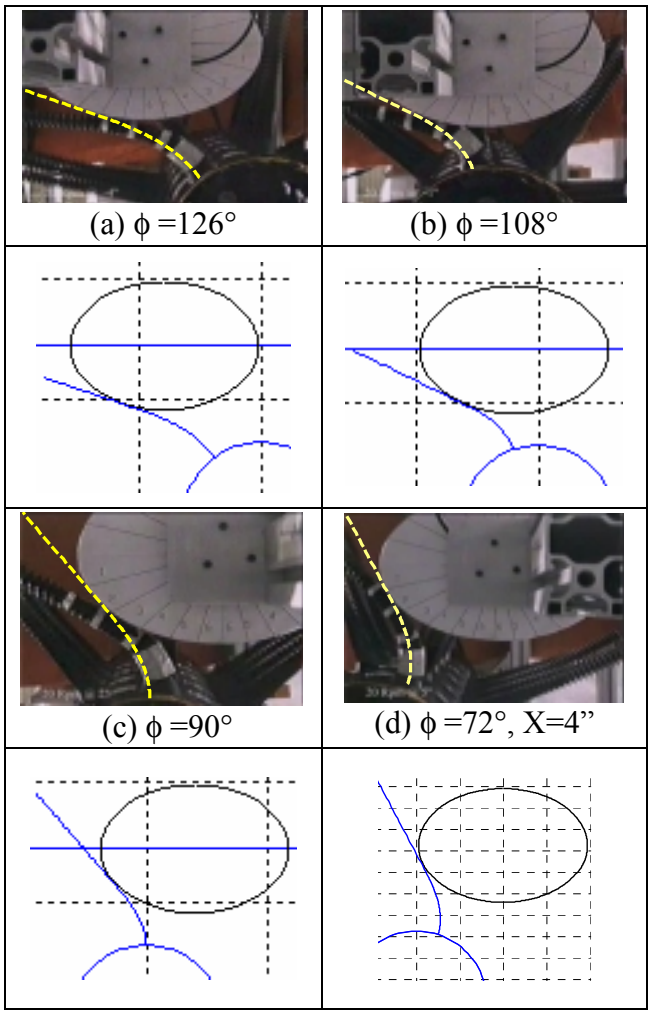

Figure 3-16 Comparison between analytical model and experiment

Contact Force Comparisons

The results of the analytical model are compared against those from both the experimental and FEM data for the motion trajectory shown in Figure 3-10. In Figure 3-17, contact forces from the analytic model, FEM computation and the experiment are

plotted. Figure 3-17 shows that the analytical contact model can predict contact forces that are close to those obtained from both FEM and experiment.

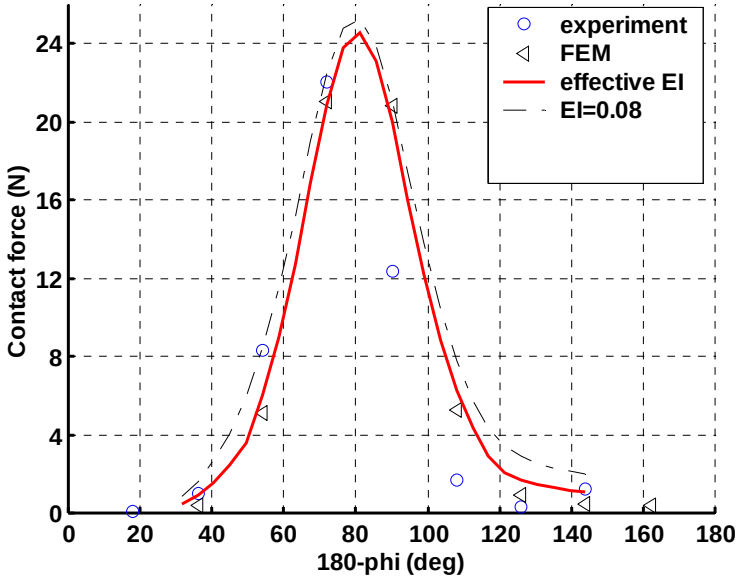

Figure 3-17 Contact force comparison

3.5 Summary

In this chapter the model to predict the contact force, which is on an object by the non-uniform compliant finger, have been presented. Two algorithms, the uniform approximation with effective EI and the FDM, to solve the non-uniform contact equations have been discussed and simulated. The Algorithm I, built upon the Frisch-Fay flexible bar theory for the uniform beam, provides an approximate closed–form solution for determining the contact points and forces. The Algorithm II in which FDM method is used to model the non-uniform beam easily goes unstable. So in the rest of the thesis the

uniform beam contact analysis together with the effective *EI* will be used in the dynamics analysis of the compliant grasper.

The contact model has been verified by experiments and FEM. The comparison results show that the contact model developed in this chapter is valid and can be used in the dynamics analysis when the drum rotates at a low angular velocity around 25rpm.

In the next chapter, on the basis of the uniform beam contact analysis presented in this chapter, a dynamic model describing the live bird grasping system will be developed.

CHAPTER IV

DYNAMICS ANALYSIS

To facilitate design of a dynamic grasper consisting of soft fingers, there is a need for a good understanding of grasping dynamics, to be used in cost-effective design and control of a high-speed compliant grasper. The objective of this chapter is to develop a dynamic model capable of predicting the motion of the bird under compliant grasping.

In the previous chapters, the finger deflections and the contact prediction between a moving object and a rotating finger have been discussed. From the experiment we found that the *finger dynamics do not have significant effects on the contact forces* for the range of speeds up to 25rpm. Therefore, the contact force calculation in a 3-D space will be searched quasi-statically in the 3-D grasping dynamics equation developed in this chapter. In other words, the dynamics, such as damping, of the finger is ignored. The compliance of the object, compared to the effects of finger stiffness on the finger force, can be ignored also. Specifically, the functions of a finger in the grasping, pull or push, are discussed. A symmetric case of the 3-D dynamics model for the high speed transfer system is used as an example to illustrate the contact model developed in this thesis. Finally numerical algorithm for the dynamics simulation is presented.

4.1 Formulation of grasping Dynamics model

For the purpose of analyzing the grasping dynamics, the system is considered to consist of three basic components as shown in Figure 4-1; namely, the bird, the rotating finger, and the conveyor. The model developed in the following section incorporates the following simplifying assumptions:

(1) The contact force is calculated quasi-statically in the 3-D grasping. In other words, the dynamics (such as damping) of the finger is neglected.

(2) The effect of the compliance (object) on contact force is negligible as compared to the stiffness of finger.

(3) Since the bird sits on the conveyor initially, we model it as an ellipsoid which includes the mass of the legs.

(4) The object rolls with slip on the conveyor surface resulting in friction forces, F_x and F_y, at the interface.

(5) The grasping process is relatively fast such that the bird does not have time to react.

In Figure 4-1, the reference coordinate C_w (XYZ) is attached at the mid-point between the two drum axes on the conveyor such that the X-axis has the same direction as the conveyor motion. The coordinate frame C_b (xyz), describes the position and orientation of the bird with respect to the reference coordinate frame C_w.

The coordinate system C_d ($X_DY_DZ_D$) is fixed as shown in Figure 4-1(a), which accounts for the inclination of the drum. The XZ and X_DZ_D are parallel and the drum is

inclined at an angle α_r from the conveyor surface as shown in Figure 4-1(b). The C_{fi3} ($x_{fi3}y_{fi3}z_{fi3}$) frame is a rotating coordinate frame (about the Z_D axis) fixed at the base of the i^{th} finger, where the positive x_{fi3}-axis points along the axis of the un-deformed finger.

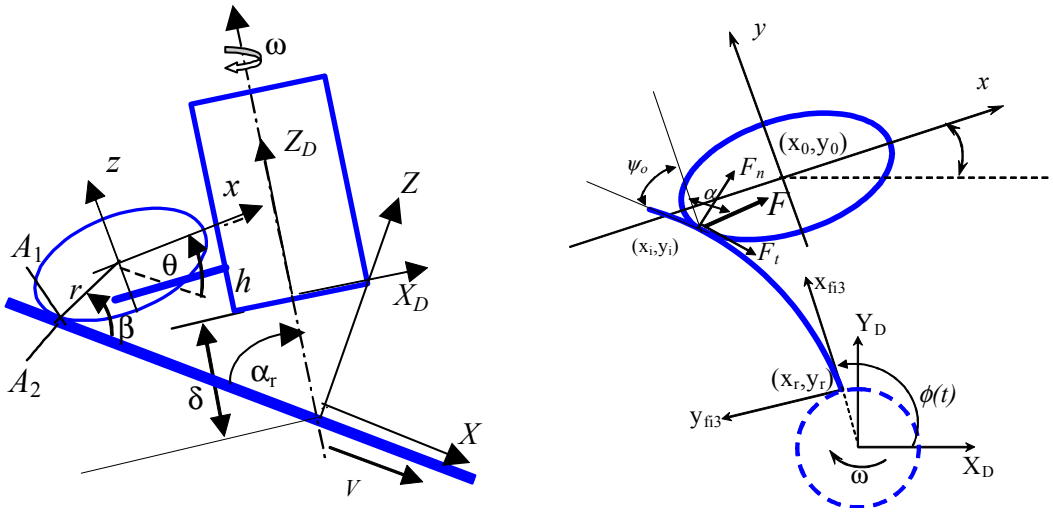

(a) Coordinate frames (b) Finger/bird interaction

Figure 4-1 Coordinate system definition

The following assumptions are made in deriving the dynamic model:

(1) The surface boundary of the object being grasped can be represented as a continuous function in 3-D space with convex and first order differential properties. As will be shown later, these properties are required for the computation of the compliant forces.

(2) As discussed in Chapter 3, the finger is flexible in its x_{fi3}- y_{fi3} plane but rigid in its x_{fi3}- z_{fi3} plane.

(3) As discussed in Chapter 3, the deflection of the rotating finger is solved quasi-statically in the grasping process.

(4) As shown in Figure 4-2, the bird sits on the conveyor initially such that its legs are represented as a lump-parameter model (its mass included in m). In addition, the object rolls with slip on the conveyor surface resulting in friction forces, F_x and F_y, at the interface.

(5) The grasping process is very fast such that the bird does not have time to react.

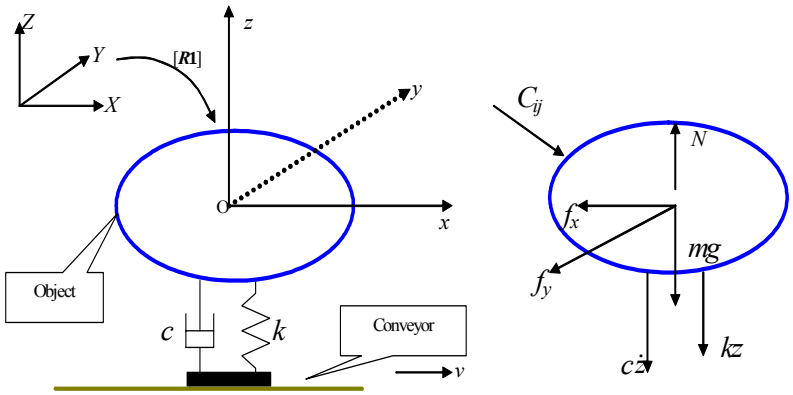

Figure 4-2 Grasping modeling and free body diagram

Based on the above assumptions, the equations of motion for the object are given in Equations (4.1a) and (4.1b) in C_w:

$$\begin{Bmatrix} Q_X \\ Q_Y \\ Q_Z \end{Bmatrix} = m \begin{Bmatrix} \ddot{X}_b \\ \ddot{Y}_b \\ \ddot{Z}_b \end{Bmatrix} \tag{4.1a}$$

where m is the mass of the object; (X_b, Y_b, Z_b) describes the mass center of the bird in C_w; and Q_X, Q_Y and Q_Z are the sum of the external forces acting on the bird along the X-, Y- and Z- axes in C_w.

$$\begin{Bmatrix} T_X \\ T_Y \\ T_Z \end{Bmatrix} = [I]_W \overline{\alpha} + \begin{bmatrix} 0 & -\omega_Z & \omega_Y \\ \omega_Z & 0 & -\omega_X \\ -\omega_Y & \omega_X & 0 \end{bmatrix} [I]_W \overline{\omega} \,. \tag{4.1b}$$

where T_X, T_Y, and T_Z are the sum of the moments contributed by the external forces about the axes in C_w; and the inertia matrix $[I]_W$ can be written in terms of the inertia matrix $[I]_b$ as follows:

$$[I]_W = [R1]^T \begin{bmatrix} I_x & 0 & 0 \\ 0 & I_y & 0 \\ 0 & 0 & I_z \end{bmatrix} [R1] \tag{4.2}$$

where I_x, I_y, and I_z are the moment of inertia of the object along its principal axes in C_b; $[R1]$ is the rotational transformation matrix describing the orientation of the object with respect to C_w. In terms of *ZYZ* Euler angles (θ, ψ, ϕ), the matrix $[R1]$ is given by [Ginsberg, 1999]:

$$[R1] = \begin{bmatrix} \cos\psi\cos\phi\cos\theta - \sin\phi\sin\psi & \cos\phi\cos\theta\sin\psi + \sin\phi\cos\psi & -\cos\phi\sin\theta \\ -\sin\phi\cos\theta\cos\psi - \cos\phi\sin\psi & -\sin\phi\cos\theta\sin\psi + \cos\phi\cos\psi & \sin\phi\sin\theta \\ \sin\theta\cos\psi & \sin\theta\sin\psi & \cos\theta \end{bmatrix} \tag{4.3}$$

In Equation (4.1b), the angular velocity of the object in C_w is given by

$$\overline{\omega} = \begin{Bmatrix} \omega_X \\ \omega_Y \\ \omega_Z \end{Bmatrix} = \begin{Bmatrix} -\dot{\theta}\sin\psi + \dot{\phi}\sin\theta\cos\psi \\ \dot{\phi}\sin\theta\sin\psi + \dot{\theta}\cos\psi \\ \dot{\psi} + \dot{\phi}\cos\theta \end{Bmatrix} \tag{4.4}$$

and the angular accelerations of the object in C_w can be expressed as

$$\bar{\alpha} = \begin{Bmatrix} \alpha_{xb} & \alpha_{yb} & \alpha_{zb} \end{Bmatrix} [R1] \begin{Bmatrix} \bar{I} \\ \bar{J} \\ \bar{K} \end{Bmatrix} \tag{4.5}$$

where $\bar{I}, \bar{J}, \bar{K}$ are unit vectors along the *X*-, *Y*- and *Z*-axis in $C_{w.}$; the accelerations in C_b is given by

$$\begin{Bmatrix} \alpha_{xb} \\ \alpha_{yb} \\ \alpha_{zb} \end{Bmatrix} = \begin{Bmatrix} -\sin\theta\cos\phi & \sin\phi & 0 & -\cos\theta\cos\phi & \sin\theta\sin\phi & \cos\phi \\ \sin\theta\sin\phi & \cos\phi & 0 & \cos\theta\sin\phi & \sin\theta\cos\phi & -\sin\phi \\ \cos\theta & 0 & 1 & -\sin\theta & 0 & 0 \end{Bmatrix} \bar{\alpha}_v ; \tag{4.6a}$$

and

$$\bar{\alpha}_v = \begin{Bmatrix} \ddot{\psi} & \ddot{\theta} & \ddot{\phi} & \dot{\psi}\dot{\theta} & \dot{\psi}\dot{\phi} & \dot{\theta}\dot{\phi} \end{Bmatrix}^T . \tag{4.6b}$$

Substituting Equation (4.6) into Equation (4.5), the angular acceleration components in C_w can be expressed in terms of *ZYZ* Euler angles as

$$\bar{\alpha} = \begin{bmatrix} \cos\psi\cos\phi\cos\theta - \sin\phi\sin\psi & \cos\phi\cos\theta\sin\psi + \sin\phi\cos\psi & -\cos\phi\sin\theta \\ -\sin\phi\cos\theta\cos\psi - \cos\phi\sin\psi & -\sin\phi\cos\theta\sin\psi + \cos\phi\cos\psi & \sin\phi\sin\theta \\ \sin\theta\cos\psi & \sin\theta\sin\psi & \cos\theta \end{bmatrix}^T$$

$$\begin{Bmatrix} -\sin\theta\cos\phi & \sin\phi & 0 & -\cos\theta\cos\phi & \sin\theta\sin\phi & \cos\phi \\ \sin\theta\sin\phi & \cos\phi & 0 & \cos\theta\sin\phi & \sin\theta\cos\phi & -\sin\phi \\ \cos\theta & 0 & 1 & -\sin\theta & 0 & 0 \end{Bmatrix} \begin{Bmatrix} \ddot{\psi} \\ \ddot{\theta} \\ \ddot{\phi} \\ \dot{\psi}\dot{\theta} \\ \dot{\psi}\dot{\phi} \\ \dot{\theta}\dot{\phi} \end{Bmatrix} . \tag{4.7}$$

Equations (4.1a) and (4.1b) describe the dynamics of the bird, where the angular velocity and acceleration of the bird are given in Equations (4.4) and (4.7) respectively; and the moment of inertia in C_w can be found from Equation (4.2) along with Equation (4.3). To solve the motion trajectory (both the position and the orientation) of the bird

under grasping, the forces exerted by the fingers on the bird and the reaction force from the conveyor surface on which the bird initially sit must be determined. These ODE's are highly coupled and nonlinear, particularly that the contact force are position dependent. In following sections, we derive the object/conveyor interface and the contact forces from the compliant fingers. Once the forces are solved, the moments due to these forces can be written.

4.2 Object/conveyor interface

The bird body (ellipsoid) could roll and slip over the conveyor surface during the process of grasping, which imposes a non-holonomic constraint on the motion of the bird. The friction forces, F_x and F_y, and the normal force N act at the contact point A.

The fact that the contacting surfaces cannot penetrate each other imposes a restriction on the velocity components perpendicular to the plane of contact (that is, the tangent plane or the surface of the conveyor). The two constraints are given by Equations (4.8) and (4.9):

$$N \geq 0 \tag{4.8}$$

and

$$\overline{V}_{A1} \bullet \overline{K} = \overline{V}_{A2} \bullet \overline{K} \tag{4.9}$$

where V_{A1} and V_{A2} are the velocities at points A_1 and A_2 on the object and the conveyor respectively; and $\overline{K}$ is the unit vector along the positive Z axis.

The friction forces generated at the interface are proportional to the supporting normal force N from the conveyor at the bird/conveyor contact, and hence we have:

$$F_x = -\text{sgn}(V_{A1x} - V_{A2x})N\mu \tag{4.10a}$$

$$F_y = -\text{sgn}(V_{A1y} - V_{A2y})N\mu \tag{4.10b}$$

where (V_{A1x}, V_{A1y}) and (V_{A2x}, V_{A2y}) are the velocities of the object and the conveyor in C_w respectively; and sgn(x) is the signum function:

$$\text{sgn}(x) = x/|x|, \text{if } x \neq 0; \tag{4.11}$$

4.3 Object/finger interface

In Chapter 3, the calculation of the contact force between a finger and a 2-D object has been discussed, which is now extended to predict the contact force of multiple rotating fingers on a 3-D object. What we need is to obtain the intersecting plane formed by the rotating finger and the ellipsoid as shown in Figure 4-3, which provides a basis to describe the object in C_{fi3} so that the contact point can be solved using techniques discussed in Chapter 3.

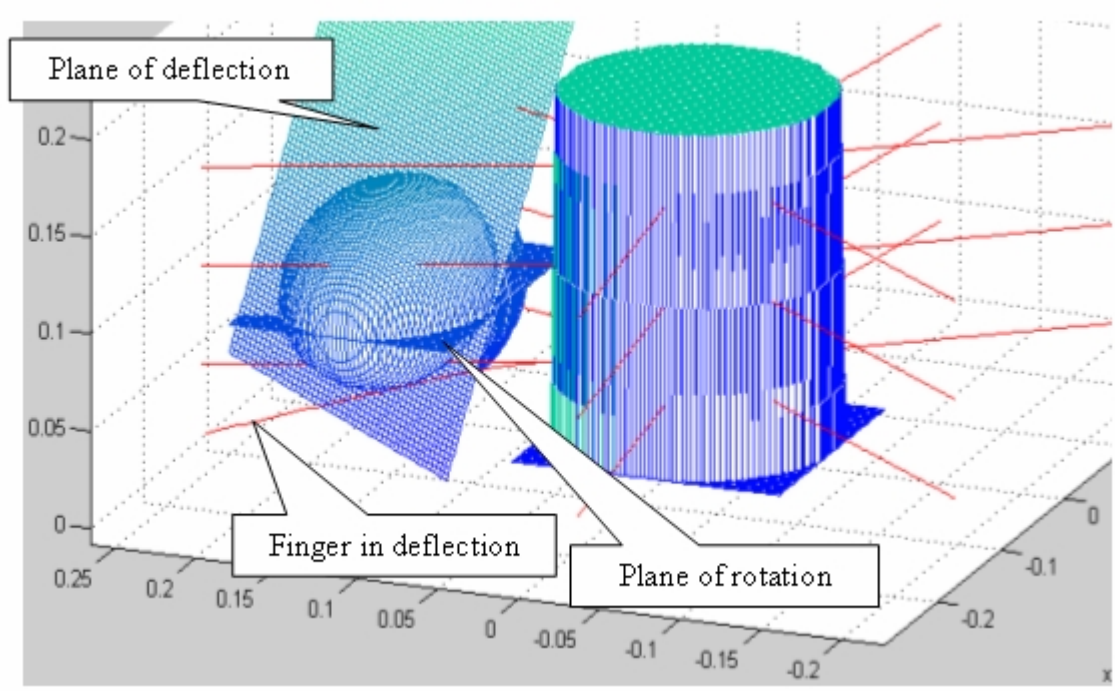

Figure 4-3 3-D contact force acting plane

4.3.1 Coordinate transformations

To facilitate the discussions, we define the following rotational matrixes for describing the coordinate transformations:

[$R1$]: transformation from C_b to C_w as defined in Equation (4.3),

[$R2$]: transformation from C_d to C_w, and

[$R3$]: transformation from C_{fi3} to C_d,

and the origins of the respective coordinate frames in C_w:

P_{b0} : origin of C_b in C_w,

P_{d0}: origin of C_d in C_w

P_{fi0}: origin of C_{fi3} at the base of the i^{th} finger in C_w.

Based on the above definitions, we have

(1) the coordinate transformation from C_b to C_w

$$P_{bw} = [R1]^{\mathrm{T}} P_b + P_{b0} \tag{4.12}$$

where $P_b = (x, y, z)^T$ and $P_{bw} = (X, Y, Z)^T$ are the position vectors describing a point on the object with respect to C_b and C_w respectively.

(2) The coordinate transformation from C_d to C_w

$$P_{dw} = [R2]P_d + P_{d0} \tag{4.13}$$

where

$$P_{d0} = (\delta - h)\begin{pmatrix} -\cos\alpha_r & 0 & \sin\alpha_r \end{pmatrix}^T; \tag{4.13a}$$

$$[R2] = \begin{bmatrix} \cos\alpha_y & 0 & -\sin\alpha_y \\ 0 & 1 & 0 \\ \sin\alpha_y & 0 & \cos\alpha_y \end{bmatrix}^T; \tag{4.13b}$$

$$\alpha_y = -\frac{\pi}{2} + \alpha_r . \tag{4.13c}$$

where $P_d = (x_d, y_d, z_d)^T$ and $P_{dw} = (X, Y, Z)^T$ are the position vectors describing a point on the drum with respect to C_d and C_w respectively; h is the height of the base point of the finger measured from the bottom of drum; δ is the distance between the origin of the C_d and the origin of the C_w.

(3) The coordinate transformation from C_{fi3} to C_d

$$P_d = [R3]P_{fi3} + P_{fi0} \tag{4.14}$$

where $P_{fi3} = (x_{fi3}, y_{fi3}, z_{fi3})^T$ is the position vector describing a point in C_{fi3}; and the rotation matrix [$R3$]

$$[R3] = [R_z(\phi_f)]^T [R_y(\phi_y)]^T [R_x(\phi_x)]^T \tag{4.14a}$$

and origins of the C_{fi3} in C_d, P_{fi0}

$$P_{fi0} = [R_z(\phi_f)]^T P_{fi10}; \tag{4.14b}$$

are derived in detail in Appendix A.

4.3.2 Ellipsoid in finger coordinate

In this section we discuss how to obtain the deflection plane of the finger for the contact force calculation. The surface boundary of the object is approximated by an ellipsoid, which can be mathematically presented in C_b as

$$f(x, y, z) = P_b^T [B] P_b - 1 = 0 \tag{4.15}$$

where

$$B = \begin{bmatrix} \frac{1}{\eta^2} & 0 & 0 \\ 0 & \frac{1}{\lambda^2} & 0 \\ 0 & 0 & \frac{1}{\gamma^2} \end{bmatrix} \tag{4.15b}$$

and η, λ, and γ are the characteristic dimensions of the bird along the *x*-, *y*- and *z*-axes of C_b.

Like those transformations derived in last section, the relationship between the bird coordinate frame C_b and the rotating finger frame C_{fi3} can be expressed in Equation (4.16):

$$P_b = [R_{\text{bfi}}]P_{fi3} + P_{bfi0} \tag{4.16}$$

where

$$[R_{bfi}] = [R1][R2][R3] \tag{4.16a}$$

$$P_{bfi0} = [R1][R2]P_{fi0} + [R1](P_{d0} - P_{b0}) \tag{4.16b}$$

For the contact force calculation the object surface function described in Equation (4.15) needs to be expressed in the final finger coordinate system, C_{fi3}. Substituting Equation (4.16) into Equation (4.15) we have

$$f(x_b, y_b, z_b) = \left[[R_{bfi}]P_{fi3} + P_{bfi0}\right]^T [B]\left[[R_{bfi}]P_{fi3} + P_{bfi0}\right] - 1 = 0 \tag{4.17}$$

and after some algebraic operations, Equation (4.17) is simplified as

$$f(x_{fi3}, y_{fi3}, z_{fi3}) = {P_{fi3}}^T M_{bfi} P_{fi3} + B_{bfi} P_{fi3} + K_{bfi} = 0, \tag{4.18}$$

where

$$M_{bfi} = [R_{bfi}]^T [B][R_{bfi}]; \tag{4.18a}$$

$$B_{bfi} = P_{bfi0}[B][R_{bfi}] + {P_{bfi0}}^T [B]^T [R_{bfi}]^T; \tag{4.18b}$$

and

$$K_{bfi} = {P_{bfi0}}^T [B] P_{bfi0} - 1. \tag{4.18c}$$

Equation (4.18) can be rewritten as Equation (4.19).

$$f(x_{fi3}, y_{fi3}, z_{fi3}) = 0. \tag{4.19}$$

To get the ellipse equation or to say, the intersection between the force acting plane and the ellipsoid, let $z_{fi3}=0$ in Equation (4.19) and the resulting Equation (4.20) is used in the force prediction analysis.

$$f(x_{fi3}, y_{fi3}, z_{fi3})\Big|_{Z_{fi3}=0} = 0 \tag{4.20}$$

If the object is approximated as an ellipsoid, Equation (4.20) essentially is an ellipse, and can be expanded in the form of Equation (3.6) using a procedure discussed in Section 3.1. The algorithm, which is presented and applied in 2-D case, is used to solve the 3-D problem here with the assumption that the finger has deformation only in its *x*-*y* plane. The resultant contact force will be treated as an input force in the dynamics analysis.

4.3.3 Finger functions in grasping: Pull or Push

Figure 4-5 shows two fingers grasping a 2D object that moves to the right at a constant speed while the drum rotates in the clockwise direction. The left red (finger #2) finger pushes the object forward while the blue finger (finger #1) pulls the object backward. The effect of the fingers on the object can be divided into two cases, push or pull. The former (finger #2) *pushes* the object forward and the latter (finger #1) *pulls* the object back resulting in a grasp on the object. The push and pull, an important property to be considered when configuring the grasper, influences the force exerted on the object, hence the dynamics of the bird.

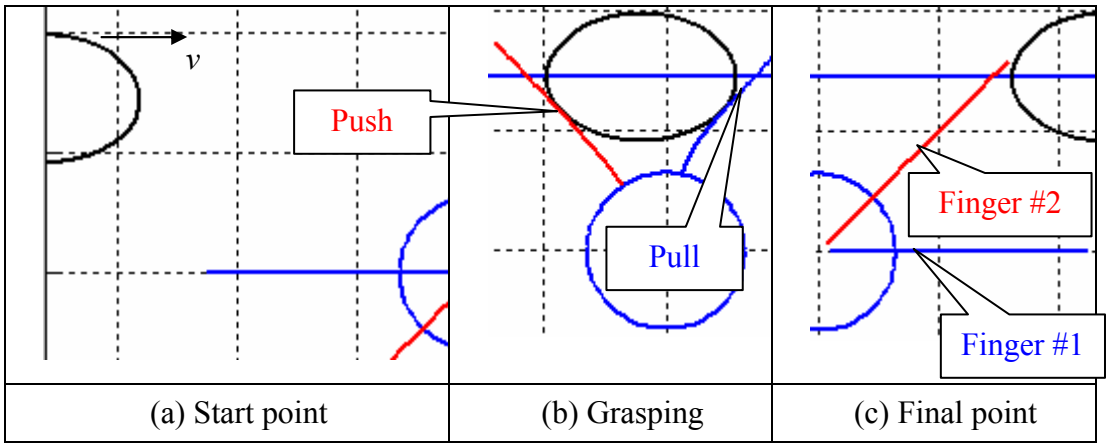

Figure 4-4 Illustration of the push and pull concept

Here we give the strict definitions for the concept of pull and push, which are required by the contact formulation. The definition is on the basis of the finger coordinate system C_{fi} ($x_{fi}y_{fi}z_{fi}$).

- Push: If the potential deformation is in the positive y_{fi} area, the function of this finger is defined as *push.*

- Pull: If the potential deformation of the finger is in the negative y_{fi} area, the function of the finger is defined as *pull*.

Figure 4-5 compares the two cases and illustrates the concepts of pull and push. Note that the primary difference is the direction of the force exerted by the finger (n=1 or 2) on the bird. More specifically, the pushing finger (n=2) results in a positive deflection. For the pulling, the slope at the contact point between the elliptic and the pulling finger (n=1) is negative.

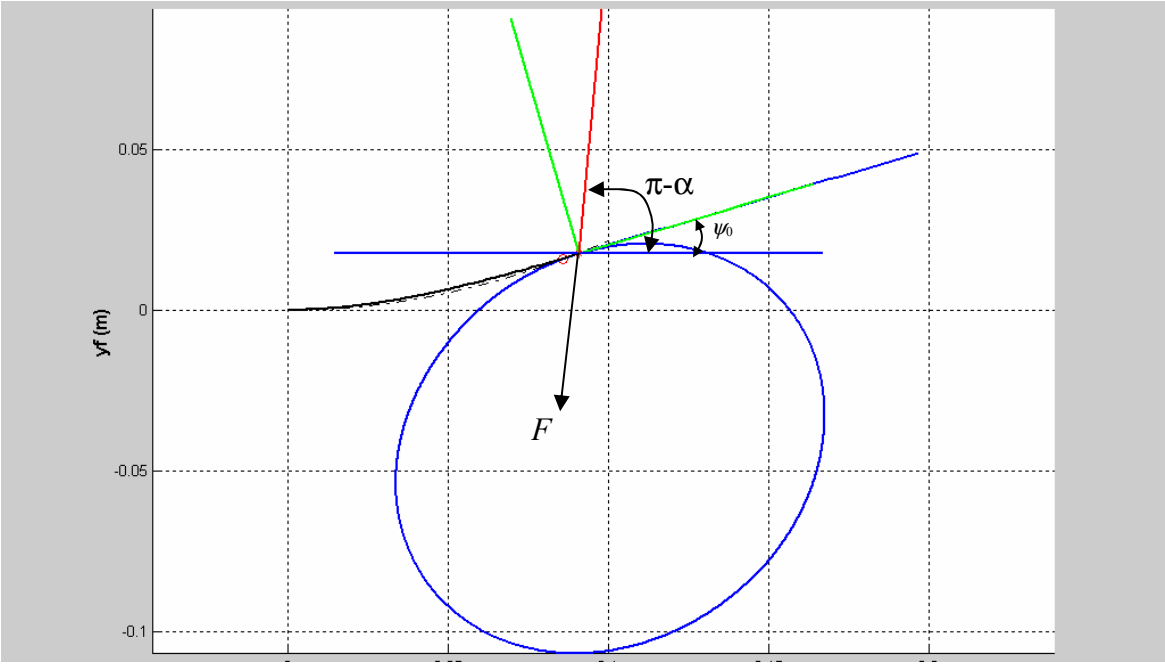

(a) Finger #1 pushing the object

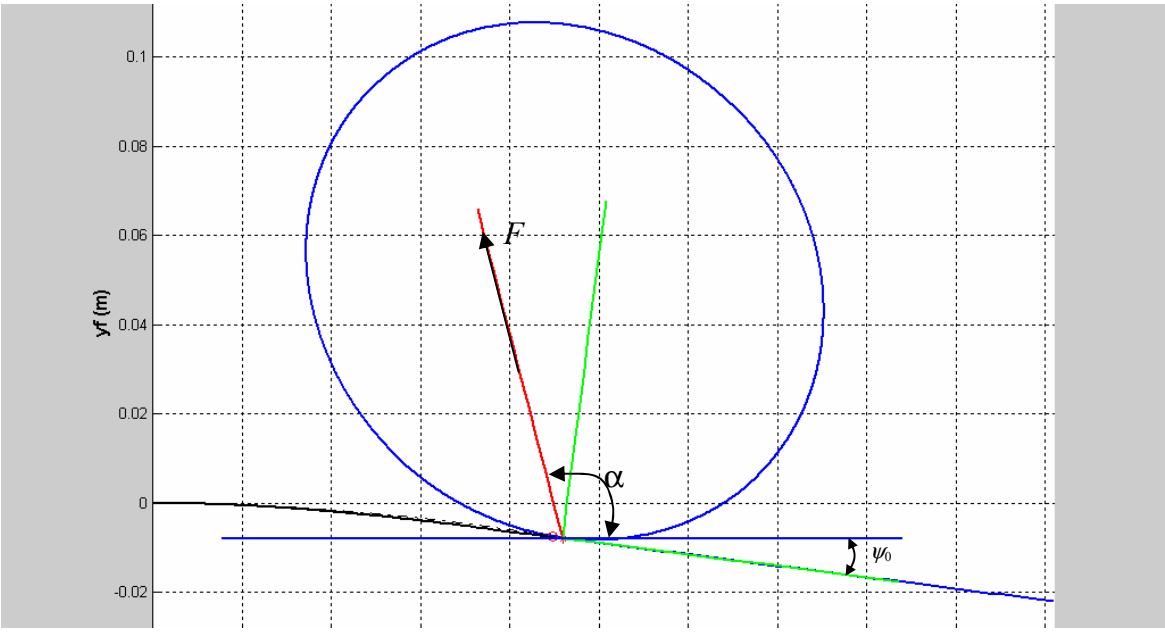

(b) Finger #2 pulling the object

Figure 4-5 Comparison between pull and push

The numerical recursive algorithm keeps the same flowchart structure as described in Figure 3-2 for the pulling case except that a few sign changes are required to get the correct contact information. Thus, Equation (3.4) that characterizes the slope at the contact point is written as

$$(-1)^n \frac{\partial f_e(x,y)/\partial x}{\partial f_e(x,y)/\partial y}\Big|_{(x=x_i,y=y_i)} = \tan(\pi + \psi_0) \tag{4.21}$$

Similarly, the initial approximation of the finger

$$y_f = (-1)^n a x_f^2; \tag{4.22}$$

$$(-1)^{n-1} 2a x_f = \frac{2b_1 x_f + b_3 y_f + b_4}{2b_2 y_f + b_3 x_f + b_5}; \tag{4.23}$$

and the equations in the computation flow chart (Figure 3-2) to update the x and y coordinate of the contact point

$$x_i = x_i - \beta y_{error} \tag{4.24}$$

and

$$y = (-1)^n \frac{1}{k}[2p\cos\alpha(\cos\varsigma - \cos\xi) + h(\psi_o)\sin\alpha] \tag{4.25}$$

In Figure 4-6, the contact force F_{f2o} (from the finger to the object) presented in the finger coordinate system is

$$F_{f2o} = (-1)^{n-1} F[R2][R3][\cos\pi \quad \sin\alpha \quad 0]^T \tag{4.26}$$

where the force in the z_f- direction is assumed to be 0; and F is the magnitude of the contact force; $[R2]$ and $[R3]$ were defined in Equation (4.13b) and (4.14a) respectively.

The resultant contact forces are used as inputs in solving the dynamic grasping problem.

4.4 Symmetric grasping

When the bird is grasped by a pair of symmetric finger systems such that the grasper is symmetric about an *XZ* plane, we may neglect the translation in *Y*-direction and the rotations about *X*- and *Z*- axes. Symmetric grasping can be commonly realized by operating the two drums (that house the flexible fingers) at the same speed in opposite directions. In addition, the bird entering the grasper tends to sit in a relatively dark environment [Lee, *et al.*, 2000], and can be constrained between two panels. For these reasons, we focus on analyzing the (X, Z,θ) motion of the bird as shown in Figure 4-6. On the above bases, Equations (4.1a) and (4.1b) can be reduced to

$$m\ddot{X} = Q_X - F_X \tag{4.27}$$

$$m\ddot{Z} = Q_Z - mg + N - c\dot{Z} - kZ \tag{4.28}$$

$$I_y\ddot{\theta} = T_Y + Nr\cos\beta + F_X r\sin\beta \tag{4.29}$$

where c and k are the effective damping and stiffness of the bird leg respectively;

r is the length of the line connecting the ellipse center and the contact; and

β is the angle between the line r and the conveyor surface.

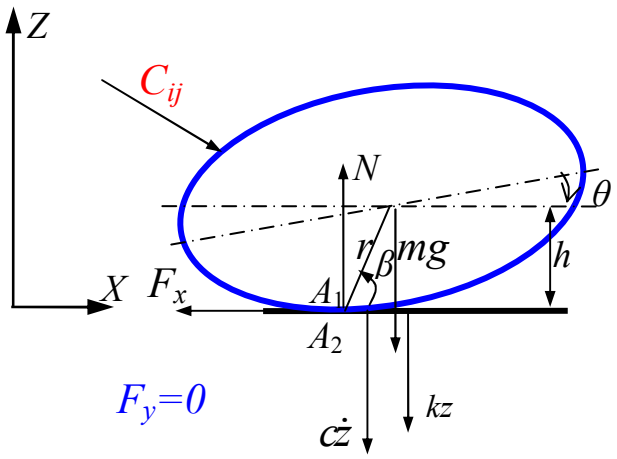

Figure 4-6 Free body diagram of the bird for symmetric case

The solution to Equations (4.27)-(4.29) requires the computation of the external forces, which include the forces acting on the bird by the rotating fingers and the reaction forces and friction from the conveyor. Since it is of interest to predict potential bruises that could be caused by the fingers, these external forces are computed in the complete three-dimensional space.

Constraints at the bird/conveyor interface

Equation (4.9) can be rewritten as

$$\dot{\theta}\, r\cos\beta + \dot{Z} = 0 \tag{4.30}$$

The bird/conveyor contact point can be expressed as a function of θ by noting that the xz and XZ planes are parallel and the ellipse inclines at an angle θ from the conveyor surface. From Equation (4.15), the cross-section of the ellipsoid represented in XZ coordinate system is

$$f_w(X,Y,Z)\big|_{Y=0} = \left\{P_w^T[R_{y'}(\theta)]^T[B][R_{y'}(\theta)]P_w\right\}_{Y=0} - 1 = 0 \tag{4.31}$$

where
$$[R_{y'}(\theta)] = \begin{bmatrix} \cos\theta & 0 & -\sin\theta \\ 0 & 1 & 0 \\ \sin\theta & 0 & \cos\theta \end{bmatrix}. \tag{4.31a}$$

Since the conveyor surface is the tangent plane at the contact, $dZ/dX = 0$, which is essentially the lowest point of the ellipse on the surface, we have

$$\frac{dZ}{dX} = -\frac{\partial f_w(X,Z)/\partial X}{\partial f_w(X,Z)/\partial Z} = 0 \tag{4.32}$$

Equation (4.32) implies $\partial f_w / \partial X = 0$, from which we obtain

$$\frac{Z}{X} = -\frac{\gamma^2\cos^2\theta + \eta^2\sin^2\theta}{\sin\theta\cos\theta(\eta^2 - \gamma^2)} \tag{4.33}$$

Since $\tan\beta = Z/X$, we have from Equation (4.33):

$$\cos\beta = \frac{(\eta^2 - \gamma^2)\sin\theta\cos\theta}{\sqrt{\gamma^4\cos^2\theta + \eta^4\sin^2\theta}} \tag{4.34}$$

The contact point (X_A, Z_A) and r in Figure 4-2 can be determined by substituting $Z = X\tan\beta$ and $\cos\beta$ from Equation (4.34) into Equation (4.31), which leads to:

$$X_A = \frac{\cos\theta\sin\theta(\eta^2 - \gamma^2)}{\sqrt{\gamma^2\cos^2\theta + \eta^2\sin^2\theta}} \tag{4.35a}$$

$$Z_A = -\sqrt{\gamma^2\cos^2\theta + \eta^2\sin^2\theta} \tag{4.35b}$$

and
$$r = \frac{(\eta^4 \sin^2\theta + \gamma^4 \cos^2\theta)^{\frac{1}{2}}}{(\gamma^2 \cos^2\theta + \eta^2 \sin^2\theta)^{\frac{1}{2}}} \tag{4.35c}$$

Friction force calculation

From Equation (4.10a) we have

$$F_x = -\text{sgn}(V_{A1x} - V_{A2x})N\mu \tag{4.36}$$

where
$$V_{A2x} = v; \tag{4.36a}$$

and
$$V_{A1x} = \dot{X} - \dot{\theta}\sqrt{\gamma^2 \cos^2\theta + \eta^2 \sin^2\theta} \tag{4.36b}$$

Below we will discuss the numerical solution to the dynamics equations. First the equations of motion will be presented in state-space form, and then the numerical method to solve it will be discussed.

State-space representation

From last section Equations (4.27)-(4.29) are written in a state-space form for numerical computation.

$$\dot{q}_1 = q_2 \tag{4.37a}$$

$$\dot{q}_2 = \frac{1}{m}(Q_X - F_x) \tag{4.37b}$$

$$\dot{q}_3 = q_4 \tag{4.37c}$$

$$\dot{q}_4 = \frac{1}{m}\left(Q_Z - mg + N - cq_4 - kq_3\right) \tag{4.37d}$$

$$\dot{q}_5 = q_6 \tag{4.37e}$$

$$\dot{q}_6 = \frac{1}{I_{by}}\left(T_Y + Nr\cos\beta + F_x r\sin\beta\right) \tag{4.37f}$$

where q_1, q_3 and q_5 denotes $X, Z,$ and θ respectively; and q_2, q_4 and q_6 are the corresponding first-order derivatives of q_1, q_3 and q_5. The two constraints imposed on the bird motion are as follows:

The supporting force

$$N \geq 0 \tag{4.38}$$

since the conveyor surface can only provide push force, and from Equation (4.38) we have the bird/conveyor contact model

$$-q_6 \frac{(\eta^2 - \gamma^2)\sin q_5 \cos q_5}{\sqrt{\gamma^2 \cos^2 q_5 + \eta^2 \sin^2 q_5}} + q_4 = 0 \tag{4.39}$$

which can be obtained by substituting r and β in Equations (4.35c) and (4.34) into Equation (4.30).

The calculation of the friction force F_x expressed in Equation (4.44) is rewritten as follows:

$$F_x = \text{-}N\mu\,\text{sgn}(q_2 - q_6\sqrt{\gamma^2 \cos^2 q_5 + \eta^2 \sin^2 q_5} - v) \tag{4.40}$$

When there is no contact, N=0. In this case Equations (4.37b), (4.37d) and (4.37f) reduce to

$$\dot{q}_2 = \frac{Q_X}{m} \tag{4.37b-1}$$

$$\dot{q}_4 = \frac{1}{m}(Q_Z - mg - cq_4 - kq_3) \tag{4.37d-1}$$

$$\dot{q}_6 = \frac{1}{I_{by}} T_y \tag{4.37f-1}$$

The six unknowns can be solved from the six state-space Equations (4.37a), (4.37b-1), (4.37c), (4.37d-1), (4.37e), and (4.37f-1).

Numerical approach

Equations (4.37a) to (4.37f) form a set of differential-algebraic equations (DAEs) that describe the dynamics of the bird as it goes through the rotating grasper subjected to constrains imposed by Equations (4.38) and (4.39). The numerical method of solving DAEs in essence is to approximate $\dot{q}$ in Equations (4.37) by a backward differentiation formula (BDF), and solve the resulting set of nonlinear algebraic equations by some iterative procedure for an approximation to $\boldsymbol{q}$. Some of the practical issues encountered in implementing the algorithm are briefly discussed as follows.

In this work, the BDF methods have been applied directly to the above DAEs. The procedure consists of substituting the backward difference approximations

$$\{\dot{\boldsymbol{q}}\}_{n+1} = \frac{1}{h\beta_0}(\{\boldsymbol{q}\}_{n+1} - \sum_{i=0}^{p} \alpha_i \{\boldsymbol{q}\}_{n-i}) \tag{4.41}$$

into the Equations (4.37a) – (4.37f) to form a set of nonlinear algebraic equations with $\{\boldsymbol{q}\}_{n+1}$ and N_{n+1} as unknowns, h is the simulation time step size. For example, when p=4, β_0=12/25; α_0=48/25; α_1=48/25; α_2=-36/25; α_3=16/25; α_4=-3/25.

In Equations (4.37b) and (4.37f), the friction expressed in Equation (4.40) between the ellipsoid and moving conveyor could have sign changes in the simulation. This friction sign change is updated at the end of each time step. The same approximation also applies to the compliant contact force from the rotating finger. In other words, within each time step, the forces remain unchanged.

The method to compute the contact force in 3-D was discussed in the last section. The algorithm differences between pull and push were also addressed in the end of the last section. Below the numerical algorithm to solve for the dynamics of the bird is presented.

Numerical algorithm

The numerical algorithm for the dynamical analysis is given below.

Computational steps:

i) Initialization of parameters such as $\{\boldsymbol{q}\}_0$, $\boldsymbol{N}_0$.

ii) Compute the net contact force and moment, $Q_x(X,Y,Z)$; $Q_z(X,Y,Z)$; $T_Y(X,Y,Z)$, based on $\{\boldsymbol{q}\}_k$ and position of the rotating finger. The step involves solving Equations (2.9a), (2.9b), (3.6), (3.7) and (3.8) for each finger and algebraically sum the components respectively, computation flow chart is shown in Figure 3-2.

iii) Substitute $\boldsymbol{Q}$ and $\boldsymbol{T}$ (forces and moment), Equation (4.40) and Equation (4.41) into Equation (4.37b), (4.37d) and (4.37f) if Equation (4.38) is met, or else Equations (4.37b-1), (4.37d-1) and (4.37f-1).

iv) Substitute Equation (4.41) into Equations (4.37a), (4.37c) and (4.37e). Solve the nonlinear algebraic equations to get $\{\boldsymbol{q}\}_{k+1}$ and $\boldsymbol{N}_{k+1}$, k=1,2,…

Repeat step ii) to v) until the end of the time duration specified.

4.5 Summary

This chapter presents first a general dynamics model of a live object grasping system. The dynamics of the object can be described by a group of differential algebraic equations, where the position dependent 3-D contact forces from the rotating fingers contribute to the net forces acting on the object. The method to calculate the 3-D contact force is discussed on the basis of a quasi-static finger model for predicting the contact force between a moving object and rotating fingers.

The second part of this chapter is to look into a special case of the dynamics formulation, the symmetrical grasper. The numerical method to solve the dynamics equation of the object for the symmetrical grasper was provided at the end of this Chapter. The dynamics simulation on the basis of a designed grasper will be presented in next chapter.

The model can be effectively used to evaluate the design parameters involved in the dynamic grasper, and to provide a rational basis for future design optimization. The existing system prototype being developed at Georgia Tech is used to do the grasping dynamics experiment in next chapter. The simulations shown in next chapter will not only help visualize the grasping process, but also save the number of experiment times and the number of live birds.

CHAPTER V

RESULTS AND DISCUSSION

In Chapter 4, we developed a dynamic simulation algorithm to analyze the motion of the bird throughout the grasping process. This Chapter begins with a brief discussion of the grasper design. Next, the results of a detailed study on the effects of the finger stiffness (on the bird motion, the contact forces, and the duration within which the rotating fingers are able to support the bird) are presented. The experimental results that were obtained using a specific grasper with an ellipsoid (football) on an existing prototype developed at Georgia Tech are then compared with the prediction.

5.1 Grasper Design Considerations

Figure 5-1 describes the coordinate systems used in the following discussion. The world coordinate system C_w (XYZ) is attached on the conveyor surface, where the X-axis is in the direction of the conveyor motion. The coordinate frame $C_b(x_b, y_b)$ is attached at the mass center (X_0, Y_0) of the bird, where the x_b- and y_b-axes are along the principal axes of the ellipse. The coordinate frame C_{fi} (x_{fi}, y_{fi}) is attached at the base of the i^{th} finger as it was defined in the previous chapters.

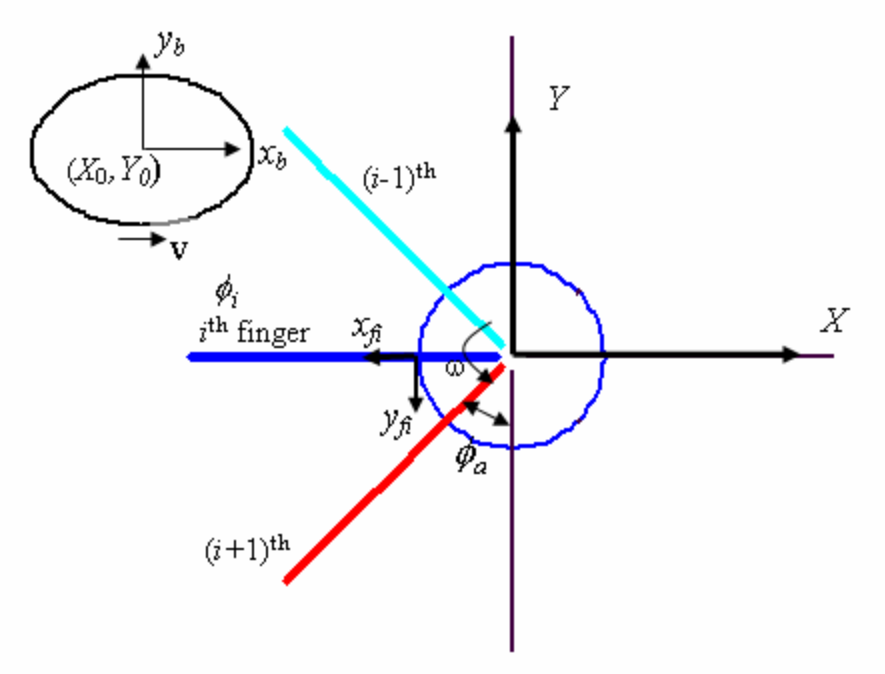

Figure 5-1 Fingers-object relationships

The parameters that could affect grasping include

(X_0,Y_0) the "initial" position of the object in C_w (XYZ) at time t=0;

ϕ_a the including angle between two neighbor fingers;

l the length of the finger;

d the spacing between two rotating drums;

r_D the radius of the drum;

ω the angular velocity of the drum; and

v the speed of the conveyor on which the bird sits.

To illustrate the effect of the finger design on the bird, we plot the un-deflected fingers as seen by the bird. As shown in Figure 5-2, the x_{fi} axis of the i^{th} finger is parallel

to y_b when $\phi_i + \omega t = \pi/2$, and the location of this x_{fi} axis repeats with a period equal to $2\pi/\omega$. As seen by the bird in its body coordinate frame C_b, the distance moved by the i^{th} finger along the x-axis is given by $v(2\pi/\omega)$. Note that any point on the i^{th} finger can be described in C_b by Equation (5.1),

$$\begin{bmatrix} x_{bi} \\ y_{bi} \end{bmatrix} = r\begin{bmatrix} \cos(\omega t + \phi_i) \\ \sin(\omega t + \phi_i) \end{bmatrix} - \begin{bmatrix} X_0 + vt \\ Y_0 \end{bmatrix} \tag{5.1}$$

where $\phi_{i+1} = \phi_i + \phi_a$;

$r_D \le r \le r_D + l$;

$Y_0 = d/2 + r$;

and ϕ_i is the "initial" angular position of the i^{th} finger. The loci of three consecutive un-deflected fingers (spaced at ϕ_a) as a function of time t can be computed as shown in Figure 5-2. The motion of the fingers, as seen by the bird, can be treated as a periodic signal in x with a period equal to

$$x_p = \frac{v}{\omega}\phi_a, \tag{5.2}$$

Figure 5-2 shows the relationship between the size and the specific grasping configuration (or the number of fingers simultaneously in contact with the object), which depends on the linear-to-angular speed ratio $\frac{v}{\omega}$, the bird's arrival X_0 and the included angle ϕ_a. Clearly, the larger the bird's size, the larger the finger would deform and hence, the larger is the contact force. Secondly, the decrease in Y_0 would result in an

increase in contact forces. Thirdly, the change in X_0 would move the ellipse to the left or right, which influences the contact forces between the fingers and the moving object.

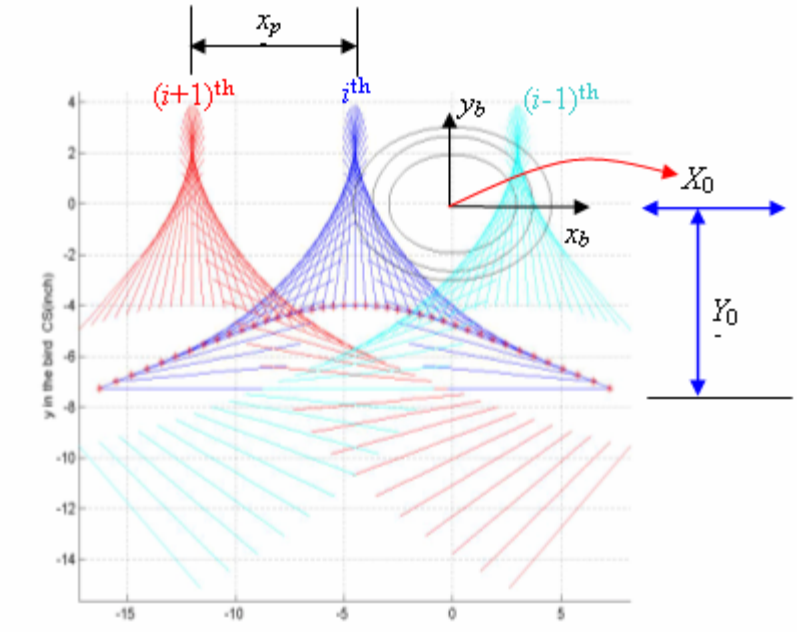

Figure 5-2 Effects of object sizes and arrival

It was shown in [Lee and Yin, 2001] that five fingers are necessary to constrain the bird for the purpose of shackling its legs. The two fingers in the upper layer are designed to restrict its movement in the Z direction, while two of the three lower fingers hold the breast of the bird and the third is placed behind the leg to support the abdomen of the bird. In addition, the bird must be held for a short time to allow time for inserting both legs into a shackle. Because the lower row of the fingers support the weight of the bird, these fingers are relatively harder and shorter than the upper rows of fingers in order to prevent them from interfering with the legs of bird. Figure 5-3 describes the relative position between the finger and the transverse intersection of the bird ellipsoids (large-, middle- and small size) where a group of fingers with different tilt angles is plotted. To accommodate a range of sizes, the spacing between the drum pair and the tilt angle of the

fingers (#1 and #2) can be tuned to function well with both large and small size birds. The tilt angle and the lengths of the finger #3, #4 and #5 are limited by the fact that all the birds arriving to the drum pair are in a sitting posture.

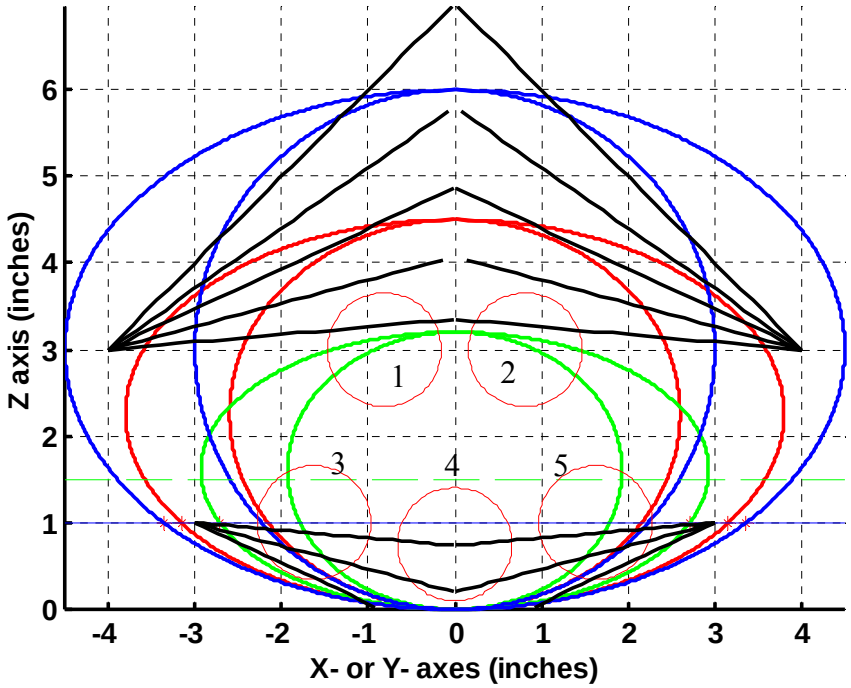

Figure 5-3 Grasper finger configurations

In addition, there are other practical considerations as briefly stated as follows:

(1) Typical processing plants require the grasper to maintain a constant throughput (birds per unit time). To ensure a smooth synchronization from the conveyor to grasper, the live objects are singulated into a queue line such that the spacing between any two consecutive birds is Δx. For a given Δx, matching the line speed implies that the speed ratio of the conveyor to the drum is

$$\frac{v}{\omega} = n\frac{\Delta x}{2\pi}, \tag{5.3}$$

where n is the integer number of finger pairs around the drum circumference given by

$$n \le \frac{2\pi}{\phi_a}. \tag{5.4}$$

(2) The included angle ϕ_a must be designed to accommodate a specified range of objects

$$2\sin^{-1}(\frac{d_f}{r_D}) < \phi_a < \pi - 2\tan^{-1}(\frac{Y_c}{X_c}) \tag{5.5}$$

where (X_c, Y_c) are the coordinate of the contact point between the straight line that representing the un-deflected finger and the largest object.

(3) The drum radius r_D must be sufficiently large to house the required number of fingers

$$r_D > \frac{nd_f}{\pi}; \tag{5.6}$$

where d_f is the diameter of the finger at the circumference of the drum.

(4) The spacing d between the drum pair should be wide enough to accommodate the largest object and the length of fingers,

$$\begin{aligned} d &\ge \lambda + \sigma_\lambda \\ d &\ge \ell . \end{aligned} \tag{5.7}$$

Based on the above considerations, the grasper configuration was designed with the aid of numerical simulations. The finger layout is plotted in Figure 5-4(a) and its

design parameters are summarized in Table 5-1. Figure 5-4(b) shows a desired grasping of a mean size bird being grasped.

Table 5-1 Design parameters for fingers

Finger #	1	2	3	4	5
Length , m (inches)	0.121 (4.75)	0.114 (4.5)	0.076 (3.0)	0.076 (3.0)	0.152 (6.0)
Height, m (inches)	0.095 (3.75)	0.095 (3.75)	0.032 (1.25)	0.025 (1.0)	0.032 (1.25)
Initial angle (degrees)	101.3	123.8	90.0	112.5	135.0
Drum radius, m	0.083	0.083	0.108	0.108	0.108
(inches)	(3.25)	(3.25)	(4.25)	(4.25)	(4.25)
ϕ_x(degs)	-45	45	45	90	-45
ϕ_y(degs)	-15.0	-15.0	15	7.5	15

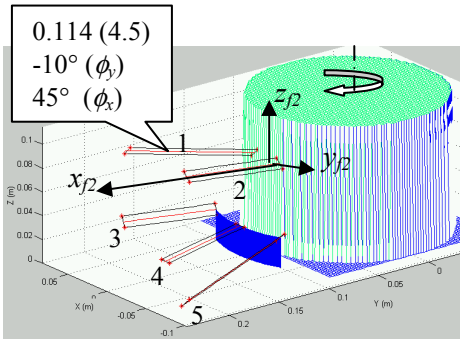

(a) Dynamic grasper structure

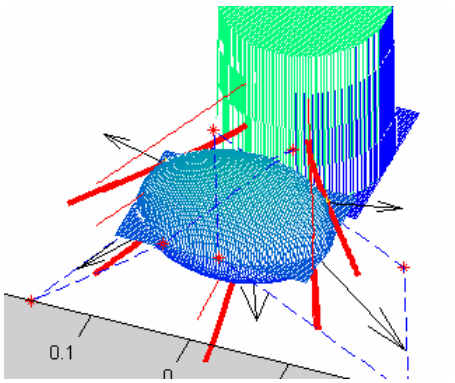

(b) Grasping illustration

Figure 5-4 Grasper configuration

5.2 Effects of Finger Stiffness through Dynamics Simulation

The simulations presented here predict the effects of the finger stiffness on the motion trajectory and the forces acting on the bird. It is expected that the results will provide useful information for developing a motion controller for the high speed grasper.

To study the effect of *EI* and the contact points on the bird, we consider two finger geometries:

1. uniform cross-section with constant EI_1 of 0.08 and
2. varying cross-section with EI_2 and EI_3 listed in Table 5-2, where EI_2 (soft) and EI_3 (hard) have the same geometry but with different *E*.

Table 5-2 shows the effective *EI* values for a uniform beam, a non-uniform soft finger, and a non-uniform hard finger. The latter two have the exactly same geometrical properties but different Young's modules, the values of which have been measured experimentally using the M system from TestResources Inc. [78] to be 4.8 MPa and 9.07 MPa respectively. The values of other simulation parameters are summarized in Table 5-3.

Table 5-2 Compare Effective *EI* of the finger

x_f mm (inch)	Case 1 EI_1 Nm^2	Case 2 EI_2 Nm^2 (soft)	Case 3 EI_3 Nm^2 (hard)
50.80 (2.0)	0.08	0.1108	0.2093
66.04 (2.6)	0.08	0.0915	0.1729
81.28 (3.2)	0.08	0.0786	0.1485
96.53 (3.8)	0.08	0.0694	0.1312
111.76 (4.4)	0.08	0.0627	0.1185
127.00 (5.0)	0.08	0.0506	0.1088

Table 5-3 Simulation parameters and values

Simulation Parameters	Values
Average bird's dimension (η, λ, γ) in mm (inches)	97, 66, 57 (3.8, 2.6, 2.25)
Bird's mass, kg	1.8
Bird's moment of inertia I_{by} in kgm^2	0.00417
"Initial" position of the bird X_0 in m (inches)	-0.075 (-18)
Distance between drum centers in m (inches)	0.368 (14.5)
Drum radius r_D in m (inches)	0.082 (3.25)
Angular velocity of the drum ω in rpm	20
Conveyor speed v in m/s (inch/s)	0.457 (18)
Coef. of friction μ, bird/finger, bird/conveyor	0.4, 0.4
Simulation time step in ms	5.6

The simulations predict the following: (1) contact forces acting on the bird, (2) support forces from the moving conveyor, and (3) displacement of the object in the *X*-direction.

(1) Displacement in *X* direction

The bird trajectory under grasping provides useful timing information essential to the development of a motion synchronizer for the overall system control. Figures 5-5 and 5-6 compare the relative *X*-displacement between the bird and the conveyor on which the live bird sits as it enters the grasping system. Figure 5-6 shows typical simulation results of a mean size bird grasped by the rotating fingers. The red star is the central point of the ellipse, which are evenly spaced in time (0.11 sec). The red line is the moving profile of the bird. As shown in Figure 5-6(a), the finger with EI_1 causes the bird center to rotate up 12mm to 37.5mm. An appropriate finger design could significantly minimize this relative

rotation as compared in Figure 5-6, which provides a basis for designing a controller to synchronize the motion among the bird, the rotating finger, and the conveyor.

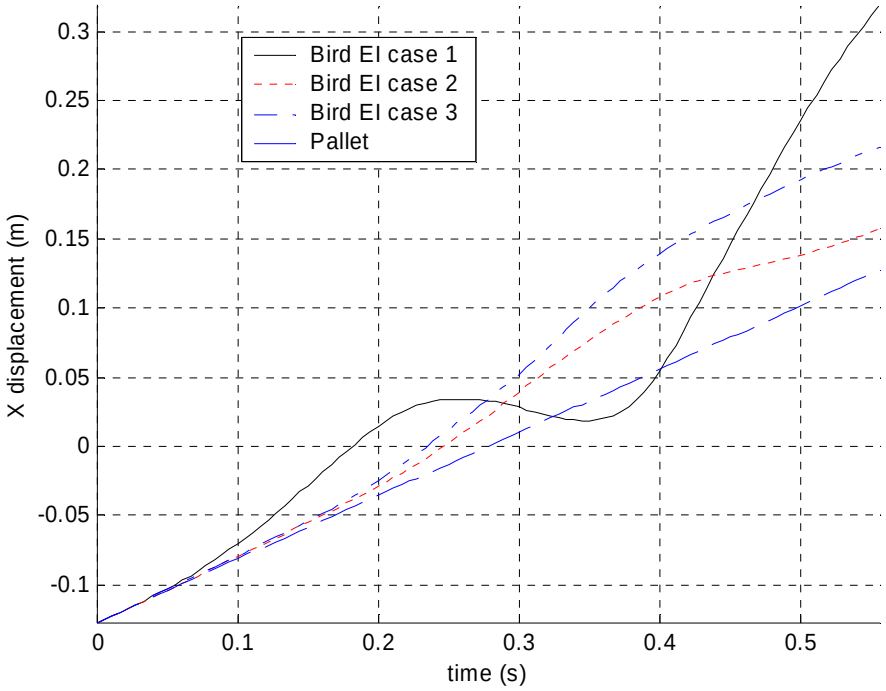

Figure 5-5 Bird motion relative to the Conveyor

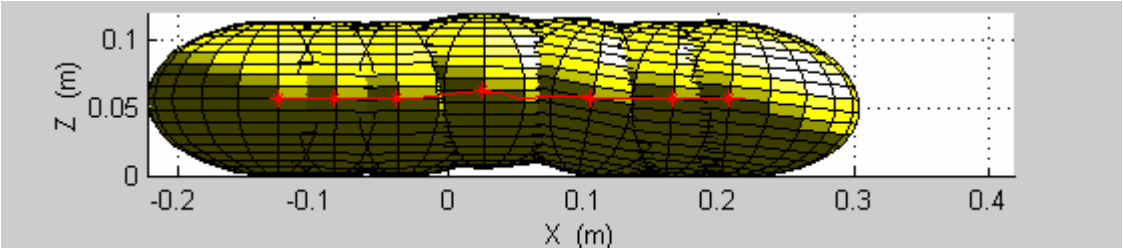

(a) *EI* table hard lower finger (case 1)

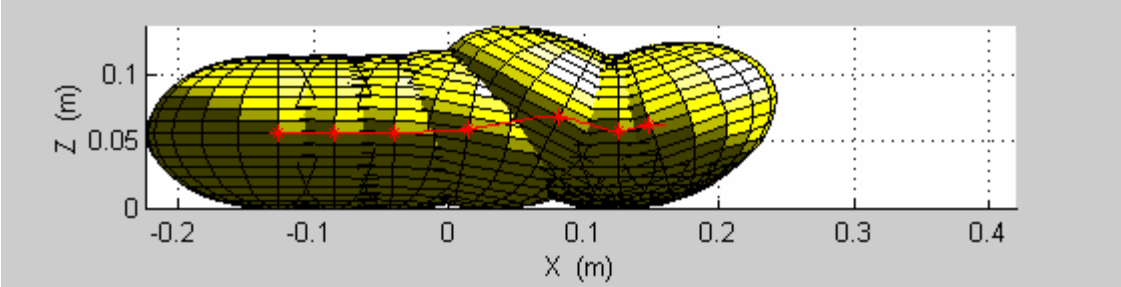

(b) *EI* table soft lower finger (case 2)

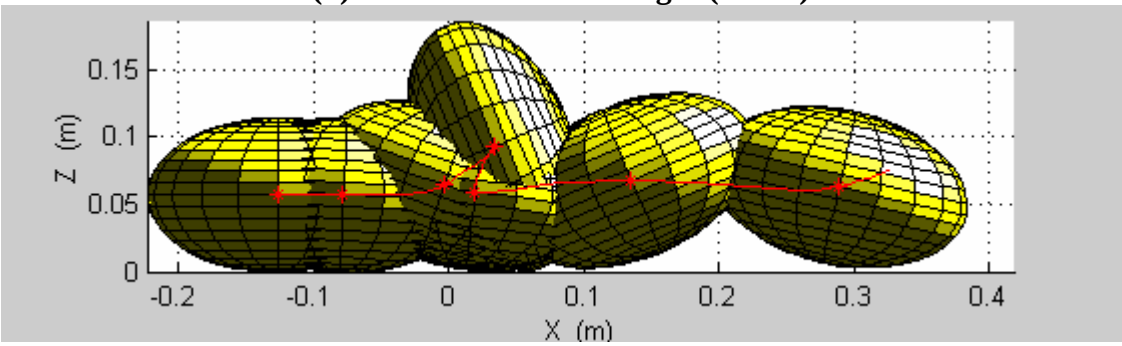

(c) Constant *EI* (case 3)

Figure 5-6 Simulated bird motions

(2) Contact forces

The contact forces contributed by the grasper on the object have a direct effect on the poultry meat quality. The forces acting on the bird depend on the structural rigidity *EI* as well as the instantaneous contact points on the fingers and the object. Figure 5-7 compares the contact forces of the five fingers between EI_2 and EI_3. It shows that there is no contact between finger #3 and the bird. The maximum contact force is exerted by finger #4 in the order of 11N. Figure 5-7 also illustrates that the contact forces concentrate densely in the area from –1.5 inches to +1.5 inches from the drum center. This is a very critical value for the successful grasping of the bird. It can help decide the best timing procedure.

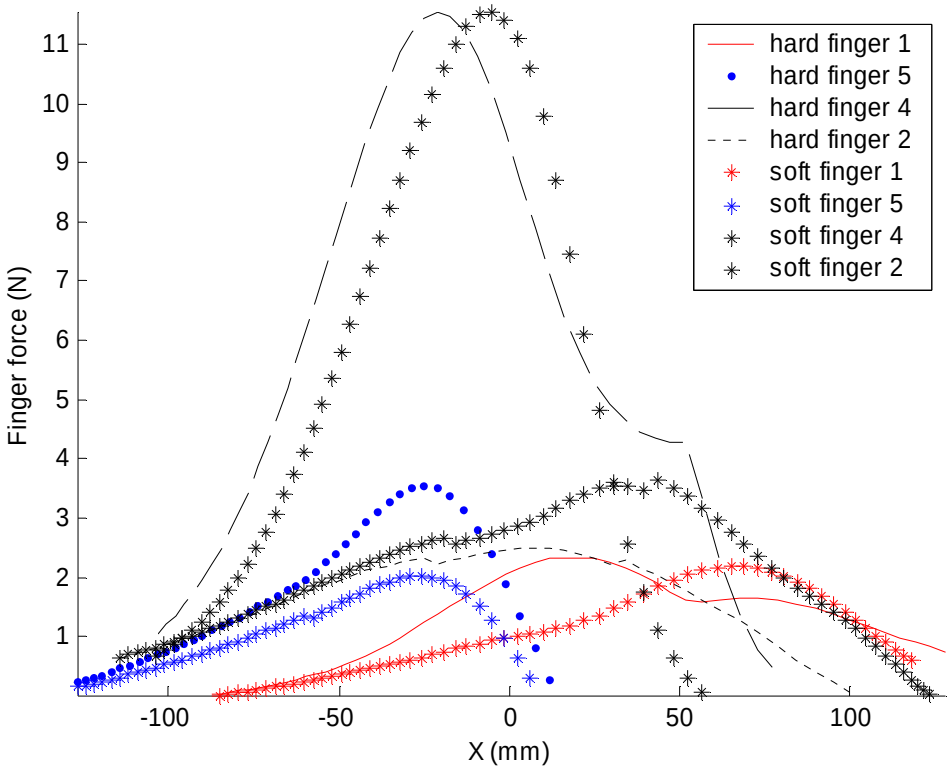

Figure 5-7 Comparison of finger forces (soft-EI_2, hard-EI_3)

Figure 5-8 shows the vector contact force field in the bird coordinate system, *xyz*, for finger #1, #2, #4 and #5 respectively. The red line on the surface of the bird is the locus of the contact points on the birds; the length of the vector illustrates the magnitude of the force. Finger #1's acting area is mainly on the upper part of the bird, as shown in Figure 5-4, which agrees very well with its position in 3-*D* space. As discussed previously, contact areas and the magnitude of the forces provides useful information for the design of the grasper.

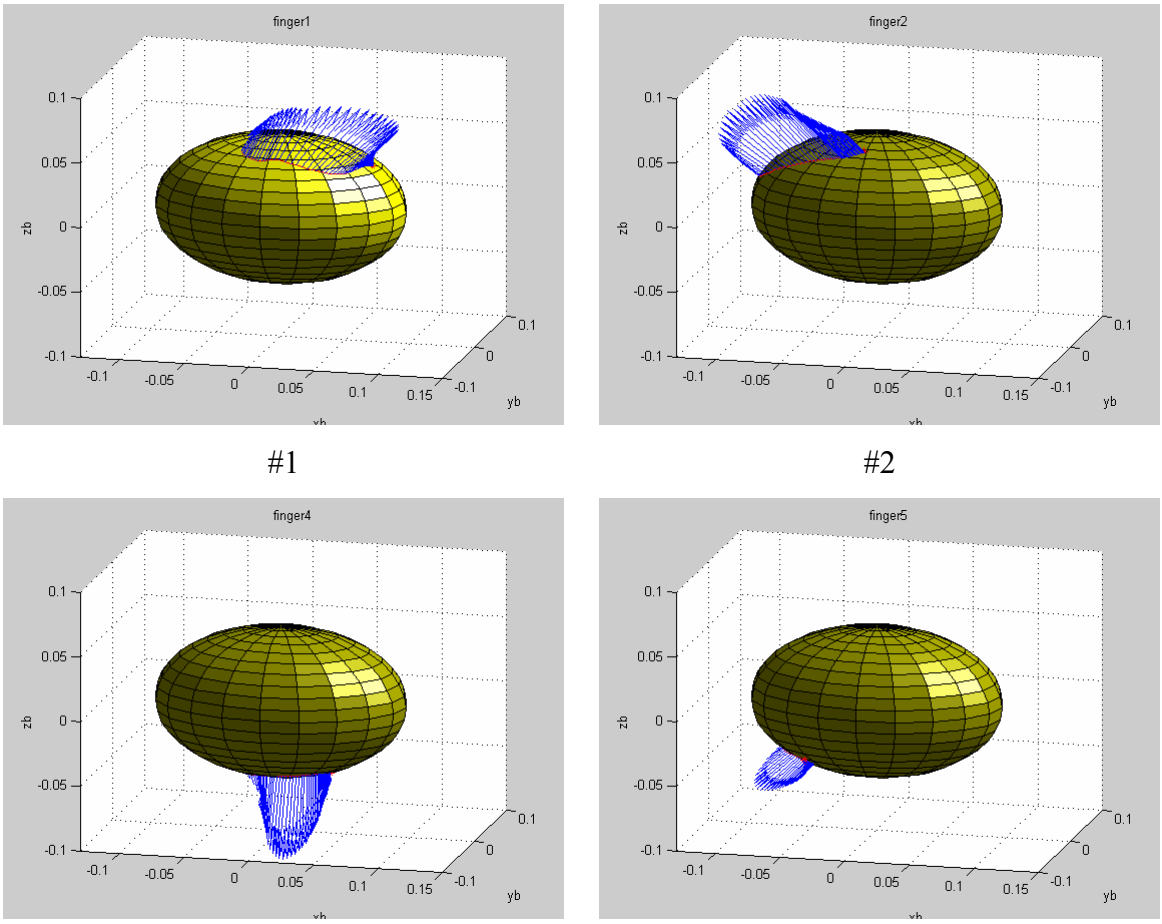

Figure 5-8 Comparison of contact force locations, (#4, 5 with EI_3) and (#1, 2 with EI_2)

(3) Normal force from the conveyor

The support force offers information on the duration the bird can be held to allow manipulation of its legs. Figure 5-9 compares the normal force at the contact between the conveyor and the bird for two cases of different finger used in the lower layer: fingers #3, #4 and #5. In the first case, these fingers are soft fingers EI_2 and EI_3 for the second case. If the fingers are sufficiently strong to support the bird, the normal force N would equal

to zero when the bird is held by the grasper. To allow adequate time to insert both legs of the bird to a pair of grippers waiting ahead, it is desired to maximize the period for which N=0. Figure 5-9 shows that when hard fingers are used the period of the support force being 0 is longer than the case when the soft fingers are used for the lower layer fingers.

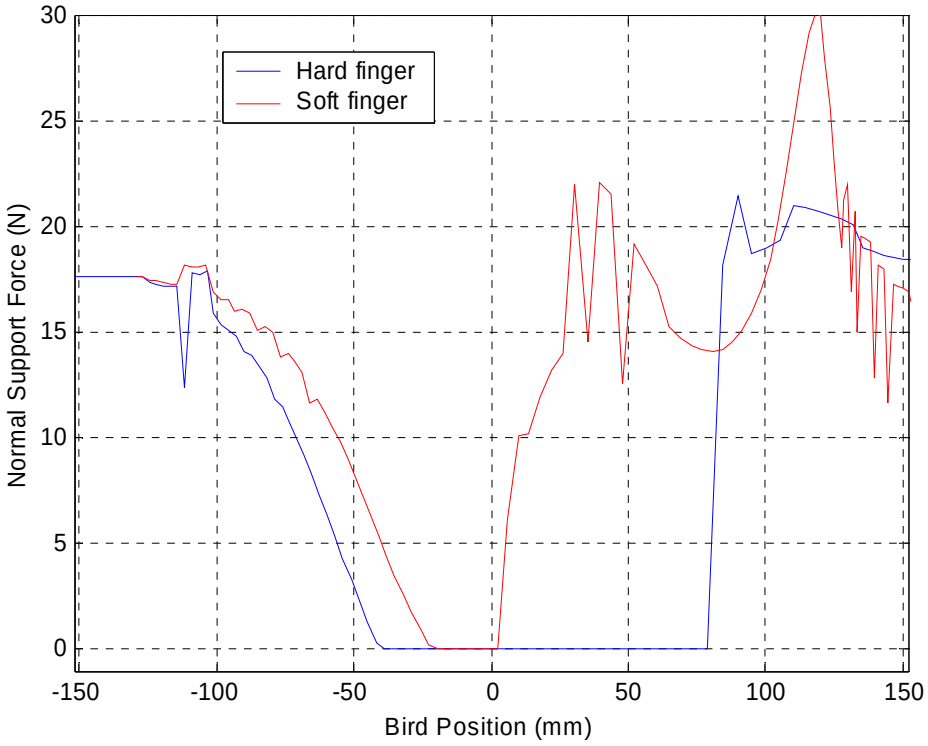

Figure 5-9 Normal force at contact with conveyor, EI_2 and EI_3

5.3 Experiment and parametric studies

As discussed in Chapter I, the transfer system uses the relative speed between the body and the legs of the bird. Specifically, while the drum rotates at a constant speed of 20rpm for the entire cycle time of one second, the conveyor (on which the birds sits) decelerates from 0.457m/s (18 inch/s) to 0.254 m/s (10 inch/s) at x=-0.142m (-5.6 inches)

or after a duration of 0.4 second. Simulations have been used to determine the optimal values for the parameters. Two sets of simulation results are presented here as an illustration. The first set of results compares the simulation to the results obtained experimentally. The second set examines the effects of some parameters on the motion of the moving object. A football has been used in the analysis since it has been a well-defined shape similar to that of a live bird, yet it allows for an experimental test in a controlled environment. The values of the parameters used in the simulation are given in Table 5-4.

Table 5-4 Simulation parameters and values for simulation of football

Simulation Parameters	Values
Football's size (η, λ, γ) in mm (inches)	122, 66, 66 (4.8, 2.6, 2.6)
Football's mass, kg	0.425
Football's moment of inertia I_{by} in kgm^2	0.0016
"Initial" position of the football X_0 in m (inches)	-0.305 (-12)
Distance between drum centers in m (inches)	0.368 (14.5)
Drum radius r_D in m (inches)	0.082 (3.25)
Angular velocity of the drum ω in rpm	20
Conveyor speed v in m/s (inch/s)	0.457 (18) and 0.254 (10)
μ, rubber-to-rubber contact	1.16 [24]
Simulation time step in ms	16.6

(1) Comparison against Experimental Results

The existing test bed (Appendix A) was used to test the dynamic grasping of a football. Figure 5-10 shows the experimentally obtained velocities of the drum (in rpm) and the conveyor (in inch/s), which are calculated from the encoder readings of the two motors.

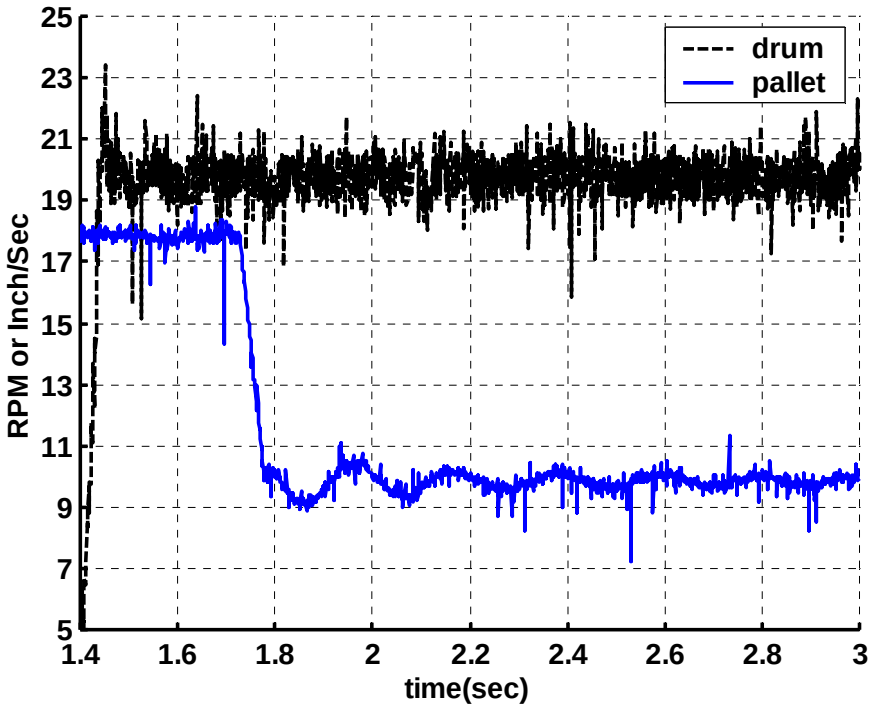

Figure 5-10 Specified drum and conveyor velocity profiles

The motion trajectory of the football was extracted from the video recording of a 30fps digital video camera. The video sequence starts when the drum began to rotate and stops at the end of one-and-a-half cycles or 43 frames. Figures 5-11(a), (b) and (c) illustrate the three phases of the grasping process; trapping, grasping and releasing respectively. Figure 5-12 compares the simulated trajectory against those captured experimentally. As shown in Figure 5-12, the experimental results well agree with the simulation results derived analytically. Figures 5-13 and 5-14 compare the simulation results against the experimental data for the displacement in the *Z* direction and the velocity in the *X* direction of the football respectively. The Reference of the *Z* direction is the surface of the conveyor. The maximum displacements in the *Z*- axis obtained from both simulation and experiment are around 0.018m (0.7inches).

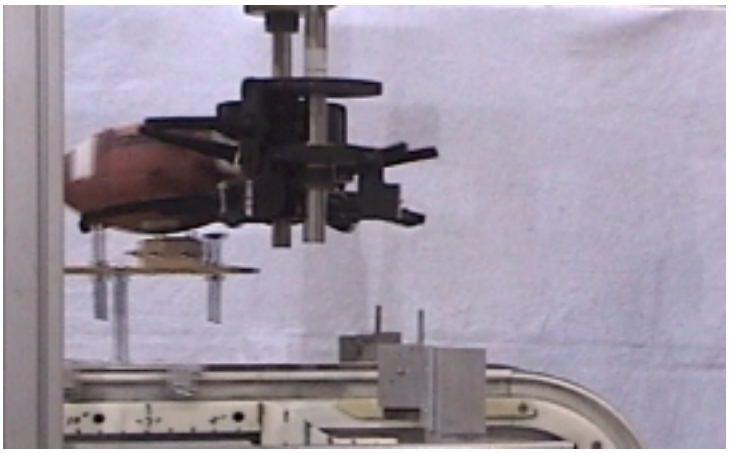

(a) Phase 1(frame 198): trapping of football

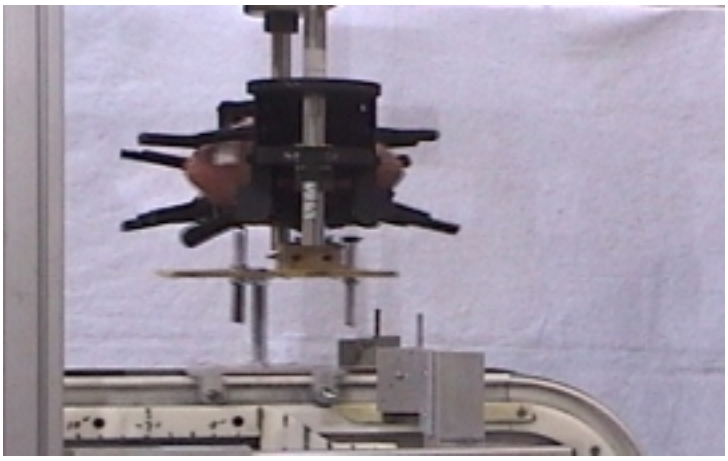

(b) Phase 2 (frame 217): grasping and holding of football

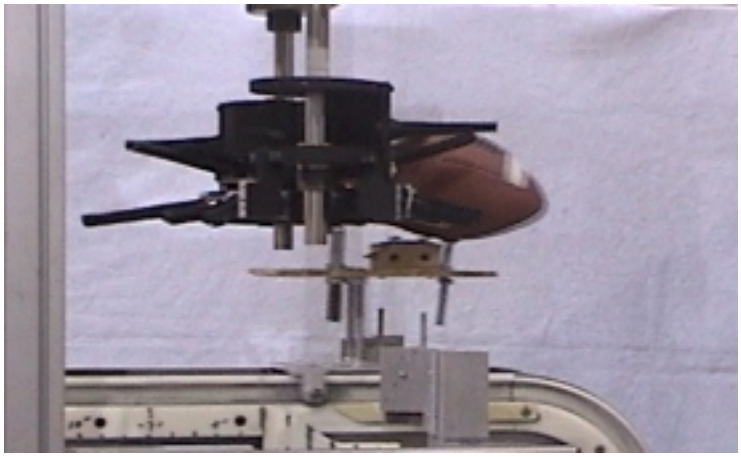

(c) Phase 3 (frame 230): release of football

Figure 5-11 Grasping process illustration

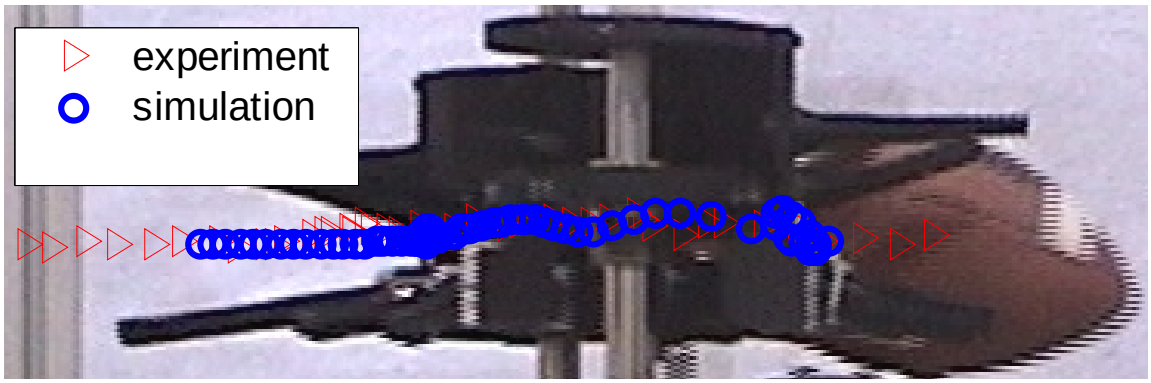

Figure 5-12 Grasping experiment with football (frame 230)

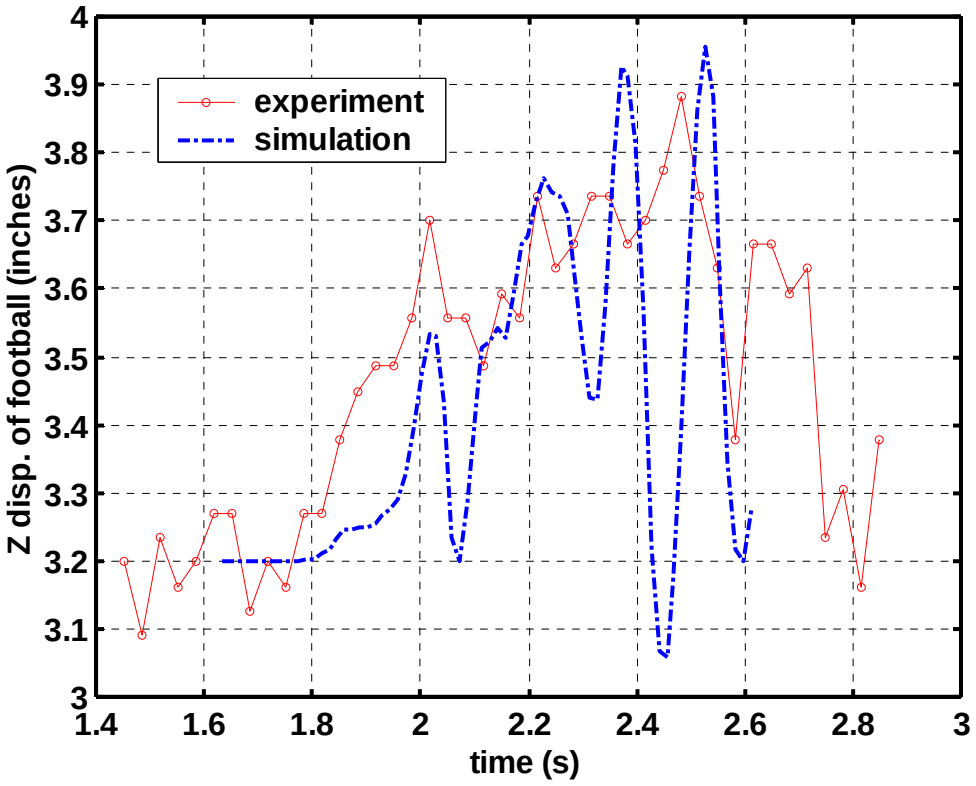

Figure 5-13 *Z*-axis displacement of football

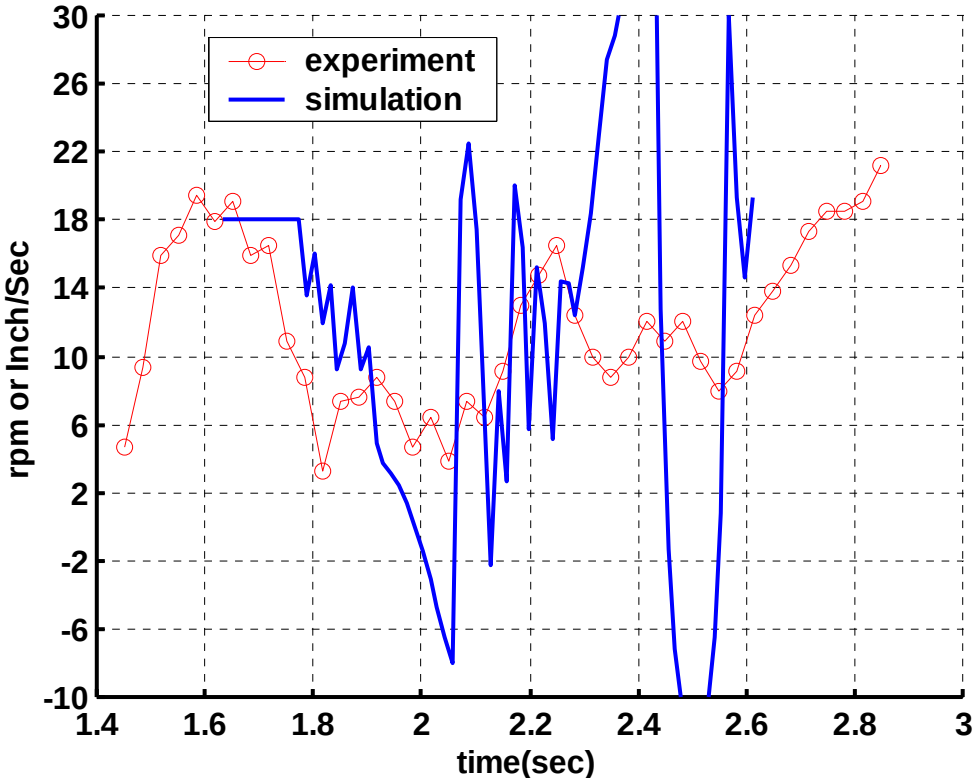

Figure 5-14 Experiment results: velocity profile of football

The overall trend of the simulated data closely follows that obtained experimentally. However, the simulated and the experimental data are rather noisy. The noises may be due to the discretization of the dynamics equation for the numerical solution, and the difficulties of locating the football in the video when the view was blocked by the rotating structure.

In Figure 5-13, the high frequency motion of the football in the simulation data implies some dynamic forces acting on the football. The acceleration can be estimated by assume that the *Z*-axis displacement follows a sine wave with an amplitude A (of no

more than 0.8 inch) and a period about 0.2 second . Thus, the largest inertia force due to the acceleration can be estimated to be

$$F = mA(\frac{2\pi}{T})^2 = 0.425 \cdot 0.8 \cdot \frac{2.54}{100} \cdot (\frac{2\pi}{0.2})^2 \approx 8.52N$$

It is close to the maximum of finger forces calculated from the simulation as shown in Figure 1-15. The large finger force is exerted by finger #4, which supports the weight of the football.

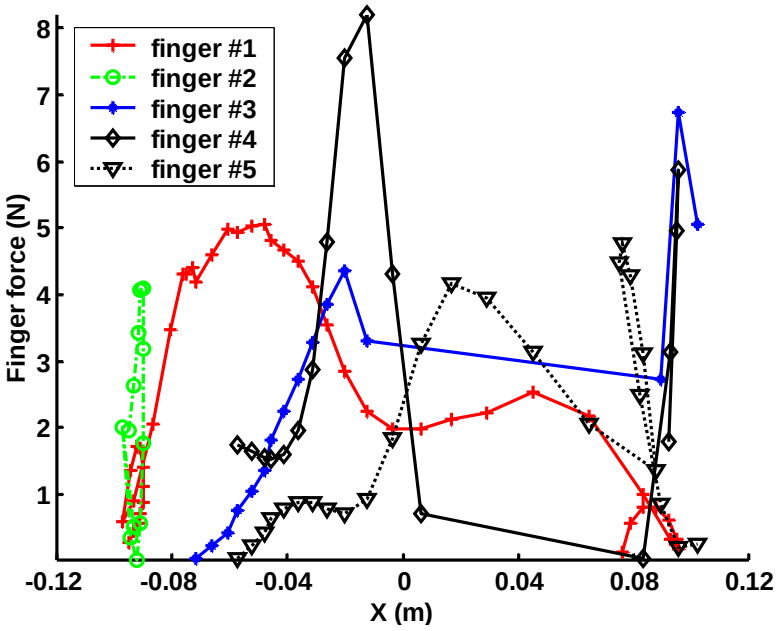

Figure 5-15 Finger forces comparison

(2) Parametric Studies

The interest here is to investigate the sensitivities of the following parameters to the object motion:

Initial position X_0 in m (inches): -0.305 (-12), -0.381 (-15), and -0.457 (-18).

Coefficient of friction μ: 0, 0.4, and 1.16.

Finger #3 configuration ϕ_x: 45˚, 60˚, and 70˚.

One of the practical issues encountered in real-world implementation is the effect of the variations of the "initial" bird position X_0 on the success of grasping, which requires a good synchronization between the conveyor and the bird arrival. Thus, the interest here is an attempt to find the tolerance of X_0 such that within the range, the grasper would work consistently. Figure 5-16 compares the motion trajectory of the football for 2 different X_0 over a range of 0.075m (or 3 inches) using the specified (drum and conveyor) velocity profiles as illustrated in Figure 5-10. The simulation demonstrates that an appropriately designed grasper has the ability to account for some variations of the "initial" position X_0 of the bird.

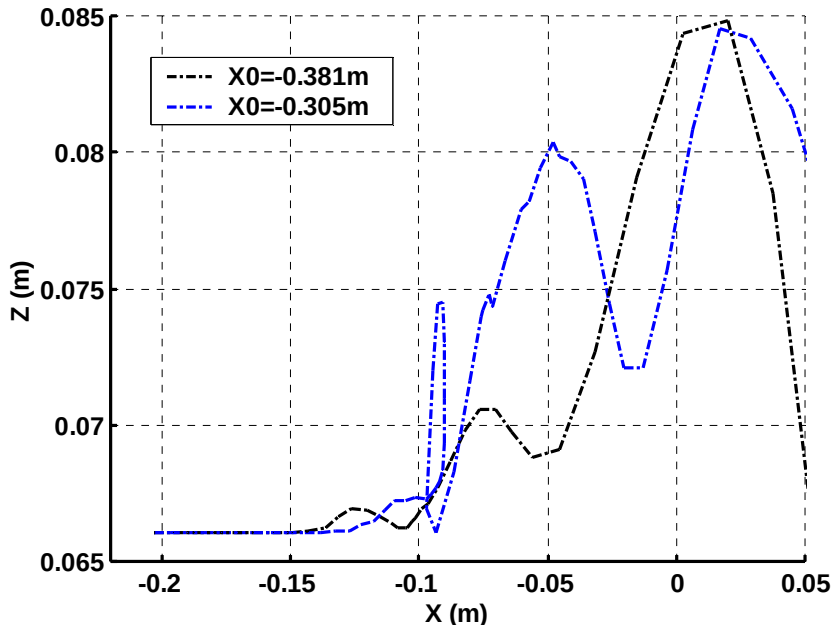

Figure 5-16 Effect of X_0 on motion trajectory (μ=1.16, ϕ_x=60°)

Figure 5-17 illustrates the effect of the friction coefficient on the football motion profile for X_0=-0.381m (-15inches). Three values for the friction coefficient were compared, corresponding to the frictionless contact (μ=0), the contact between a rubber finger and bird feathers (μ=0.4), and the contact between a rubber finger and rubber football (μ=1.16, [24]). Simulation results show that some frictional forces are necessary for the system to grasp the football, especially in the early phase when the football touches the first one or two fingers. As shown by the solid line in Figure 5-17, the football is pushed back when contacts are frictionless, and the motion is periodic afterwards. In addition, the system is able to handle a range of friction coefficients (0.4 - 1.16).

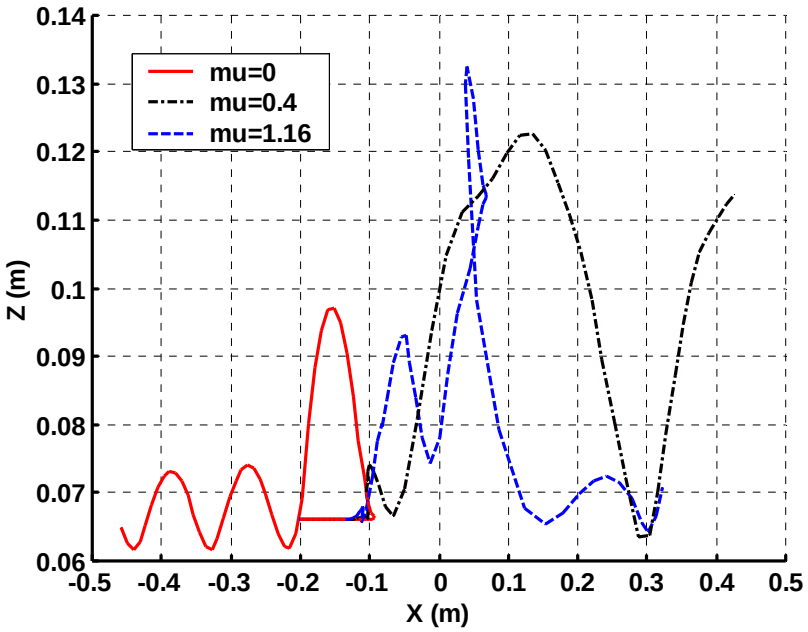

Figure 5-17 Effect of μ on motion trajectory (X_0=-0.381m, μ=1.16)

The motion trajectory is a function of both the friction coefficient and the orientation angle ϕ_x at which the finger is mounted on the drum. As ϕ_x increases the contact force in the X- direction decreases. Figure 5-18 compares the simulated motion trajectories of the football for three different ϕ_x of Finger#3, 45˚, 60˚ and 70˚ for a given μ of 1.16. Simulation results show that when ϕ_x <60˚ the football was pushed back by finger #3 and was unable to pass through the grasper.

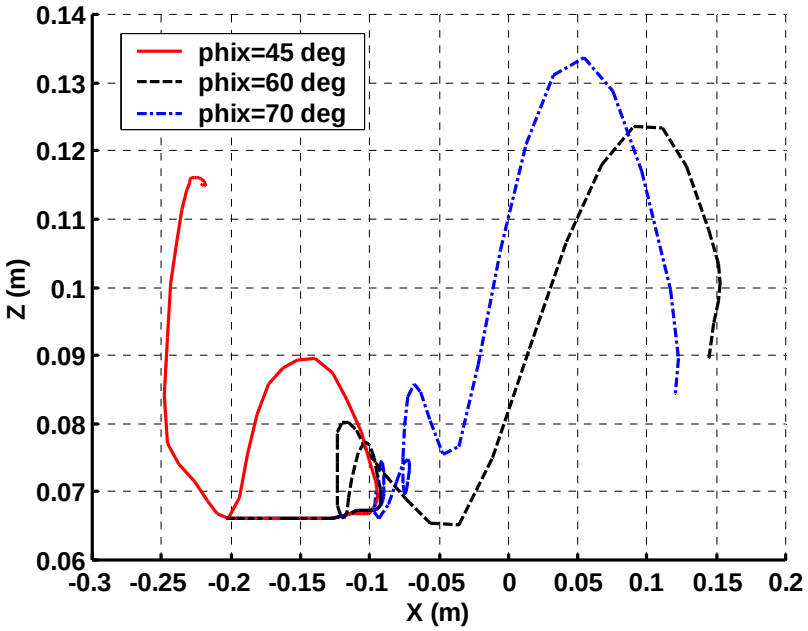

Figure 5-18 Effect of ϕ_x on motion trajectory (X_0=-0.381m, μ=1.16)

5.4 Discussion of results

We have presented the parametric studies using a football in Section 5.3. This section examines the effects of size and weight variations on the motion trajectory of a

typical bird. The primary differences between a football and a bird are the coefficient of friction and the weight. Table 5-5 lists all the cases considered in the simulations.

Table 5-5 Simulation cases for bird (X_0 =-15 inches, μ=0.4)

Case number	Weight (kg)	Sizes (a, b, c) inches & meters
Case #1	1.20	Small (3.1, 2.0, 1.80), (0.079 0.051 0.046)
Case #2	1.66	Mean1 (3.8, 2.6, 2.25), (0.097 0.066 0.057)
Case #3	1.80	Mean2 (3.8, 2.6, 2.25), (0.097 0.066 0.057)
Case #4	2.05	Large1 (4.35, 2.9, 2.6), (0.111 0.074 0.066)
Case #5	2.30	Large2 (4.90, 3.2, 3.0), (0.125 0.081 0.076)

Figure 5-19(a) predicts the motion trajectories of four different sizes of birds. Figure 5-19(b) shows the nutation of the bird as a function of the bird position. The results show that the lift occurs at about the same point along the motion trajectories for all cases and that the grasper has the ability to accommodate a relatively wide size/weight range of birds. For the weight range of 1.66 to 2.05kg, the grasper is able to lift the bird to the same height of 80mm. However, the support of the fingers tails off sooner for a very small bird. It is expected that the bird would tend to tilt upward as it leaves the grasper, as the finger experiences a much larger deflection (and hence results in a larger contact force) on the back of the bird.

Figure 5-20 compares the motion of two birds that have the same size but different weight of 1.66kg and1.80kg. It is worth noting that the two motion (position and orientation) trajectories have similar shape but the 1.66kg-bird is lifted higher than the 1.80kg-bird.

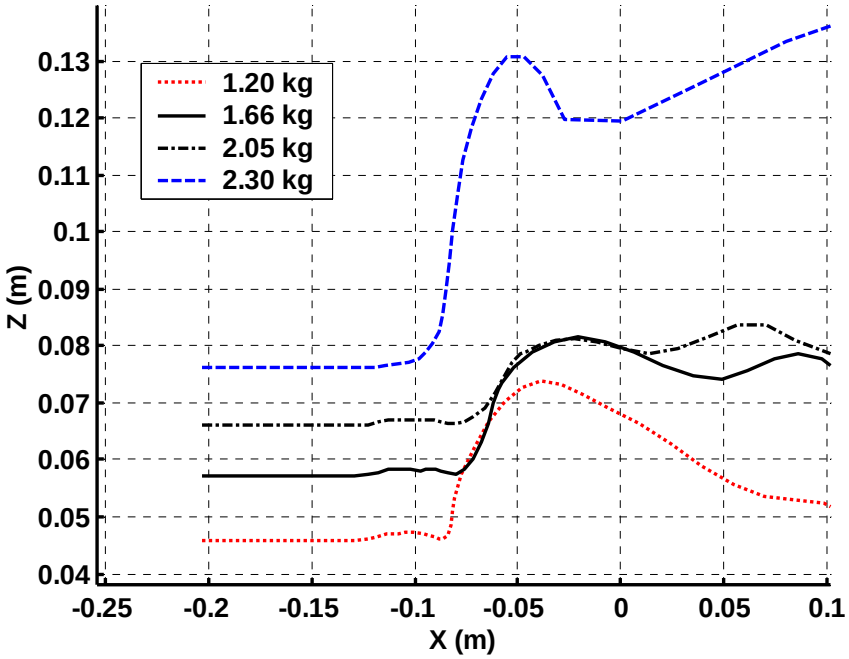

(a) Moving profiles

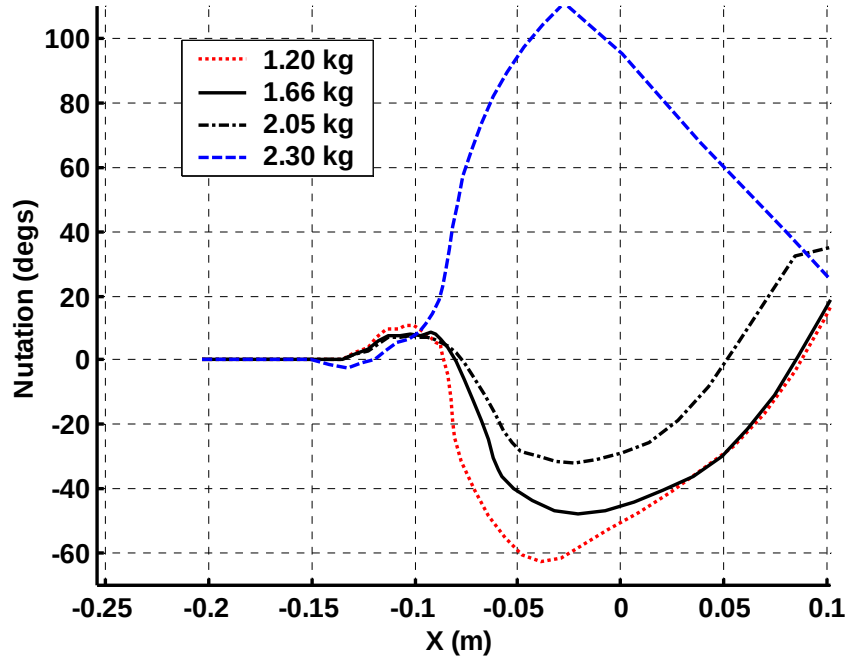

(b) Nutations

Figure 5-19 Comparisons for birds

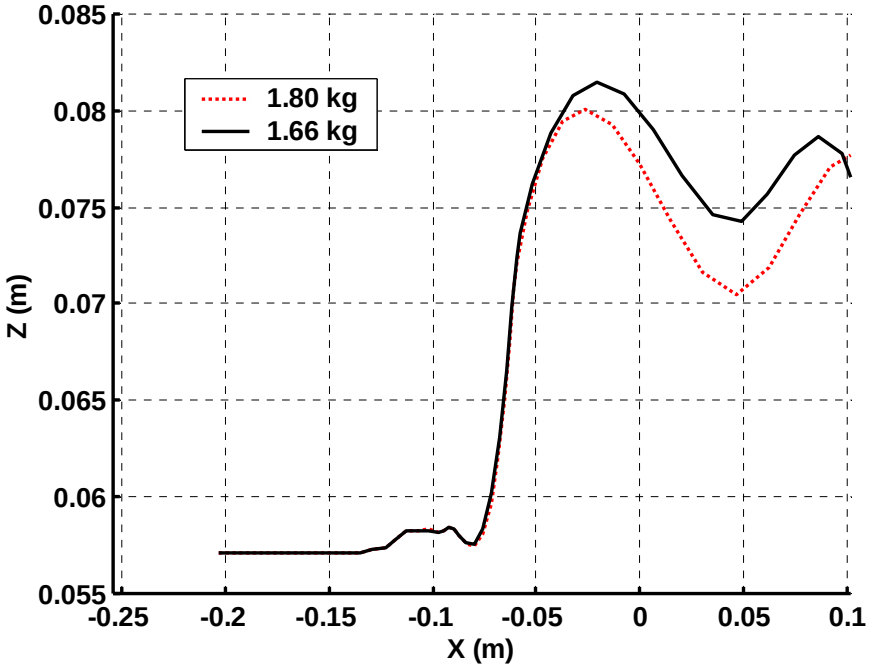

(a) Moving profiles

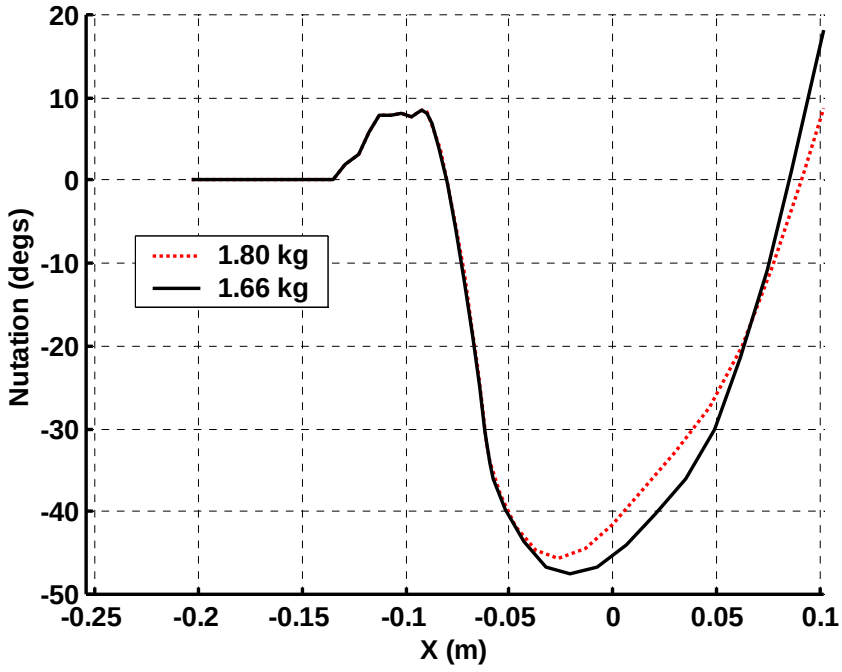

(b) Nutations

Figure 5-20 Comparisons for birds

As illustrated above, the simulations help provide a good understanding on the effects of different parameters on the grasper performance.

CHAPTER VI

CONCLUSIONS AND RECOMMENDATIONS

6.1 Accomplishments and Contributions

This thesis contributes to the development of an analytical method for modeling the dynamic contact between rotating flexible fingers (quasi-static) and a moving object, which is essential for the design optimization and controller development of a high-speed grasper for the manufacturing of natural products (such as poultry meat). Specifically, this thesis offers the following:

- ***Solutions to the equations that characterize the large deflection of a flexible beam (with non-uniform cross-section) under a point force have been derived.***

In this thesis, the problem of computing the deflection of a flexible beam, which has many engineering applications, has been solved. Particular focus has been placed on beams (with non-uniform based on its cross-section along the length of the finger) undergoing large deflections. Two algorithms based on the shooting method and the FDM have been developed, which extend the solution offered by the Frisch-Fay flexible bar theory that is only valid for beams with a uniform cross-section to large-deflection

beams with non-uniform cross-sections. The basic idea of the shooting method is to construct an initial value problem for the ODE, which requires two initial guesses of the derivatives (for the beam equation) at one end. While the shooting method can easily achieve the fourth- or higher order accuracy; however, the cost is that it needs a recursive algorithm to match the boundary conditions. The essence of the FDM for solving the ODE is to transform a calculus problem into an algebra problem. It is often referred to as a global method satisfying the boundary conditions automatically. It is relatively easy to implement the FDM but it is difficult to obtain higher than second-order accuracy.

The analysis is followed by simulations for the large deflection of the beam, where the shooting method and the FDM were compared. The beam deflection calculation provides a solid basis for the contact analysis involving the flexible beam. Concept of effective EI, which characterizes the ability of the finger resisting deformation under external force, has been introduced. It can be used to approximate the deflection of a non-uniform beam by a uniform beam with the effective EI, which has also been used in the contact analysis.

- ***A quasi-static model has been developed for predicting the contact force between a moving object and a rotating finger.***

The force acting on the live object and the contact point is calculated using the geometrical properties of the object and the mechanical properties of the finger. The contact problem is characterized by a set of coupled nonlinear equations, which include the object geometry, the shape of the deflected finger, the frictional forces between the finger and the object, and the location at which the force is applied. The coupled

equations are rather involved because of the compliant property of the finger. An algorithm and its flowchart for solving the coupled nonlinear equations have been presented.

The contact model has been validated by the experimental data and the computed results using FE methods. Experimental results show that, when the finger rotates at a low speed of about 20rpm, the contact model can be used to predict the contact force between a rotating finger and a moving object. The contact models developed in this thesis have been applied to the design of a live bird grasper. The contact prediction provides a rational basis for design optimization and force measurement of a grasper using flexible rotating fingers.

- ***The dynamic grasping model has been implemented numerically and simulated for an illustrative example based on the mean size of the live birds.***

A dynamic model has been developed to predict the motion of a live bird going through a rotating grasper. It has been implemented numerically using MatLAB. As illustrated in the simulation results, the computational algorithm provides an effective means to predict the locations at which the fingers exert the contact force on the moving bird, and the motion of the bird with respect to the pallet (conveyor). The magnitude of the contact force can be used as a basis for predicting potential bruises that may be caused by the rotating fingers on the bird. The relative motion of the bird with respect to the pallet provides information for the design and control of the grasper.

With the help of the kinematic analysis and all the constraints considered, values of a set of parameters are selected for a grasper, on the basis of which the 3-D dynamics simulations are implemented. The dynamic model has been validated by using a football because the football (ellipsoid like) has a well defined shape similar to that of a bird and allows for an experimental test in a controlled environment. The simulation results well agree with those from the experiment.

After being validated by the experiment using a football, the dynamics simulation has been used to evaluate the effects of the weight/size of the live bird. The simulation results show that the grasper design presented in this thesis is capable of accommodating a range of sizes and weights of the bird for the function of grasping if the appropriate motion controls of both the drum and the conveyor are provided.

The dynamics has helped provide a good understanding of the mechanical grasping of a singulated live object, which is essential for the design and development of a high speed LBTS with few or no injuries. The simulation has also reduced the number of live birds to be used experimentally.

- ***Results of a detailed study on the effects of the finger stiffness for the design of a grasper have been presented.***

The effects of the finger stiffness on the bird motion, the contact forces, and the duration within which the rotating fingers are able to support the bird have been studied by comparing three types of fingers (different effective EIs) in the dynamic simulation.

6.2 Recommendations for Future Research

Some recommendations for future work to further improve understanding the dynamics for the high speed grasper are summarized below.

In the contact force analysis, the uniform beam with an effective EI profile along its length is used to approximate the non-uniform beam. The FDM can solve the non-uniform beam contact problem more accurately. However, it sometimes becomes unstable in the recursive solution using the Newton method. In the future a more stable algorithm can be developed to improve the accuracy of the contact prediction.

The contact model discussed in Chapter III has been experimentally verified and also compared against the FEM. The contact, in reality, occurs in a finite area on the interface between the finger and the object. The size of the contact area depends on the local geometries, the elasticity of both the finger and the object and the normal component of the contact force. In general the area contact results in not only contact force but also the contact moment, which sometimes causes the torsional displacement of the finger. Therefore, further research in the finger/object contact model is needed to improve the accuracy of the contact force calculation. One of the possible approaches is to use the FEM for in-depth effects investigation. Then the effects of the area contact can be added to the contact model presented in Chapter III.

The 3-D contact force model has only considered the force component in the acting plane of the rotating finger. Actually there should be force components outside of the acting plane. The effects of these force components on the contact force prediction,

which finally influences the dynamics simulation, are not discussed. In further studies, a model which accounts for these effects on the dynamics needs to be developed. In the contact force analysis, the push or pull function of the finger are manually set. So an algorithm which can automatically determine the finger's functions is needed.

In Chapter IV, the ellipsoid that models for the live bird is a very good model to describe the geometrical shape of the bird. However, a more accurate dynamics model needs to consider the two ignored components in this thesis: the pair of legs and the long slim neck with head.

APPENDIX A

EXPERIMENTAL SYSTEM

An existing test bed mentioned in Chapter V to test the dynamic grasping of the live bird is presented. The test-bed is controlled by a PC which serves as a host to facilitate data acquisition for offline analysis. Data recorded through two NI PCI cards, **AT_MIO_16XE** and **PCI-6602** [62]**.** Motion of the bird is also recorded using a video camera for offline analysis. The control system consists of a microcomputer-based controller that controls the chain-conveyor carrying a few pallets on which the bird sits and a rotating grasper. The block diagram illustrating the operations is shown in Figure A-1. The grasping system is a sequence of singulated birds. The bird (transported on the conveyor) triggers the machine vision system that determines the orientation of the bird and the controller as it passes through a beam-switch (that can detect the arrival of the bird). The detailed orientation determination is discussed in [Lee *et al*, 2000].

Figure A-2 shows the structure of the two axes industrial motion controller, which has an on-board motion controller, two IDC's (961 and 962) Indexers, digital and analog I/O, and an AC power supply integrated in a single unit. Axis 1 is driving the rotating drum pair, and Axis 2 the drive train. The host computer communicates with the IDC terminal using RS-232c serial port.

Computer user interface is written using Visual C++ on windows 2000. The C++ program provides a flexibility to select a specific program stored in IDC controller for different motion operations as shown in Figure A-3, and to monitor the overall system in real-time, which shows the machine's status, images captured by the USB camera that can be reviewed on the computer immediately after the experiment. An output window is at the left side of the screen for text output that can record the actions of the system.

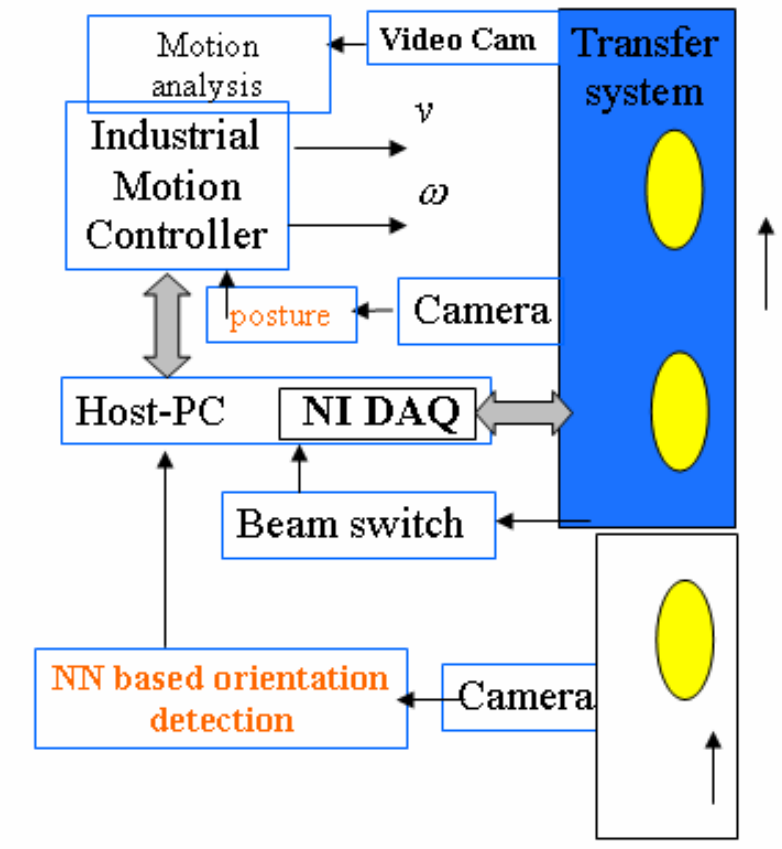

Figure A-1 Block diagram of the prototype live hang system

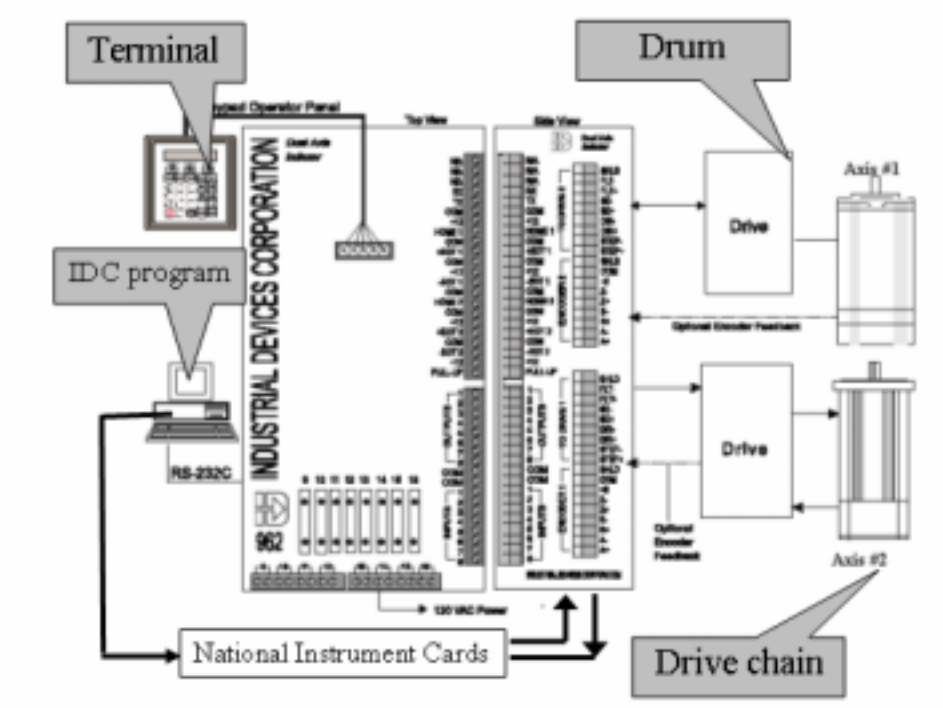

Figure A-2 System components of the prototype live hang system

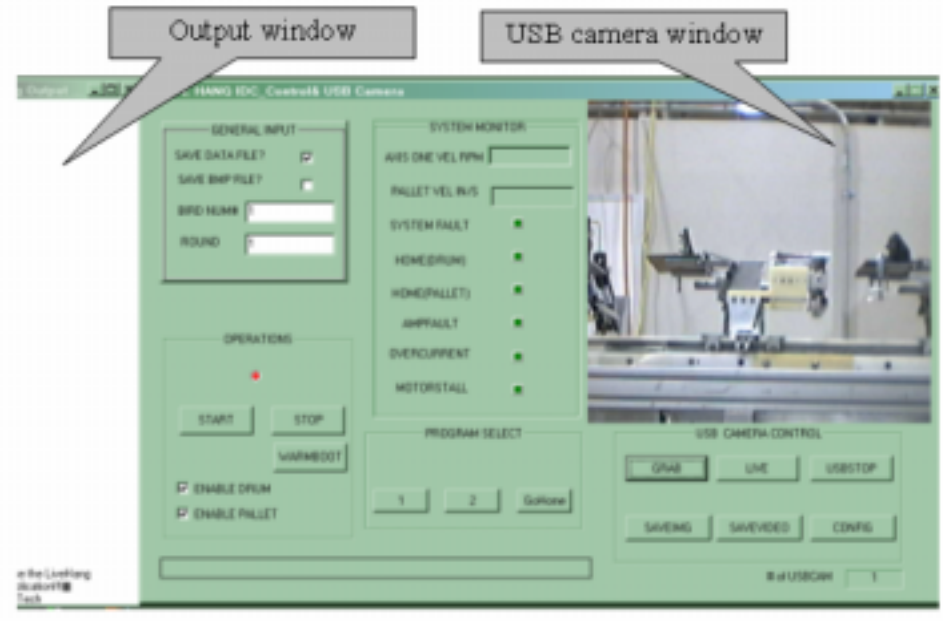

Figure A-3 Control panel of the prototype live hang system

APPENDIX B

TRANSFORMATION FROM THE C_F TO C_D

The transformation matrix [$R3$] and the position vector P_{fi0} in Equation (B.15) are derived with aid of Figure B-1, which shows the rotation sequences to get to the final posture of the i^{th} finger and its attached coordinate system C_{fi3}. The transformation involving three sequential rotations that begins with the initial finger coordinate system C_{fi} ($x_{fi}y_{fi}z_{fi}$).

The first rotation is about the fixed Z_d axis from C_d to an intermediate frame C_{d1}; and it is defined as

$$P_{d1} = [R_{Z_d}(\phi_z)]P_d \tag{B.16}$$

where
$$[R_{Z_d}(\phi_z)] = \begin{bmatrix} \cos\phi_z & -\sin\phi_z & 0 \\ \sin\phi_z & \cos\phi_z & 0 \\ 0 & 0 & 1 \end{bmatrix} \tag{B.16a}$$

Equation (B.16a) defines the orientation of C_{d1} in C_d with an angle of rotation denoted ϕ_z as

$$\phi_z(t) = \omega t + \phi_i; \tag{B.16b}$$

where ϕ_z takes into account both the drum rotations and the initial angular position of i^{th} finger as shown in Figure B-1(b); and $P_{d1} = (X_{d1}, Y_{d1}, Z_{d1})^T$ is the position vectors in C_{d1}. The finger coordinate system after the rotation is denoted as C_{fi1} ($x_{fi1}y_{fi1}z_{fi1}$) as shown in the Figure B-1.

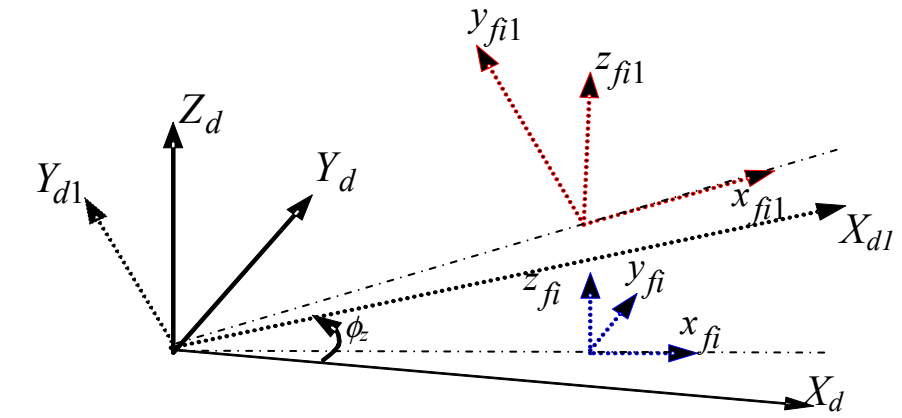

(a) ϕ_z

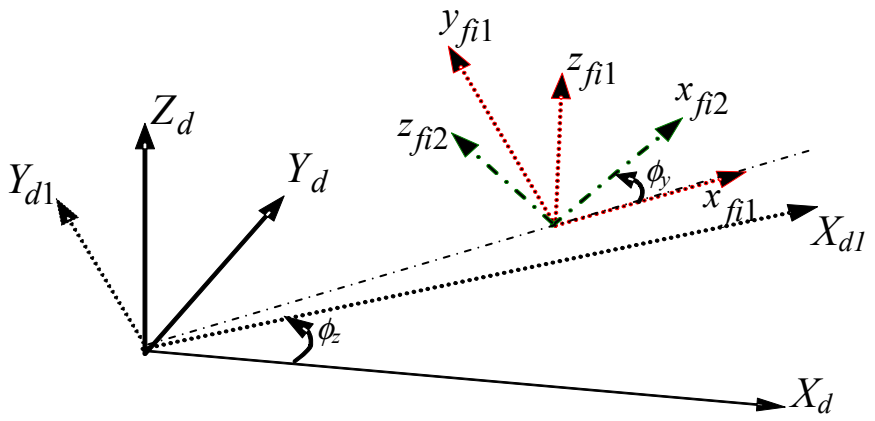

(b) ϕ_y

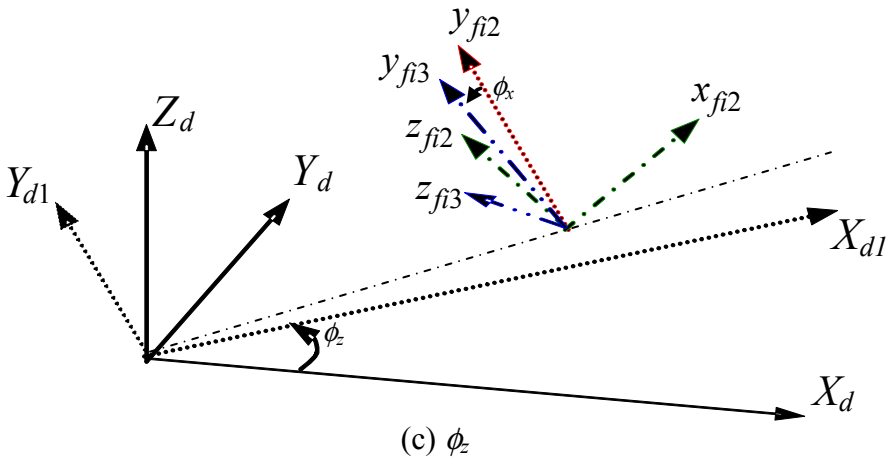

(c) ϕ_z

Figure B-1 Coordinates transformation from C_d to C_{fi3}

The second rotation ϕ_y is about the y_{fi1} axis. The orientation of the moving reference frame after this rotation is denoted C_{fi2} ($x_{fi2}y_{fi2}z_{fi2}$) in Figure B-4. The transformation from C_{fi1} to C_{fi2} is

$$P_{fi2} = [R_{\text{yfi1}}(\phi_{\text{y}})]P_{fi1} \tag{B.17}$$

where
$$[R_{yfi1}(\phi_y] = \begin{bmatrix} \cos\phi_y & 0 & -\sin\phi_y \\ 0 & 1 & 0 \\ \sin\phi_y & 0 & \cos\phi_y \end{bmatrix}^T; \tag{B.17a}$$

defines the orientation of C_{fi1} in C_{fi} with a angle of rotation denoted ϕ_y ; and $P_{fi1} = (x_{fi1}, y_{fi1}, z_{fi1})^T$ and $P_{fi2} = (x_{fi2}, y_{fi2}, z_{fi2})^T$ are the position vectors describing the same point in 3-D space but in C_{fi1} and C_{fi2} respectively

The third rotation ϕ_x is about the x_{fi2} axis. The orientation of the moving reference frame after this rotation is denoted C_{fi3} ($x_{fi3}y_{fi3}z_{fi3}$) in Figure B-4. The transformation from C_{fi1} to C_{fi2} is

$$P_{fi3} = [R_{\text{xfi2}}(\phi_{\text{x}})]P_{fi2} \tag{B.18}$$

where
$$[R_x(\phi_x)] = \begin{bmatrix} 1 & 0 & 0 \\ 0 & \cos\phi_x & -\sin\phi_x \\ 0 & \sin\phi_x & \cos\phi_x \end{bmatrix} \tag{B.18a}$$

defines the orientation of C_{fi1} in C_{fi} with an angle of rotation denoted ϕ_x.

The relationship between the C_{d1} to C_{fi1}as shown in Figure B-3 is

$$P_{fi1} = P_{d1} + P_{fi10} \tag{B.19}$$

where

$$P_{fi10} = \begin{pmatrix} r_D & 0 & h \end{pmatrix}^T \tag{B.19a}$$

is the origin of C_{fi1} in $C_{d1;}$ and r_D is the radius of the drum.

In order to get the transformation matrix and the translation vector in Equation (B.8), P_{fi1} in Equation (B.8) can be expressed in P_{fi3} by combining Equations (B.18) and (B.19), and P_{d1} can be replaced by expression of P_d using Equation (B.9). After some algebraic manipulations the resulting equation can be written as follows:

$$P_d = [R_z(\phi_f)]^T [R_y(\phi_y)]^T [R_x(\phi_x)]^T P_{fi3} - [R_z(\phi_f)]^T P_{fi10}. \tag{B.20}$$

Matching Equation (B.20) and Equation (B.8), the transformation matrix [$R3$] and translation vector P_{fi0} are represented as follows:

$$[R3] = [R_{Z_d}(\phi_z)]^T [R_{yfi1}(\phi_y)]^T [R_{xfi2}(\phi_x)]^T \tag{B.21}$$

and

$$P_{fi0} = [R_z(\phi_f)]^T P_{fi10} \tag{B.22}$$

BIBLIOGRAPHY

[1] Allen, P.K., Timcenko, A., Yoshimi, B. and Michelman, P., 1993, "Automated tracking and grasping of a moving object with a robotic hand-eye system," *IEEE Transactions on Robotics and Automation*, Vol. 9, No. 2, pp 152 -165.

[2] Akella, P. and M. Cutkosky, 1989, "Manipulating with Soft Fingers: Modeling Contacts and Dynamics," Proceedings of *IEEE International Conference on Robotics and Automation*, Vol.2, pp 764-769.

[3] Ananthasuresh, G. K. 1995, http://www-mtl.mit.edu/~suresh/CompMech.html.

[4] Asada, H., 1979, "Studies on Prehension and Handling by Robot Hands with Elastic Fingers," *Ph.D Dissertation*, Massachusetts Institute of Technology.

[5] Asada, H., and A. B., By, 1985, "Kinematics Analysis of Workpart Fixturing for Flexible Assembly with Automatically Reconfigurable Fixtures, " *IEEE Journal of Robotics and Automation*, Vol. 1, No. 2, pp 86-93.

[6] Ascher, URI M., Robert M. M. Mattheij, Robert D. Russell, 1988, *Numerical Solution of Boundary Value Problems for Ordinary Differential Equations*, Prentice-Hall Inc.

[7] Baraff D., 1994, "Fast Contact Force Computation for Non-penetrating Rigid Bodies," *Proc.of SIGGRAPH 94*, Orlando, pp 23-34.

[8] Baselt, David 1993, http://stm2.nrl.navy.mil/how-afm/how-afm.html.

[9] Berry, P. S., *et al.*, 1993, "Poultry Harvesting Assembly," US Patent 4,513,689, November 9.

[10] Briggs, D. V., *et al.,* 1994, "Poultry Harvester," US Patent 5,325,820, July 5.

[11] Bicchi, A. and V. Kumar, 2000 "Robotic Grasping and Contact: A Review," *Proceedings of the IEEE Int. Conf. on Robotics and Automation (ICRA'01)*, San Francisco.

[12] Burden, R. L., J. D. Faires, 1997, *Numerical Analysis*, Sixth Edition, Brooks/Cole Publishing Company.

[13] Burns, R. H., 1964, "The Kinetostatic Synthesis of Flexible Link Mechanisms," *Ph.D. Dissertation*, Yale University, New Haven, Connecticut.

[14] Buttazzo, Giorgio C., Benedetto Allotta, and Felice P. Fanizza, 1994 "Mousebuster: A robot for Real-Time Catching," *IEEE Control Systems*, pp 49-56.

[15] Cheng, H-M., M. T. S. Ewe, R. Bashir, and G. C. T. Chiu, 2001, "Modeling and Control of Piezoelectric Cantilever Beam Micro-Mirror and Micro-Laser Arrays to Reduce Image Banding in Electrophotographic Processes", *Journal of Micromechanics and Microengineering*, pp 487-498

[16] Chu, M. T., 1996, Numerical Methods for Boundary Value Problems in Ordinary Differential Equations (lecture notes), http://www4.ncsu.edu:8030/~mtchu/Teaching/Lectures/MA583/ma583.html.

[17] Croft, E. A., R. G. Fenton and B. Benhabib, 1998, "Optimal Rendezvous-point Selection for Robotic Interception of Moving Objects," IEEE transactions on *Systems, Man and Cybernetics*-part B: Cybernetics, Vol. 28, No. 2, April, pp 192-204.

[18] Comaniciu, D., V. Ramesh, and P. Meer, 2003, "*Kernel-Based Object Tracking*", IEEE Trans. Pattern Analysis Machine Intelligence, Vol. 25, No. 5.

[19] De Los Santos, H. J., Y.-H. Kao, Caigoy, A.L. and Ditmars, E.D., 1997, "Microwave and mechanical considerations in the design of MEM switches for aerospace applications," *Aerospace Conference, IEEE Proceedings*, Vol.3, pp 235-254.

[20] DeMeter, E. C., 1998, ''Fast Support Layout Optimization,'' International Journal of Machine Tools and Manufacture, Vol. 38, No. 10-11, pp 1221–1239.

[21] Devoe, D. L. and A. P. Pisano, 1997, "Modeling and Optimal Design of Piezoelectric Cantilever Microactuators," *Journal of Microelectromechanical Systems*, Vol. 6, No. 3, Sep., pp 266-270.

[22] Doug L. J. and D. K. Pai., 1999, "ArtDefo - Accurate Real Time Deformable Objects," *Proceedings of SIGGRAPH* 99, pp 65-72.

[23] Doug L. J., and D. K. Pai, 2003 "Multiresolution Green's Function Methods for Interactive Simulation of Large-scale Elastostatic Objects," *ACM Transactions on Graphics*, Vol. 22, No. 1.

[24] Friction coefficients, http://hypertextbook.com/physics/mechanics/friction/

[25] Frisch-Fay, R., 1962, *Flexible Bars*, Washington, Butterworths.

[26] Gascuel, M. P., 1993, "An implicit formulation for precise contact modeling between flexible solids," ACM SIGGRAPH 93, p.313-320, September 1993.

[27] Ginsberg, J. H., 1999, *Advanced Engineering Dynamics*, Cambridge University Press.

[28] Houshangi, N., "Control of a robotic manipulator to grasp a moving target using vision," 1990. Proceedings., 1990 *IEEE Inter. Conf. on Robotics and Automation*, May 1990, Vol. 1, pp604 -609.

[29] Harley, J, A., 2000 "ADVANCES IN PIEZORESISTIVE PROBES FORATOMIC FORCE MICROSCOPY," *Ph.D Dissertation*, Stanford University.

[30] Hill, J. and W. T. Park, 1979, "*Real-time control of a robot with a mobile camera*," in Proceedings, 9th lnt. Syrnp. Indus. Robots (SME), Washington, D.C.

[31] Hunt, A. E. and A.C. Sanderson, 1982, *Vision-Based Predictive Robotic Tracking of a Moving Target*, tech. report CMU-RI-TR-82-15, Robotics Institute, Carnegie Mellon University, January.

[32] Hurtado, J. F., and Melkote, S., 1998, "A Model for the Prediction of Reaction Forces in a 3-2-1 Machining Fixture," *Trans. of the NAMRI of SME*, Vol.26, pp 335–340.

[33] Hoffman, J. D., 1992, *Numerical Methods for Engineers and Scientists*, McGraw-Hill, Inc.

[34] Howard, W. S. and Vijay Kumar, 1996, "On the Stability of Grasped Objects," *IEEE Trans. on Robotics and Automation*, Vol. 12, No. 6, December.

[35] Hrishikesh, P. G., "Automated manipulation of dynamic natural objects," *Master Dissertation*, Georgia Institute of Technology, April 1998.

[36] http://psa-rising.com/medicalpike/detect/microchip0801.shtml

[37] Javier, G. D. J. and B. Eduardo, 1994, *Kinematic and Dynamic Simulation of Multibody System*, Springer-Verlag.

[38] Joni, H. J., 2000, "Force analysis of an automated live-bird transfer system," *Master Dissertation*, Georgia Institute of Technology.

[39] Kaneko, M., K. Harada and T. Tsuji, 2002, "Dynamic Friction Closure," Proc. Of *IEEE Conference on Robotics and Automation*, Washington, DC, May, pp1584-1589.

[40] Kazerooni, H. and Foley, C., 2003, "A robotic end-effector for grasping postal sacks," 2003 IEEE/ASME International Conference on AIM 2003, Vol. 1, pp260 - 265.

[41] Kettlewell, P. J. and M. J. Turner, 1985, "A Review of Broiler Chicken Catching and Transport Systems," *J. of Agricultural Engineering Research,* Vol. 31, pp 93-114.

[42] Kerr, J., B. Roth, 1986, "Analysis of Multifingered Hands," *International J. of Robotics Research*, Vol. 4, No. 4.

[43] Koivo, A. J., 1991, "On Adaptive Vision Feedback Control of Robotic manipulators," Proceedings of *IEEE Conference on Decision and Control*, Brighton, England, Dec., pp1883-1888.

[44] Kolesar, Edward S., and Frank L. Lewis, 2002, http://arri.uta.edu/acs/jmireles/MEMSclass/MAINpage.htm

[45] Lee, J. D., and L. S. Haynes, 1987, "Finite-element Analysis of Flexible Fixturing System," *Transactions of the ASME Journal of Engineering for Industry*, Vol. 109, pp 134-139.

[46] Lee, K.-M. and S. Arjunan, 1988, ″Force/Torque Sensing and Micro-Motion Manipulator of a Spherical Stepper Wrist Motor,″ *Proceedings of the 1988 Joint American Control Conference (ACC),* Atlanta GA, June 15-17.

[47] Lee, K.-M., and Y. Qian, 1995a, "Development of a Flexible Intelligent Control for Target Pursuit," *Int. Conf. on Recent Advances in Mechatronics* (ICRAM'95), Istanbul, Turkey, August 14-16, Vol. 1, pp 310-317.

[48] Lee, K.-M., and Y. Qian, 1995b "Intelligent Part-feeding based on Dynamic Pursuit of Moving Object," *Proc. of SPIE Photonics East*, August 25-26, Philadelphia, PA, pp 172-183.

[49] Lee, K.-M., R. Carey, M. Lacey, and B. Webster, 1996, "Automated Singulating System for Transfer of Live Broiler," *Proposal to US Poultry and Egg Association*, June 30.

[50] Lee, K.-M., 1999, "On the Development of a Compliant Grasping Mechanism for On-line Handling of Live Objects, Part I: Analytical Model," *Int. Conf. on Advanced Intelligent Mechatronics Proc. (AIM'99)*, Atlanta, September 19-23, pp 354-359.

[51] Lee, K.-M., A. B. Webster, J. Joni, X. Yin, R. Cary, M. P. Lacy, and R. Gogate, 1999, "On the Development of a Compliant Grasping Mechanism for On-line Handling of Live Objects, Part II: Design and experimental investigation," *AIM'99 Proc*., Atlanta, September 19-23, pp 360-365.

[52] Lee, K.-M., 2000 "Design criteria for developing an automated live-bird transfer system," *IEEE ICRA'2000*, San Francisco.

[53] Lee, K-M., J. Joni, and X. C. Yin, 2000, "Compliant Grasping Force Modeling for Handling of Live Objects," *Proceedings of the IEEE ICRA2000*, May 21-26, Seoul, Korea, pp 1059-1064.

[54] Lee, K.-M., J. Joni and X. C. Yin, 2000, "Imaging and Motion Prediction for an Automated Live-bird Transfer Process," *Proc. of the ASME DSCD 2000*, DSC-Vol.69-1, IMECE, Orlando, Nov. 5-10, pp 181-188.

[55] Lee, K.-M. and Y.-F. Qian, 1998, ″Development of A Flexible Intelligent Control For Target Pursuit,″ *ASME Trans. Journal of Manufacturing Science and Engineering,* August 1998.

[56] Lee, K-M. and X. Yin, 2001, "Design Algorithm for Automated Dynamic Grasping of Live Birds," *IEEE/ASME AIM'01 Proceedings, July 8–11 2001, Como, Italy, pp 207-212.*

[57] Lei, Ming and Ghosh, B. K., 1993, *"*Visually guided robotic tracking and grasping of a moving object," *Proceedings of the 32nd IEEE Conference on Decision and Control,* vol.2, pp 1604 -1609.

[58] Li, B., and Melkote, S. N., 1999, ''An Elastic Contact Model for the Prediction of Workpiece-Fixture Contact Forces in Clamping,'' *ASME J. Manuf. Sci. Eng*., Vol.121, pp 485-493.

[59] Linthorne, Nicohlas P. 2000, "Energy loss in the pole vault take off and the advantage of flexible pole," *Sports Engineering* (2000), Blackwell Science Ltd, March, pp 205-218.

[60] Liu, Y. H. and M. Wang, "Qualitative test and force optimization of 3D frictional force-closure grasps using linear programming," *IEEE International conf. On Robotics and Automation*, Leuven, Belgium, May.

[61] Markenscoff, X, L. Ni, and C. H. Papadimitriou, 1990, "The geometry of grasping," *International Journal of Robotics Research*, Vol. 9, No. 1, pp 61-74.

[62] Mason, M. T. and J. K. Salisbury, Jr., 1985, *Robot Hands and the Mechanics of Manipulation*, The MIT Press.

[63] Minne, S. C, G. Yaralioglu, S. R. Manalis, J. D. Adams, J. Zesch, A. Alalar, and C. F. Quate, 1998 "Automated parallel high-speed atomic force microscopy," *Applied Physics Letters*, Vol. 72, Number 18, May, pp2340-2342.

[64] Montana, David J., 1988 "The Kinematics of Contact and Grasp," *Int. J. of Robotics Research*, Vol. 7, No. 3, June.

[65] Murray R. M., Li Z. X., Sastry S. S, 1994, *A Mathematical Introduction to Robotic Manipulation*. CRC Press, Boca Raton, Florida.

[66] National Instrument Corporation, http://www.ni.com/products/

[67] Nguyen, V. D., 1988, "Constructing Force-closure Grasps," *Int. J. Robotics Research*, Vol. 7, No. 3, pp 3-16.

[68] Okamura, A. M., M. L. Turner and M. R. Cutkosky, 1997, "Haptic Exploration of Objects with Rolling and Sliding," *Proc. of the IEEE ICRA'97*, New Mexico, April.

[69] Okamura, A. M., N. Smaby and M. R. Cutkosky, 2000 "An Overview of Dexterous Manipulation," *Proc. of the IEEE ICRA'00*, San Francisco, April.

[70] Reilly, D. K., L. N. Cooper, and C. Elbaum, 1982, "A Neural Model for Category Learning." *Biological Cybernetics*, Vol. 45, pp35-41

[71] Reuleaux, F., 1876, The kinematics of Machinery, New York: Macmillan Publiations, 1876, reprint, New York, Dover Publications, 1963

[72] Salisbury, J. K., 1982, "Kinematic and force analysis of articulated hands," *Ph.D dissertation*, Dept. of Mechanical Engineering, Stanford University, Stanford, CA.

[73] Shampine, L. F., 1994, *Numerical Solution of Ordinary Differential Equations.*

[74] Sinha, P. R., and J. M. Abel, 1992, "A contact stress model for multifingered grasps of rough objects*," IEEE Transactions on Robotics and Automation*, Vol. 8, No. 1, pp 7-22.

[75] Smith, C.E. and Papanikolopoulos, N.P., 1995 "Grasping of static and moving objects using a vision-based control approach," Proceedings of 1995 IEEE/RSJ International Conference on *Intelligent Robots and Systems*, Aug., Vol.1, pp 329 -334.

[76] Somov, P., 1900, "Uber Gebiete von Schraubengeschwin- digkeiten eines starren Korpers bie verschiedener Zahl von Stutzflachen,", Zeitricht f¨ur Mathematik und Physik, Vol. 45, pp 245--306.

[77] Summer, Matthew D., 2002 "Design algorithm of a novel computer-controlled gripper for a live bird transfer system," *Master Dissertation*, Georgia Institute of Technology, Nov.

[78] TestResources, 2003, http://www.testresources.com/research.htm.

[79] Thierry C. Leïchlé, Martin von Arx, and Mark G. Allen, 2001, "A Micromachined Resonant Magnetic Field Sensor", *Proceedings IEEE Micro Electro Mechanical Systems*, Interlaken, Switzerland, 21-25 January.

[80] Timoshenko, S. P., 1953, *History of strength of materials*.

[81] Tortonese, M., H. Yamada, R. C. Barrett, and C. F. Quate, 1991 "Atomic force microscopy using a piezoresistive cantilever," *Transducers 1991 International Conference on Solid-State Sensors and Actuators*, pp 448-451.

[82] Vogel, S., 1995, "Better Bent than Broken," *Discover*, May Issue, pp 62-67.

[83] Wang, M. Y., D. M. Pelinescu, 2003, "Contact force prediction and force closure analysis of a fixtured rigid workpiece with friction," *ASME Journal of Manufacturing Science and Engineering*, May, Vol. 125, pp 325-332.

[84] Wang, M. Y., 2000, "An optimum design for 3-D fixture synthesis in a point set domain," *IEEE transactions on Robotics and Automation*, Vol. 16, No. 6, pp839-846

[85] Wu, G., R. H. Datar, K. M. Hansen, T. Thundat, R. J. Cote and A. Majumdar, 2001, "Bioassay of prostate-specific antigen (PSA) using microcantilevers," *Nature Biotechnology*, Sep., Vol. 19, No. 9, pp 856 – 860.

[86] Xiong, C. - H., Y. Li, H. Ding and Y. Xiong, 1999, "On the Dynamic Stability of Grasping," *Int. J. of Robotics Research*, Vol. 18, No. 9, September.

[87] Yaakov, B. S. and T. E. Fortmann, 1988, *Tracking and Data Association*, Academic Press, Inc.

[88] Yang, T. Y., 1973, "Matrix displacement solution to elastica problem of beams and frames," *Int. J. of Solids and Structures*, Vol. 9, No. 7, pp 829-842.

[89] Yin, X. and K.-M. Lee, 2002, "Modeling and Analysis of Grasping Dynamics for High Speed Transfer of Live Birds," *Proceedings of the 2nd IFAC Conference on Mechatronic Systems*, Berkeley, California, December 9-11.

[90] Zhang, M. and Buehler, M., 1994 "Sensor-based online trajectory generation for smoothly grasping moving objects", *Proceedings of the 1994 IEEE International Symposium on Intelligent Control*, 16-18 Aug., pp 141 -146.

VITA

Xuecheng Yin, son of ShiSun Yin and XueYu Liu, was born on April 20, 1972. He grew up in JiangXi Province, China, and attended TsingHua University from September, 1989 to July 1994, where he received his B.S. degree in Mechanical Engineering. After another 3 years in Institute of Automation, Chinese Academy of Science he received his M.S. degrees in Electrical and Computer Engineering.

Following completion of his M.S. study, Xuecheng got a research assistantship from Nanyang Technological University, Singapore, a very beautiful city country. He did research there for 4 months, and then he joined Semiconductor Technology & Instrument, a company developing vision inspection system for semiconductor industry. After 6 months working in STI he got the research assistantship from Woodruff School of Mechanical Engineering at Georgia Institute of Technology to be a Ph.D student. He joined the Mechatronics and Automation group and worked on Live Bird Transfer System under the guidance of Dr. Kok-Meng Lee. His research interests are automation and control, dynamics simulation, computer vision, digital signal processing and MEMS.